AN EXPERIMENTAL INVESTIGATION OF AN AEROTHERMOPRESSOR HAVING A GAS FLOW CAPACITY OF 25 POUNDS PER SECOND

by

Arthur A. Fowle

SUBMITTED IN PARTIAL FULFILLMENT

OF THE REQUIREMENTS FOR THE

DEGREE OF DOCTOR OF PHILOSOPHY

at the

MASSACHUSETTS INSTITUTE OF TECHNOLOGY

February, 1972

Signature of Author_____

Certified by_____
Thesis Supervisor

Accepted by_____
Chairman, Departmental Committee on Graduate Students

ABSTRACT

AN EXPERIMENTAL INVESTIGATION OF AN AEROTHERMOPRESSOR HAVING A GAS FLOW CAPACITY OF 25 POUNDS PER SECOND

by

ARTHUR A. FOWLE

This is a report on an experimental investigation of a medium-scale Aerothermopressor - a device having an 11 inch diameter subsonic entry to its evaporation section and a gas flow capacity of 25 pounds per second.

The fundamental characteristics of Aerothermopressor behavior are revealed by the illustration and interpretation of the results of tests made on this device when fitted with a constant area evaporation section 11 inches in diameter and 7 feet long. The measured influences of initial temperature, water injection rate, and Mach Number on performance are shown to be entirely compatible with the concepts and theory relating to the Aerothermopressor process.

Extrapolation of these experimental results indicates that the ultimate stagnation pressure rise to be expected of an Aerothermopressor having a subsonic inlet, a constant area evaporation section, and a conventional injection system is about 8%.

The important influence which the contour of the evaporation section has on Aerothermopressor performance is demonstrated experimentally. A net rise in stagnation pressure from the inlet to evaporation section to the exit of the diffuser of about 5% is reported for the variable area experiment showing most promising performance.

These results are extrapolated to an Aerothermopressor having the same basic size as the experimental unit but designed to eliminate certain parasitic losses inherent only to it. It is concluded that a stagnation pressure rise in the range of 10-15% is an assured performance for the medium-scale Aerothermopressor having a subsonic inlet, a variable area evaporation section, and an injection system of conventional design. Theory suggests design refinements can lead to further increases.

The experimental results of both constant area and variable area operation are compared with theoretical calculations. The theoretical prediction of over-all performance is shown to be surprisingly accurate. Theoretical computations duplicate all the qualitative aspects of Aerothermopressor behavior and provide quantitative results useful for design purposes. Interesting differences between experimental and theoretical results are illustrated and the reasons underlying these differences are explored.

FOREWORD

This work reports the results of an experimental study of a medium-scale Aerothermopressor made at the Massachusetts Institute of Technology. The study represents a phase in the project for the development of this device which has continued here under contract with the Office of Naval Research since 1952. The project is supervised by Professor Ascher H. Shapiro, of the Department of Mechanical Engineering. The test facilities are located at the Gas Turbine Laboratory of M.I.T.

The scale on which the experimental work was carried out suggests a certain maturity of the Aerothermopressor development. Prior work had led to a rather full understanding of the physical processes taking place within the Aerothermopressor. A theoretical model of the Aerothermopressor process had been devised which explained all the qualitative features of behavior of this device and gave useful quantitative results. The major objectives of this phase of the work have been to consolidate, to clarify, and to refine previous concepts; to demonstrate Aerothermopressor performance approaching practical significance; and to evaluate the future prospects of the device.

The content of this report is divided into two parts. The main body presents the skeleton of the investigation fleshed with the lean meat of the more significant results. It presents the highlights of the recent progress in the development of the Aerothermopressor. Interpretation of the

results presented in this section assumes some prior knowledge of the behavior of this device.

The second portion of the report appears as a series of appendices. These appendices present material in support of the main body. They are designed to serve three functions: (i) to provide the newcomer with the essential physical concepts and the mathematical treatment of the Aerothermopressor process, (ii) to present to the critic the details of various experimental and mathematical techniques used, (iii) to give to the interested engineer some knowledge of the construction details of the test apparatus and how they were determined.

As with any such undertaking, this thesis reports the results of efforts and ideas contributed by many individuals besides the author. It is a fitting and pleasant task to give thanks to those who cooperated in this venture.

I am particularly pleased to express by appreciation for the guidance and cooperation of Professor A. H. Shapiro, my thesis supervisor. He is primarily responsible for the concept of the Aerothermopressor and the theory underlying its operation. His ideas and supervision have made the development of the Aerothermopressor possible. It has been a most rewarding experience to work with Professor Shapiro as superior and counselor.

To Dr. Bruce D. Gavril, who organized the theoretical analyses appearing herein for computation by M.I.T.'s Whirlwind Digital Computer, and who, together with Mr. Alve J. Erickson and Professor Kenneth R. Wadleigh, contributed many useful ideas and critical judgments, I am indebted.

My hearty thanks go to Mr. Harry Foust and Mr. James F. Fenske, who participated whole-heartedly in the successes and blunders associated with the design, construction, and testing of the experimental apparatus. Many features of the test rig stem directly from their own ingenuity and labor.

Thanks also are due to Professor E. S. Taylor and R. C. Dean, and Mr. Dalton Baugh, of the Gas Turbine Laboratory, and to Professors H. C. Hottel and G. L. Williams and Mr. Paul Jensen, of the Fuels Research Laboratory, who cooperated to make the installation and testing of this Aerothermopressor possible.

Finally I wish to express my appreciation to Miss Margaret Tefft for computational aid, and to Mrs. Mary L. Regnier and Miss Catherine V. Ahearn for secretarial help.

TABLE OF CONTENTS

TABLE OF CONTENTS, cont'd

TABLE OF CONTENTS, cont'd

LIST OF TABLES

LIST OF FIGURES

LIST OF FIGURES, cont'd

NOMENCLATURE

a	function defined by equation D.11
A	function defined by equation D.10
A	cross-sectional area of duct
B	function defined by equation D.12
c_p	specific heat at constant pressure
$\bar{c}_{pa}$	mean specific heat of air defined by equation D.2
$\bar{c}_{pv}$	mean specific heat of water vapor defined by equation D.3
C	function defined by equation D.13
d	diameter of spherical water droplet
d_{oj}	initial diameter of water droplet given by Japanese correlation
D	hydraulic diameter, equals duct diameter for circular duct
D_o	outside diameter of annular cross-section
D_i	inside diameter of annular cross-section
f	skin friction coefficient of pipe
$\bar{f}$	apparent wall friction factor defined by equation D.6
h_{fg}	enthalpy of evaporation
k	ratio of specific heats for gas phase
ℓ	length of evaporation section
M	Mach Number of gas phase
M_{CR}	critical value of initial Mach Number
p	static pressure of gas phase

NOMENCLATURE, cont'd

p_o	stagnation pressure of gas phase
$\mathbb{P}$	parameter defined by equation D.7
r_o	outside radius of annular cross-section
r_i	inside radius of annular cross-section
R_a	gas constant of air
T	absolute temperature of gas phase
T_ℓ	temperature of droplet
T_o	stagnation temperature of gas phase
v	specific volume of substance
V	gas velocity
V_ℓ	droplet velocity
w	mass rate of gas flow
w_a	mass rate of air flow
w_ℓ	mass rate of water flow
$w_{\ell o}$	mass rate of water injected
W	molecular weight of gas phase
W_a	molecular weight of air
W_v	molecular weight of water vapor
x	fraction evaporated, ω/Ω_o
y	V_ℓ/V
Y	parameter defined in equation 6.1
z	axial distance along evaporation section from inlet plane
η_D	diffuser efficiency

NOMENCLATURE, cont'd

K	thermal conductivity of gas phase
μ	viscosity of gas phase
γ	wall shear stress
ω	specific humidity of gas phase, pounds of water vapor per pound of dry air
Ω_o	initial water-air ratio w_{lo}/w_a

Subscripts

o	at location upstream of water injector and entrance nozzle
1	at inlet of evaporation section
2	at exit of evaporation section
3	at exit of diffuser
7	at plane of tap number 7
r	radial distance from duct axis

INTRODUCTION

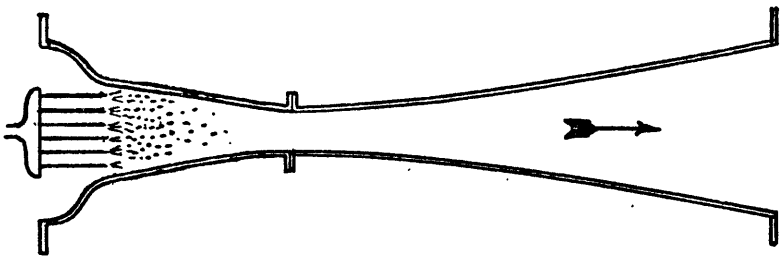

The Aerothermopressor is a device designed to increase the stagnation pressure of a high-temperature gas stream by evaporative cooling. It performs the function of a compressor but has an extremely simple mechanical form involving no moving parts. To produce a stagnation pressure rise, it depends on the interplay of thermodynamic and dynamic effects accompanying water injection into a high-velocity, high-temperature gas flow.

The form of an Aerothermopressor is essentially that of a continuous circular duct comprised of three sections which follow one another downstream in this order: an inlet nozzle, an evaporation section, and a diffuser. Water is injected into the gas flow at the exit plane of the inlet nozzle.

Many uses may be envisioned for the Aerothermopressor, but one of its most promising applications is to the gas turbine power plant. If attached to the exhaust of the power turbine of a simple gas turbine cycle, it can make good use of the hot gases which otherwise would be exhausted to the atmosphere. If an Aerothermopressor supplied with these hot gases and exhausting to the atmosphere can produce a rise in stagnation

pressure, it will lower the pressure at the turbine exit. The reduction of back pressure on the turbine betters the performance of the power plant by increasing the power output and fuel economy of a plant of given size.

Cycle calculations made by Gavril[4]* show that, with high turbine inlet temperatures and high component efficiencies, the percentage rise in power output and thermal efficiency approximate the percentage increase in stagnation pressure across the Aerothermopressor.

This description of the application of the Aerothermopressor to the gas turbine power plant is not complete[2], but shows the motivation for this work.

The Aerothermopressor evolved directly from concepts first articulated by Shapiro and Hawthorne[5]. In 1947 they showed that an increase in stagnation pressure of a flowing gas stream could result from cooling, if the cooling were accomplished by injection and evaporation of a volatile liquid, and not if it were done by conventional heat exchangers.

Having in mind its promise as an adjunct to the gas turbine power plant, theoretical and experimental research on the Aerothermopressor began at M.I.T. in 1949 under the supervision of Shapiro. Work on this device has continued at M.I.T. since 1952 under the sponsorship of the Office of Naval Research.

---

*Numbers in parentheses refer to the bibliography.

Progress in the development of the Aerothermopressor can be followed through the reports (7), (8), (6), (3), (4), and (2). Results of the comprehensive experimental study by Wadleigh[3] on a small Aerothermopressor and the theoretical study reported by Gavril[4] indicated that significant rises in stagnation pressure could be obtained in sufficiently large Aerothermopressors. Consequently the decision was made to build and test an Aerothermopressor large enough to demonstrate an appreciable stagnation pressure rise. This work reports the result of experimental tests on this device.

The physical concepts underlying the behavior of the Aerothermopressor are those common to gas dynamics and thermodynamics. Their application to the Aerothermopressor process has reached a rather refined state of development. References (5), (3), (4) and (2) show the growth of the theory of the Aerothermopressor to its present state. A convenient review of the concepts and theory of the Aerothermopressor is given in Appendix A as a necessary background and complement to the main body of this thesis.

CHAPTER I

TEST APPARATUS AND MEASUREMENTS

1.1 Flow System

The flow system used in all experimental tests is pictured in Figure 1. Air in amounts up to 27 pounds per second was supplied by a positive displacement compressor (1)* to a combustion changer (7) where it was heated by firing with fuel oil. The heated air then passed through a long sweeping elbow to the test section (9). From the latter it flowed through a system of quench sprays (11) into a water eliminator (14) and out through a sound muffler (16) to the atmosphere. More complete and detailed information on the major components comprising the experimental test facility is given in Appendix B of which this section is an abstract.

1.2 The Aerothermopressor Test Section

The essential structural features of an Aerothermopressor are an entrance nozzle, an evaporation section, a diffuser, and a water injection system.

In this investigation a basic Aerothermopressor was tested with both constant area and variable area evaporation sections.

The Aerothermopressor with a constant area evaporation section is pictured in the top illustration of Figure 2. The inlet nozzle had an inside contour which reduced the

---

*Circled numbers correspond to those in Figure 1.

duct diameter along an arc of a circle from 24 to 11 inches. A straightsection, 11 inches in diameter and 85½ inches long, identified as the evaporation section, followed. The diffuser was a cone 222 1/8 inches long having an included angle of nearly 5°. Fifty static pressure taps were spaced along the length of the test section, and it was fitted with 13 access ports to permit the introduction of measuring probes.

In order to obtain a variable-area evaporation section, the simple constant-area Aerothermopressor was modified as shown in the bottom illustration of Figure 2. In this modification, provision was made to suspend plugs from an overhead track within the Aerothermopressor and to traverse them axially.

A photograph of the Aerothermopressor test section, together with some of its measuring instrumentation and operating controls, is shown in Figure 3. A geometric description of all the plugs which were constructed for purposes of area variation and a photograph of one of them appear in Figure 4.

The water injector used in all tests is pictured in Figure 5. It was constructed of a number (208) of small parallel injection tubes about 7 inches long arranged to give good distribution over an 11 inch diameter circle. These tubes were fed from an airfoil-shaped manifold which in turn was connected to a single header pipe. This water injector was mounted within the entrance nozzle such that

the exit plane of the injection tubes coincided with the inlet to the 11 inch diameter section.

Provision was also made to inject water into the boundary layer next to the duct wall through a porous metal ring located 6 inches downstream from the inlet to the 11 inch diameter section.

Those persons interested in the details of the design of the test section and in the criteria underlying its design are referred to Appendix B.

1.3 Measurements

The following properties of the Aerothermopressor system were determined:

(i) The mass flow rate of gas entering the Aerothermopressor was determined by metering the air flow rate in advance of the combustion chamber with a sharp-edged orifice and adding to it the fuel flow rate measured by a Shutte and Koerting Rotameter.

(ii) The stagnation temperature of the flowing gas was measured upstream of the entrance nozzle by means of a five-shielded chromel-alumel thermocouple probe and potentiometer.

(iii) The stagnation pressure immediately upstream of the entrance nozzle was computed on the basis of a one-dimensional flow at this location having the measured properties of static pressure, stagnation temperature, and mass flow rate.

(iv) The stagnation pressure at the inlet to the evaporation section was determined by a calibration procedure

which correlated measured values of this quantity with the upstream stagnation pressure and inlet Mach Number. In calibration tests, both the inlet stagnation pressure and the inlet Mach Number were measured by making pitot tube traverses at the inlet section while operating the Aerothermopressor without water injection. The assumption was made that the correlation determined would hold in cases of water injection. The difference between the upstream stagnation pressure and the inlet stagnation pressure is often referred to as the entrance nozzle loss.

(v) The inlet Mach Number was determined as a result of calibration tests which correlated this value with the upstream stagnation pressure and the pressure drop across a portion of the entrance nozzle. As in the case of the evaluation of the inlet stagnation pressure, the calibration tests were made while operating the Aerothermopressor dry and the inlet Mach Number was measured by means of pitot traverses.

(vi) The stagnation pressure at the diffuser exit was determined in either of two ways: it was measured directly with a special impact probe; or it was computed on the basis of a one-dimensional flow at the exit to the diffuser having the measured value of static pressure, an estimated value of stagnation temperature, and an estimated mass flow rate.

(vii) The static pressure distributions along the length of the test section were indicated by connecting the wall

taps to a manometer board.

(viii) The radial distribution of stagnation pressure was measured at the various port locations by making horizontal traverses at these sections with a special impact probe [11]. The radial distribution of Mach Number was inferred from the measured values of stagnation pressure and static pressure.

(ix) The amounts of water injected from the water nozzle and boundary layer ring were metered by a rotameter and sharp-edged orifice respectively. In computing the water-air ratio referred to in the experimental results, only the water injected from the nozzle is included; for no significant effect of boundary layer water on Aerothermopressor performance could be found experimentally.

(x) The specific humidity of the inlet gases was computed by adding the water vapor formed in the combustion process to the water vapor content of the entering air. The latter was obtained from the local U. S. Weather Bureau.

Precise definitions of the measured properties, technical details and problems of measurement, estimate of measuring errors, and some details and results of the calibration procedures used appear in Appendix C.

CHAPTER II

LOSSES IN AEROTHERMOPRESSOR OPERATION WITHOUT WATER INJECTION

In its performance, the Aerothermopressor must rise above a basic handicap imposed by what may be termed "inherent" losses associated with its flow. At the upstream end, the flow of gas over the water injection system and through the nozzle gives rise to aerodynamic drag and wall friction losses. Wall friction exacts its toll within the evaporation section. The diffuser efficiency is a measure of the stagnation pressure loss in the diffuser. Determinations of the entrance nozzle loss, the duct-wall friction factor in the evaporation section, and the diffuser efficiency were made while operating the Aerothermopressor dry in order that they might serve as indices of the handicap imposed on normal Aerothermopressor operation.

2.1 Entrance Nozzle Loss

Figure 6 may be regarded as a chart of entrance nozzle losses. This plot resulted from the calibration procedure briefly described in Article 1.3, subsection (iv). Dimensional reasoning suggests that the percentage loss in stagnation pressure over the water injector and through the entrance nozzle could be correlated with the inlet Mach Number and the duct-diameter Reynolds Number. However, for the range of Reynolds Numbers (1×10^6 to 3×10^6) occurring in the calibration tests, no separate influence of Reynolds Number could be detected from the measured data.

Separate analysis of the core region of the flow yielded stagnation pressure losses of about 80 percent of those in Figure 6. Accordingly, we concluded that the aerodynamic drag of the injection system was responsible for 80 percent of the total loss. Losses in the boundary layer of the entrance nozzle accounted for the remaining 20 percent.

2.2 Dry Duct-Wall Friction Factor

The determination of the wall friction factor, f, is necessary to the theoretical evaluation of the Aerothermopressor process and to the interpretation of the experimental data. The duct-wall friction factor is defined by the equation

$$f \equiv \frac{\tau}{k p M^2/2}$$

where, in the case of a non one-dimensional flow, some average value of the Mach Number may be used in the definition.

The friction factor enters in the theoretical analysis of the fluid flow problem in the momentum equation to account for wall shear forces. However, in a simplified one-dimensional analysis of a problem involving two and three-dimensional flows, an "apparent" friction factor is sometimes used which accounts also for momentum flux terms associated with a changing velocity profile. The presence of liquid water in the Aerothermopressor further complicates an accurate evaluation of momentum effects. This water may well impinge on the walls, run along the walls,

and be re-entrained in the gas stream, an action which must modify the shear stresses at the wall and the water and gas velocity profiles.

Regardless of the apparent complexity of this problem, the experiments of Wadleigh[3] indicated that the measured values of the apparent friction factor made with and without water injection corresponded closely. Accordingly, experiments were made to determine the dry duct-wall friction factor for the constant area evaporation section of the test device.

In these experiments the inlet Mach Number and the static pressure distributions along the evaporation section were measured. Using the properties of the Fanno line[12], an average friction factor was determined. Two sets of experiments were made, one with and one without the internal tracks in the evaporation section. Results of these tests are given in Table I.

2.3 Diffuser Efficiency

We chose to define the diffuser efficiency as the isentropic change in enthalpy between the state entering the diffuser and the pressure at its exit divided by the actual change in enthalpy across the diffuser. For future reference, the relation between diffuser efficiency entrance Mach Number, and stagnation pressure loss for the one-dimensional flow of a perfect gas (air), is shown plotted in Figure 7. For comparison, Figure 8 shows a

corresponding relationship derived for a similar flow through the diffuser of the test Aerothermopressor assuming all losses were due to wall friction.

The tests to determine diffuser efficiencies were carried out on the Aerothermopressor operating without water injection. The Mach Number and stagnation pressure at its entrance and the stagnation pressure at its exit were measured. Diffuser efficiencies were evaluated before and after modification of the test device for area variation. A summary of experimental results appears in Table II.

CHAPTER III

PERFORMANCE OF THE AEROTHERMOPRESSOR WITH A CONSTANT AREA EVAPORATION SECTION

3.1 Objectives

At the outset it was realized that optimum performance is not to be demonstrated by an Aerothermopressor having a constant area evaporation section. Rather, initial tests were conducted on this simplified device to most readily meet the following objectives:

(i) To check the "scale effect" on Aerothermopressor performance. Based on theoretical calculations and the extrapolation of previous small-scale experiments, tests designed on this medium scale gave promise of demonstrating significant stagnation pressure increases.

(ii) To gather data with which to critically review the theory.

3.2 Experiments

A general study of the operational characteristics of the Aerothermopressor pictured in the top illustration of Figure 2 was made by systematically varying conditions present at its inlet end. The variables under control were (i) inlet stagnation temperature, (ii) inlet stagnation pressure, (iii) inlet Mach Number (or shock position when the inlet Mach Number was critical), and (iv) water injection rate. The first 34 runs appearing in Table III refer to tests carried out in this study. In these experiments,

the static pressures along the length of the test section were measured in addition to the inlet conditions. The separate influence of the inlet stagnation pressure was not experimentally determined.

In order to get more detailed information about the Aerothermopressor process, total pressure traverses were made for a few selected runs. The last four entries in Table III represent the operating conditions for these experiments.

3.3 Interpretation of Static Pressure Curves

Figures 9, 10, 11 and 12 illustrate some typical experimentally determined static pressure distributions. In numerical sequence they represent the progressive changes which took place in the pressure patterns with increasing Mach Numbers in the evaporation section. The major qualitative features of all these distributions can be explained on the basis of the known influences that area change, evaporation, wall friction and droplet drag have on the static pressure as given in Table V.

In particular, Figures 9 and 10 show some static pressure distributions resulting from operation of the Aerothermopressor with subsonic flows throughout. The following general features of these curves are to be noted; (i) a rapid drop in pressure accompanying accelleration in the entrance nozzle, (ii) a further drop in pressure due to the drag of the injected water,* (iii) a rapid rise in the

*See page 12.

forward regions of the evaporation section where cooling predominates, (iv) a leveling of the static pressure rise as wall friction takes over in the downstream portions of the evaporation section, and finally, (v) pressure recovery in the diffuser.

An increased inlet temperature produces more rapid evaporation of the water and allows greater amounts to be evaporated. Therefore, with sufficient water present, greater rates of increase in static pressure and a greater overall rise in pressure accompany the higher inlet temperatures. It is interesting to note that evaporation had already become predominant over droplet drag at a distance of only 10 inches downstream from the plane of injection. This fact, together with the steep slopes of the pressure curves, emphasize the tremendous rates of evaporation which were present in this region. The fact that in Figure 10 the pressure curves corresponding to Runs Number 541216-7 and 541216-6 cross over one another in the forward portion of the diffuser indicates that the higher temperatures in this region for Run Number 541216-7 produced more evaporative cooling even though less water was present.

At the same temperature, the rate of pressure rise increased with increased Ω_o in the flow zones where evaporation

---

*The pressure drop in this region is somewhat obscured by the fact that the pressure registered at the exit to the entrance nozzle is lower than the average pressure at this section because of the curvature of the streamlines in the region of the pressure tap, and because the flow undergoes a sudden expansion at the termination of the water injection tubes.

predominated, due primarily to the larger heat transfer surface of the liquid drops. The greater initial pressure drops which likely followed the larger water injection rates were obscured.

Because the influences of area change, evaporation, etc. on pressure are dynamic in nature, the rates of pressure change were larger at the higher Mach Number level. Further, at the higher Mach Numbers smaller drops were produced which resulted in a greater fraction of water being evaporated per unit of length[2][3]. This latter fact further enhanced the rates of pressure rise in those regions where evaporation effects were dominant. The net result was better Aerothermopressor performance for tests at the higher subsonic Mach Number.

In all the subsonic runs, the static pressures increased very little over the downstream half of the evaporation section. This fact indicates that, in this region, evaporation is extravagantly spending its influence in a stand-off battle with wall-friction. Somewhat better performance might be expected if the evaporation section were shorter.

Figures 11 and 12 reveal pressure data measured in experiments carried out at critical inlet Mach Numbers. In the experiments of Figure 11, the back pressure of the Aerothermopressor was adjusted to place the shock in its most forward stable position. In Figure 12 the shock was adjusted to occur at about 53 inches downstream from the plane of injection.

The characteristics of these pressure plots are similar, and from them we can deduce the main events in the history of these Aerothermopressor processes. First, there is a large drop in pressure in the converging portion of the entrance nozzle. This drop continues (neglecting certain spurious indications previously explained) immediately downstream of the injection plane due to the predominant influence of droplet drag. As the droplets accelerate, their drag effect on the main stream progressively lessens in respect to their cooling effect. When these effects balance,* the stream passes through Mach Number unity. Continuing downstream, evaporation takes over in the supersonic flow further reducing the pressure. These are the events typical of the passage of an Aerothermopressor flow through unity in a constant area duct operated at the critical inlet Mach Number[2][4]. Next, a shock (probably a series of shocks) is present at a location dependent on the back pressure. A very rapid rise in pressure accompanies the shock and the large evaporation rates present downstream from it. Wall friction suppresses the pressure rise as evaporation rates become less. Finally, the pressure recovers due to the predominant influence of area increase in the diffuser.

In Figure 11 the region of predominant evaporation upstream of the shock is very narrow. Even though the amounts

---

*In this discussion attention has been confined to the principal factors influencing Aerothermopressor behavior.

of evaporation up to the shock location must have varied widely in the cases reported, the balance between droplet drag and evaporation was such that little differences in pressure are evident. After the shock, the increased rates of evaporation for the runs having the larger water contents and the higher gas temperatures are revealed by the increase in their rates of pressure rise. The "negative drag" of the water droplets in this region contribute substantially to the pressure rise. This probably accounts for the rapid rise shown in Run Number 541218-4.

Operation of the Aerothermopressor as shown in Figure 11 gave the best constant area performance. For the reasons outlined in the case of the subsonic runs, somewhat better performance might be expected if the evaporation section were shorter.

The more extensive region of supersonic flow in front of the shock is the primary difference between the curves of Figures 11 and 12. In this region a pressure decrease accompanies the predominant influence of evaporative cooling. The larger decreases for the experiments having higher temperatures and water contents are consistent with expectations.

The performance of the Aerothermopressor worsened as the shock moved downstream in the evaporation section. In the subsonic region in advance of the shock the Mach Numbers were high and the static temperatures were low. The low

temperatures evidently inhibited evaporation to such an extent that the influence of cooling was ineffectual in spite of the high Mach Numbers, and friction again became important if not masterful. Evaporation took place but its cooling effect was wasted. Further, the shock became stronger as it moved downstream, and the additional stagnation pressure losses associated with its increase in strength acted to decrease the over-all performance.

3.4 Effect of Initial Conditions on Over-all Performance

The influences of Ω_o, T_{o1}, and M_1 on the over-all performance of the Aerothermopressor with a constant area evaporation section are summarized in Figures 13, 14, 15, and 16. One must be cautious not to draw too general conclusions from the results shown here. The over-all change in stagnation pressure in an Aerothermopressor depends not only on its inlet conditions but on its size, its configuration, and, in the case of a critical inlet Mach Number, on its back pressure. Nevertheless, one can expect certain consistent influences of the inlet conditions on Aerothermopressor behavior, and it is these influences which are to be emphasized.

Figure 13 represents all the measured data taken in the survey of Aerothermopressor performance. Figures 14, 15, and 16 result from cross-plotting this data to better reveal the separate influences of certain inlet variables.

As shown in Figure 13, for each set of initial parameters (M_1, T_{o1}, P_{o1}), there is an optimum value of Ω_o

giving rise to the greatest percentage increase in stagnation pressure. For values of Ω_o less than the optimum, too little cooling takes place to offset wall friction; above this value, the added drag of the injected water overbalances evaporative cooling which is limited by the saturation of the stream. The preceding conclusions appear to be logically well founded in spite of the fact that, in some cases, too few data points are present to clearly reveal an optimum Ω_o; and, in the case of $M_1 = 0.66$ and $T_{o1} = 1480$, the data appears a bit inconsistent.

Figure 14 shows the optimum value of Ω_o taken from Figure 13 and plotted against T_{o1}. As would be expected, the optimum value of Ω_o increases with increasing T_{o1}. The higher temperatures provide a greater driving force for more rapid evaporation; and this fact, coupled with the greater heat transfer surface accompanying the larger injection rates, places the optimum balance between cooling, friction, and initial drag at higher values of Ω_o. The highest optimum value of Ω_o was about 60 percent in excess of the amount needed for saturation, while the lowest value was about equal to that for saturation.

It comes as no surprise that increases in T_{o1} result in an increase in the optimum Aerothermopressor performance as shown in Figure 15. However, increasing T_{o1} does not always increase its performance. As shown in Figure 13, for cases in which Ω_o was very small, a decrease in

performance accompanied an increase in T_{o1}. The explanation for this behavior lies in the fact that evaporative cooling was limited by an insufficient amount of injected water, and, consequently, the percentage change in the stagnation temperature decreased with an increasing inlet temperature. As shown by equation A.2 (Appendix A), other things being equal, the percentage rise in stagnation pressure is approximately proportional to the percentage decrease in stagnation temperature. Therefore, for the cases cited, a decrease in performance was the result of increasing T_{o1}. For the range of variables considered in these experiments, a decrease in performance with increasing T_{o1} could easily be avoided by increasing Ω_o and allowing more water to evaporate.

With very high inlet temperatures, the optimum Aerothermopressor performance would decrease with increasing temperature for reasons similar to those given above. However, in this case, the amount of cooling would be limited by saturation of the stream and not by insufficient injection water.

The curves of Figure 16 show that the over-all performance of the Aerothermopressor improved as the Mach Number increased through a range of values up to the critical. In recognition of the dynamic nature of the phenomena occurring within the Aerothermopressor, the ordinate of Figure 16 is the so-called "performance coefficient"[2][3]. A rising performance coefficient with Mach Number indicates that a

greater fraction of water is evaporated in a given length of duct at the higher Mach Numbers. The smaller droplet produced by the atomizing process at the higher Mach Numbers is responsible for this behavior. The fact that the top curve in this figure has a slight negative slope is not considered too significant. It is known that operation of the Aerothermopressor at these high temperatures and at lower values of the Mach Number than have been recorded result in negative values of the performance coefficient. Therefore, the optimum performance coefficient must rise sharply in a lower Mach Number range.

Again it might be well to emphasize that the performance of an Aerothermopressor depends, not only on its inlet conditions, but also on the Mach Number present at each point in the process. Independent control of this Mach Number distribution can be obtained by varying the Aerothermopressor geometry, or, in the case of a critical inlet Mach Number, through changes in the back pressure.

CHAPTER IV

PERFORMANCE OF THE AEROTHERMOPRESSOR WITH VARIABLE AREA EVAPORATION SECTIONS

4.1 Objectives

As explained in some detail in references (2) and (4), control of the Mach Number at each point in the Aerothermopressor process is required for optimum performance. Variation of the cross-sectional area of the evaporation section is one method by which the Mach Number distribution may be regulated. To demonstrate the promise of better Aerothermopressor performance through the mechanism of area variation was the immediate goal of the series of tests to be described.

4.2 Experiments

The simple constant-area Aerothermopressor was modified as shown in Figure 2 in order to obtain variable area evaporation sections. The details of this modification are given in Appendix B. The use of internal plugs was not the ideal way to demonstrate good performance through area variation for reasons to be discussed fully in Section 6.2. The justification for use of this scheme was that it would quickly and economically give valuable technical information on variable area operation.

The series of tests outlined in Table VI were made to demonstrate the operation of the Aerothermopressor with variable area evaporation sections. In most of these experiments the following inlet conditions were fixed:

$T_{o1} = 1000^{o}$ F, $P_{o1} \cong$ 5 psig, and $\Omega_{o} \cong$ its optimum value. With plugs numbers 1, 2, and 3 set at various locations and with the inlet Mach Number a variable, static pressure distributions were recorded. No tests were made with plug number 4, for it was felt that they would provide no additional information of value. The last entry in Table VI refers to a run in which total pressure traverses were made.

4.3 Interpretation of Static Pressure Curves

As might be expected, the three plugs tested in their many positions gave rise to a great complexity in the operational character of the Aerothermopressor as illustrated by the great variety of the static pressure distributions observed. Only a few modes of operation determined by particular area variations were of any practical significance. Nevertheless, it might be of interest to illustrate the nature of some of the characteristic forms of operation. Figures 17 and 18 are included to serve this purpose.

In Figure 17 are shown some typical static pressure distributions observed in operation with plug number 2. These curves are also representative of those resulting from operation with plug number 1.

Runs Number 550513-2, 550513-4, and 550513-5 show operation with subsonic flow throughout with the nose of the plug located at 5, 20, and 43.5 inches, respectively, from the plane of injection. The decrease in pressure accompanying the acceleration of the flow over the forward half of

the plug is evident. The performance of the Aerothermopressor in all these runs is less than in their constant area counterparts for two reasons. The plug introduced additional parasitic losses (wall friction, aerodynamic drag of mountings, etc.) and it acted to increase the Mach Number in the downstream regions of the evaporation section where friction becomes dominant, making its effect more disastrous.

Runs Number 550512-1, 550512-3, 550422-4 are the supersonic counterparts to the tests previously described. In these experiments the entrance Mach Number is critical and a region of supersonic flow appears.

Run Number 550512-1 gave rise to the greatest increase in stagnation pressure recorded with an inlet temperature of 1000° F. It illustrates the mode of operation which was calculated in advance of the plug design to be superior. These calculations were based on considerations discussed fully in reference (2). Briefly stated, the Mach Number was made to tread a narrow path avoiding, on the one hand, operation at too low Mach Numbers suffering from too little dynamic action and, on the other hand, operation at too high Mach Numbers suffering from too little evaporation. To follow this path requires the Mach Number to rise rapidly in the first stages of the process, and thereafter, to gradually decline.

For this particular experiment, after a speedy rise to supersonic values from its initial critical value, the Mach

Number gradually decreased over the forward portions of the plug as the flow took place in a converging section. It then increased on the downstream side of the minimum area section, decreased rapidly across a weak shock, and further diminished in the divergent portion of the evaporation section and diffuser. Operation with a weak shock was found necessary for stable operation.

These changes in Mach Number can be inferred from the static pressure distributions. Proceeding downstream, we note a rapidly falling pressure as the flow becomes supersonic, a decrease in pressure over the forward portion of the plug accompanying the area decrease, an increase in pressure as the supersonic flow expands immediately downstream of the minimum area, a rapid pressure rise across the shock, and a continuing rise in the remaining divergent sections.

The changes in area force the character of the static pressure curve after the acceleration zone; however, evaporative cooling, wall friction, etc. have their influence. For instance, the maximum pressure in the region of the geometric throat does not occur at the point of minimum area.

Run Number 550512-3 has a static pressure distribution similar to the one previously described, but the area variation for this run was evidently less favorable. It delayed reducing the Mach Number in the evaporation section too long.

Run Number 550422-4 has a static pressure curve illustrating another behavior. In this experiment, in order to meet the back pressure condition, a shock appeared at 11 inches with subsequent subsonic acceleration of the flow over the forward half of the plug. If the back pressure were further reduced from the value shown, the shock position would shift downstream until a condition was reached in which the flow was again choked near the minimum flow area.

The area reduction provided by plug number 3 prevented the favorable operation illustrated in Run Number 550512-1. The minimum flow area was made so small that the flow choked in the region of minimum area before the critical inlet Mach Number could be reached, as illustrated in Figure 18, Run Number 550405-5. The flow for 550405-1 was very close to being choked. A slight decrease in back pressure would bring this condition about. A critical inlet Mach Number could not be reached until the plug was moved about 50 inches downstream in the evaporation section. At this location, with sufficiently low back pressures, one observed the behavior illustrated in Run Number 550404-3. This operation was similar to that previously described for Run Number 550422-4.

CHAPTER V

COMPARISON OF EXPERIMENT AND THEORY

As outlined in Appendix A for a one-dimensional system, the state of the flowing gas and liquid at any location downstream in an Aerothermopressor of fixed geometry and given inlet conditions is determined by 6 independent properties. If the temperature and velocity is assumed and the friction factor is considered an unknown, simultaneous application of the momentum, continuity, and energy equations, together with two measured properties, is sufficient to determine an appropriate average friction factor and the local state of the stream. With these facts in mind, measurements of total pressure and static pressure were made for a few selected runs, as listed in Chapters II and III, and as described in detail in Appendix C. The dual purpose of these experiments was to gain more complete information about the Aerothermopressor process and to gather data for comparison with theoretical calculations.

The theoretical model of the Aerothermopressor process, the methods employed in its analysis, and the assumptions inherent to the theoretical calculations are described in Appendix A. In the particular theoretical computations computed for the studies of this chapter, the size of the water droplets produced by atomization were taken to be equal to the volume-surface mean drop size predicted by the correlation

of Nukyama and Tanasawa[9] and were held constant in the evaporation process; the friction factor in the evaporation section was set equal to the appropriate measured "dry" duct-wall friction factor; and the friction factor for the diffuser was set to give the diffuser efficiency determined in dry tests for the same Mach Number at the diffuser entrance.*

5.1 Apparent Wall Friction Factor

A determination of the wall friction factor is necessary to the theoretical evaluation of the Aerothermopressor process. Some of the problems associated with the definition and evaluation of this quantity for the Aerothermopressor system have been mentioned in Article 2.2. An estimation of an "apparent" friction factor could be made for those runs in which both static and stagnation pressures were measured by making use of a "discontinuity" analysis whose details are given in Appendix D. The results of this analysis as applied to Runs Number 541221-1, 541223-1, and 550621-1 gave an apparent duct-wall friction factor of .0043 in all cases. The apparent friction factor therefore agreed closely with the measured values of the friction factor for dry operation.

5.2 Static Pressure, Stagnation Pressure, and Mach Number

Figures 19, 20, and 21 summarize the results of some detailed experimental observations together with some corresponding theoretical calculations. Figures 19 and 20 depict

---

*Figures 7 and 8 were used for this purpose.

Aerothermopressor operation with a constant area evaporation section, while Figure 21 refers to an experiment made with a variable area evaporation section. The particular modes of operation shown in these figures have been described previously in Articles 3.3 and 4.3.

The experimental values of stagnation pressure and Mach Number shown plotted in these figures (except for the duct-centerline or maximum values) are mass flow weighted average values computed from data obtained from total pressure traverses as described in Appendix C.

An examination of these figures shows that a gratifying similarity exists between measured and calculated properties, their differences never exceeding 13 percent of local values. All the qualitative features of the experimental Mach Number and static pressure curves are duplicated by the theoretical computations. Although perhaps coincidence, in all cases the theoretical prediction of overall stagnation pressure change is remarkably accurate. Both measurement and theory show essentially no change in the stagnation pressure for the flow in the diffuser.

Some major differences between experiment and theory are made evident by an inspection of the various stagnation pressure curves. In all cases, the measurements indicate a much more rapid rise in stagnation pressure in the initial stages of the Aerothermopressor process. The non one-dimensional nature of the flow is shown by the differences

between the curves of measured average stagnation pressure and the curves of measured centerline or maximum stagnation pressure.

In the real flow one does not observe the abrupt change in properties which would take place across a normal shock. Rather, the changes observed in the shock region are more gradual probably occurring over a series of shocks rather than over a single normal one because of shock-boundary layer interaction.

The rather large differences which exist in the initial stages of the Aerothermopressor process between the experimentally and theoretically determined stagnation pressure curves give rise to more questions about the true nature of the differences between the real and model Aerothermopressor process than the limited experimental data can answer. The experiments show a complete recovery of stagnation pressure in the first 10 inch length of the evaporation section, indicating a more favorable balance between droplet drag and evaporative cooling up to this point than predicted by theory. One may rationalize that the disagreement is due to the difference between the real and model atomization process, to differences between the real and model heat and mass transfer relations, or to errors in measurement.* The precise reasons for disagreement must await a much more extensive investigation of the acceleration zone** of the Aerothermopressor

---

*See page 29.
** " " "

process. That further knowledge of events taking place within this zone is important to the development of the Aerothermopressor is obvious, for these tests indicate action in this zone contributed a great deal to the eventual Aerothermopressor performance.

The two-dimensional character of the real flow is further illustrated by the Mach Number profiles of Figures 22, 23 and 24. Although these figures show that the development of the boundary layer as the flow proceeds in the evaporation section is not very different from that to be expected of a flow without the complications resulting from water injection, they make evident the fact that elements of the stream located at different radial distances from the duct centerline have quite different process histories. It seems likely that the longer residence times afforded the droplets travelling near the boundaries of the duct give rise to humidity profiles having maximums at these boundaries and temperature profiles having much the same character as the Mach Number profiles. With a uniform distribution of water over the inlet to the evaporation

---

*It is true that the curves of measured gas stagnation pressure agree more closely with the theoretically determined curves of mixture stagnation pressure (2) than with the theoretical curves of gas stagnation pressure. Yet there was no good reason to believe that the special pitot probes used measured other than the gas stagnation pressure for which purpose they were designed (11).

** The region at the forward end of the evaporation section where the droplet cloud is formed and where differences between droplet speed and gas speed are large.

section, one can visualize an ever widening zone of saturated gas extending from the boundaries downstream. A penalty is paid for accelerating the excess amounts of water which must exist within this saturated zone and from which no benefits from evaporative cooling can be derived. All this suggests a modification of the water injection scheme to effect a reduction in the amounts of water introduced near the duct walls.

5.3 Humidity

As outlined at the beginning of this chapter, for those experiments in which both the static and stagnation pressure are measured, the local specific humidity can be inferred from the measured data and a knowledge of the inlet conditions. The precise methods used to determine the specific humidity are described in Appendix D.

For Runs Number 541221-1, 541223-1 and 550621-1, Figure 25 compares the specific humidity determined by these methods to those computed by theory. The computation of specific humidity using measured data showed the result to be sensitive to the accuracy of the measurements. For variable area Run Number 550621-1, consistent results throughout the evaporation section could not be obtained due primarily to the uncertainties involved in the evaluation of a $\int_0^z pdA$ term appearing in the computations.

The comparisons of Figure 25 indicate rather close agreement. The fact that values of the specific humidity computed from the measured data are initially higher than those given

by the complete theoretical analysis and thereafter rise more gradually would lead to a more favorable balance between droplet drag and evaporative cooling in the upstream portion of the evaporation section followed by a less favorable balance between cooling and friction as evaporation proceeds. Comparison made previously between measured and calculated stagnation pressure supports this generalization.

5.4 Core Flow

An examination of the Mach Number profiles illustrated in Figures 22, 23 and 24 shows that, in the developing flow within the Aerothermopressor, the effects of wall friction do not penetrate the core region of the flow until it has proceeded downstream in the evaporation section some 4 feet or so. It was reasoned that a comparison between experimentally measured and theoretically calculated properties of the flow in a centrally located stream tube would be particularly revealing, for in such a comparison the uncertainties due to wall friction and two-dimensional effects are eliminated. Accordingly, theoretical calculations were carried out which applied to the core region of the flows in Runs Number 541221-1, 541223-1, and 550621-1. In these calculations, the inlet conditions and the Mach Number distributions were set to match the measured values. Under these conditions, if the heat, mass, and drag interactions between the drop and surrounding gas in the real and model flows are the same, their corresponding properties will be identical.

In order to match the prescribed Mach Number distributions of Runs Number 541221-1, 541223-1, and 550621-1 required that the corresponding theoretical flows have gradually decreasing cross-sectional areas. The increasing displacement thickness of the boundary layer confined the core region of the real flows but not necessarily to the same extent. However, comparisons based on stagnation pressure do not reflect differences in area variation.

In Figures 26, 27, and 28 the distributions of stagnation pressure within the evaporation section resulting from theoretical calculations are compared to the measured distributions. In all cases, the measured values of stagnation pressure are initially higher than the theoretical values and, thereafter, rise somewhat more slowly. Again the experiments indicate, on the average, a more favorable balance between droplet drag and evaporative cooling in the acceleration zone than predicted by theory. The theory predicts a considerable initial loss in stagnation pressure which is associated with the acceleration of the droplet mass. The measurements do not show this loss or, at least, they show a very rapid recovery from it. Yet, for those runs having a subsonic critical inlet Mach Number, passage through Mach Number unity to supersonic values requires that the stream first suffer a stagnation pressure loss. If, at each point within the acceleration zone, evaporative cooling has relatively more influence than droplet drag on the behavior of the real flow

than in the case of the model flow, it follows that the measured values of the critical inlet Mach Number should be higher than the calculated values. Unfortunately, within the accuracy with which the inlet Mach Number was measured this relationship was not evident. Further investigation of the acceleration zone of the Aerothermopressor process is indicated.

As the flow proceeds in the evaporation section, the distance between the theoretical and experimental stagnation pressure curves gradually lessens. This behavior is consistent with the smaller rates of evaporation for the experimental runs, as illustrated in Figure 25. However, a comparison of the slopes of the corresponding stagnation pressure and humidity curves shows that differences in evaporation rates in the region immediately downstream of the acceleration zone are small.

The theoretical stagnation pressure curves for Runs Number 541223-1 and 550621-1 rise sharply immediately downstream of what amounts to the shock locations in the corresponding real flows. Similar rises are not observed for the real core flows. The increase in the rate of evaporation and the "negative drag" of the decelerating droplet clouds that accompany the increase in gas temperature and the decrease in gas speed which take place after the shock locations explain the stagnation pressure rises exhibited by the theoretical flows. Three factors probably account for

the fact that the measured stagnation pressures do not show the rise predicted by theory. First, at the shock locations the effects of wall friction have already penetrated the core flow. This is particularly true for Run Number 550621-1 which uses an evaporation section of smaller hydraulic diameter. Second, the extreme turbulence present in the shock zones effectively mixes the core flow with surroundings having lower stagnation pressure. Third, stagnation pressure losses accompany the shocks present in the real flow. In short, the advantages of this particular comparison do not extend downstream of the shock locations in Runs Number 541223-1 and 550621-1.

CHAPTER VI

EXTRAPOLATED PERFORMANCE OF THE AEROTHERMOPRESSOR

6.1 Aerothermopressor with Constant Area Evaporation Section

If we compare two Aerothermopressors with different transverse dimensions but having the same inlet conditions, the same lengthwise Mach Number distributions in their evaporation sections, and the same effective diffuser efficiencies, equation A.2 (Appendix A) can be integrated to the form

$$\frac{p_{03} - p_{01}}{p_{01} M_1^2} = Y - 2 f k \frac{\ell}{D} \qquad (6.1)$$

where Y is the so-called "performance coefficient"[2][3] which includes the influence of all terms except wall friction. Using equation 6.1 and assuming a value for f, Y may be computed from data obtained from experiments made on one scale and then used (subject to the restrictions listed above) to compute the performance of a device of different scale. In line with this procedure, assuming f = .004 and k = 1.35, and utilizing the measured data from those constant area experiments demonstrating the greatest increases in stagnation pressure, the following results were obtained:

Run No.	T_{01} (°R)	p_{01} (in. HG.)	M_1	Ω_0	$\frac{p_{03}-p_{01}}{p_{01} M_1^2}$	ℓ/D	Y
541218-3	1238	37.93	.73	.19	.037	7.76	.121
541218-9	1464	40.13	.78	.18	.054	7.76	.138
541218-3	1660	42.39	.77	.30	.061	7.76	.145

Now, the stagnation pressure rise is computed for a device having a duct diameter approaching infinity and operating with the inlet conditions of Run Number 541218-9.

$$\frac{p_{o3} - p_{o1}}{p_{o1}} = M_1^2 Y = .084$$

How might this figure of 8.4 percent compare with the extrapolated performance of a large Aerothermopressor having a constant area evaporation section?

To answer this question one must recognize that the Mach Number distribution in the extrapolated unit will differ from that present in the medium-scale experiment. The comparatively larger frictional effect in the smaller device tends to drive its Mach Number distribution nearer unity. For the operation considered, the alteration of the Mach Number distribution by increased friction makes the separate influence of evaporative cooling more effective and actually gives rise to a larger performance coefficient for the smaller unit.

This fact is borne out by making a comparison between the performance coefficients computed for the tested Aerothermopressor and those calculated for similar small-scale tests reported by Wadleigh[3]. For instance, Y = 0.22 was computed for a small scale test in close agreement with Run Number 541218-9.

It seems likely that the performance coefficients for a constant area Aerothermopressor approaching infinite size

would be less than those measured on the medium-scale unit, leading to a stagnation pressure rise of less than 8.4 percent for the operating conditions of Run Number 541218-9.

A lower friction factor accompanying a greater pipe Reynolds Number and an improvement in diffuser design would increase the performance of the large Aerothermopressor somewhat, but, unless marked gains are realized through improvements in the water injection scheme, an 8 percent stagnation pressure rise is representative of the limitation in the performance of an Aerothermopressor having a constant area evaporation section and a subsonic inlet flow.

6.2 Aerothermopressor with Variable Area Evaporation Section

The best variable area performance demonstrated by the experimental unit was handicapped by certain parasitic losses introduced by the use of internal plugs. The problem is to interpret the measured "best" performance of the experimental unit in terms of what performance one might expect of an Aerothermopressor of "clean" aerodynamic design having the same (or better) Mach Number distribution.

Run Number 550621-1 was selected as representative of the most promising variable area performance. A comparison between the losses inherent to the experimental unit in this test and those expected of a device having an external area variation giving the same Mach Number distribution appears below. The techniques used to compute these losses are explained in Appendix E.

ESTIMATE OF STAGNATION PRESSURE LOSSES

Nature of Loss	Estimated Percent Stagnation Pressure Loss	
	Experiment with Plug (Internal area variation)	Similar Operation (External area variation)
Air nozzle loss and losses due drag of water injector	2.5	2.5
Wall friction loss	12.8	8.0
Diffuser loss	3.6	2.0
Loss associated with reacceleration of water impinging on plug	3.1	0.0
Total loss	22.0	12.5
Net difference: 9.5		

A penalty of 9.5 percent stagnation pressure loss seems attributable to the fact that the area control was achieved by an internal plug rather than by external area variation. On this basis, a stagnation pressure rise $[p_{o3}-p_{o1}/p_{o1}]$ of 14.2% is foreseen for the device of clean aerodynamic design.

In addition to the losses tabulated for the tested Aerothermopressor there were additional ones due to:

i) loss of heat transfer surface due to impingement of water on the plug;

ii) roughnesses at flanges, access ports, boundary layer water injector, etc.

The magnitude of these additional losses are difficult to estimate, but may total 2 or 3%, and may be eliminated in a design built for best performance rather than experimental flexibility.

As an additional check on the extrapolated performance of the experimental Aerothermopressor, a complete theoretical calculation was carried out for a device having the area variation and inlet conditions of Experiment Number 550621-1. The unit in these calculations was considered to have clean aerodynamic design with its area variation achieved by external diameter control. The results of this theoretical calculation are plotted in Figure 29 and are to be compared with those shown in Figure 21. The stagnation pressure rise $[p_o - p_{o1}/p_{o1}]$ of 10.7 percent predicted by this computation compares with the 14.2 percent rise resulting from the previous estimate. It is to be remembered that the latter computation did not take account of losses due to water deposit on the plugs and it was based on a device having the same area variation and not Mach Number distribution as the experimental device.

In conclusion, it appears reasonable that an Aerothermopressor with an 11 inch diameter subsonic inlet and with an external area variation the same as that produced internally in Run Number 550621-1 would have a stagnation pressure rise in the range of 10 to 15 percent. It seems improbable that this particular area variation is "best"; therefore, further increases seem likely by more closely approaching the area variation for optimum performance of a clean design. Modifications in the water injector design as suggested in Article 5.2 give expectations of improved performance.

Whatever figure, 10, 15, or 20%, is selected a representative of the ultimate performance of this medium-scale variable area Aerothermopressor, the methods of the previous article suggest that the ultimate performance of a variable area device approaching infinite size is about 5 percentage points greater.

An evaluation of the future promise of the Aerothermopressor would not be complete without mention of the possibilities of operation with a supersonic inlet flow. Theoretical studies* made to date indicate superior performance can be realized by injecting the water into a stream previously accelerated to supersonic velocity.

---

*Studies being made at this writing by Bruce D. Gavril, Division of Industrial Cooperation, Massachusetts Institute of Technology.

APPENDIX A

A REVIEW OF CONCEPTS AND THEORY

The concepts which underlie and explain the unique behavior of the Aerothermopressor are embodied in the equation first introduced by Shapiro and Hawthorne[5] in 1947.

$$\frac{dp_o}{p_o} = -\frac{kM^2}{2}\left[\frac{dT_o}{T_o} + 4f\frac{dz}{D} + 2(1-y)\frac{dw}{w} - \frac{dW}{W}\right] \quad (A.1)$$

This equation results from a one-dimensional analysis of a fluid stream flowing in a duct in which (for application to the Aerothermopressor process) changes in state are brought about by the external actions of area change, pipe-wall friction, and the stepwise injection of a liquid. It evaluates the change in stagnation pressure,* dp_o, taking place in an infinitesimal length of duct, dz, accompanying a change in stagnation temperature,** dT_o, the introduction of liquid mass, dw, and a change of the molecular weight of the gas phase, dW. In the model considered, the liquid is injected with a forward component of velocity, V_l, and the ratio of this velocity to the local gas velocity, V, is y. It is further assumed that this liquid is completely

---

*The stagnation pressure, p_o, is defined as that pressure which the gas phase would have if it were reduced isentropically in steady flow to zero velocity.

**The stagnation temperature, T_o is defined as that temperature which the gas phase should have if it were reduced adiabatically in steady flow to zero velocity.

evaporated and mixed at the end of the interval, dz. The evaporation of this liquid is responsible for the change in molecular weight and stagnation temperature of the gas phase. p_o, T_o, f, D, w, and W are the local values of the gas phase stagnation pressure, the gas phase stagnation temperature, Mach Number, duct-wall friction coefficient, duct diameter, mass flow rate of the gas phase, and the molecular weight of the gas phase, respectively.

Equation A.1 shows that cooling, which reduced the stagnation temperature, acts to increase the stagnation pressure. Wall friction, the drag associated with the injection of liquid (for $y < 1$), and a reduction in molecular weight act to decrease the stagnation pressure. Whether or not, the stagnation pressure rises in the interval, depends on the balance between these favorable and unfavorable effects. Further, equation A.1 shows the strong influence of Mach Number on the magnitude of the stagnation pressure change produced by these effects. Indeed, it points up the fact that changes in stagnation pressure result only from dynamic processes, and for a significant change in the stagnation pressure operation at reasonably high Mach Numbers is indicated.

Changes in the cross-sectional area of the duct have no direct influence on the local change in stagnation pressure. However, variations in the cross-sectional area of the duct have a very important, indirect effect on the

integrated change in stagnation pressure, for they strongly influence the local values of the Mach Number.

It is to be noted that the effect of the size of the Aerothermopressor on the change in stagnation pressure enters in the wall friction term, $4 f dz/D$, of equation A.1. For given gas properties at the beginning of the differential interval, dz, and for no significant heat exchange with the surroundings, analysis shows that the change in stagnation temperature is very nearly fixed by the ratio of the mass of liquid evaporated per unit of time to the mass flow rate of the gas phase. The advantage, therefore, lies in evaporating the injected liquid in as short a length and in as large a duct as possible. Of course, in order to increase the size of the duct and at the same time hold the properties of the flow at any section the same, requires greater mass flow rates. For this reason, Aerothermopressor performance is better in systems of greater flow capacity.

In order to evaporate as much water as possible in as short a duct length as possible, it appears reasonable to inject all the water at the inlet end of the Aerothermopressor. With this injection method, each portion of the injected water has a maximum residence time within the evaporation zone and a good opportunity to evaporate. This is the injection scheme used in all experimental Aerothermopressors tested to date.

The manner in which the water is introduced is very important to the Aerothermopressor process. Evaporation in a

short duct length requires that the injected liquid presents a large surface for heat and mass transfer to the surrounding gas. In the Aerothermopressor the water is injected at low velocity into a high-speed zone of the gas flow, and it is atomized into tiny droplets by virtue of the relative velocity between the two merging fluid streams.

In line with the preceding remarks, the model of the Aerothermopressor process with stepwise injection (the one used in deriving equation A.1) is abandoned in favor of one in which a cloud of finely divided water droplets is presented at the inlet section. An analysis of the Aerothermopressor process, using this model, has been completed (2)(3)(4). This analysis derives from the application of the energy, momentum, and continuity equations, and the equation of state of a perfect gas to the two-phase system occupying a control volume formed by the inside duct wall and two planes perpendicular to the duct axis and separated by a differential distance, dz. It retains the assumption of a one-dimensional flow; that is, one in which there are no radial variations in properties; accounts for the simultaneous external influences of heat transfer, area change, wall friction, and liquid injection; and considers variations in specific heat and molecular weight of the gas phase.

Tables IV and V, from (2), summarize the results of this analysis. By way of comparison with equation A.1, some

rearrangement of the terms listed in Table IV give the equation:

$$\frac{dp_o}{p_o} = -\frac{KM^2}{2}\left[\frac{dT_o}{T_o} + 4f\frac{dz}{D} - \frac{dW}{W} + \frac{2w_\ell}{w}\frac{dV_\ell}{V} + 2(1-y)\frac{dw}{w}\right]$$

$$+\left[\frac{K/K-1\ M^2/2}{1+\frac{K-1}{2}M^2} - \frac{KM^2}{1+\frac{K-1}{2}M^2} - \frac{K}{(K-1)^2}\ln\left(1+\frac{K-1}{2}M^2\right)\right]\frac{dK}{K} \qquad (A.2)$$

The similarity of this equation to equation A.1 is obvious, but it also includes drag effects associated with the evaporating liquid droplets and the influence of a changing specific heat ratio.

A stepwise numerical solution to the Aerothermopressor problems is obtained in the following manner (reference Table IV): For known properties at any given location in the duct, the change in these properties (left column Table IV), taking place in a small, finite interval downstream, can be computed if the change in the properties listed in the top row can be determined. In order to compute the change in these properties, a wall friction factor is assumed; the heat, mass, and momentum interactions between the liquid cloud and the surrounding gas are analyzed; and Gibbs-Dalton Law for perfect gas mixtures is applied. Having computed the change in the properties taking place in the small interval, the new state at the downstream end of this interval is determined, and the computing

process repeated. A complete solution to any particular Aerothermopressor problem is a tedious and time consuming endeavour. For this reason it has been found necessary to utilize automatic machine computations in the theoretical solution to the Aerothermopressor problem[4].

In order to summarize the theoretical attack on the Aerothermopressor problem, consider the following: at any station, z, downstream in an Aerothermopressor of fixed geometry, the state of the flowing gas and liquid is described by the 6 variables p, T, M, T_ℓ, V_ℓ and ω. By simultaneous application of the energy, momentum, and continuity equations together with the three equations relating to the heat, mass, and drag interactions between the liquid drop and the surrounding gas, the downstream state of the system is determined for any fixed condition at the inlet end. The state of the air-water mixture at the inlet end of the device is determined by the independent properties M,* T_o, p_o, Ω_o, ω, V_ℓ, T_ℓ** and A.

---

*For a certain value of M, designated as the critical Mach Number, a continuous progression from subsonic to supersonic flow is possible even in a constant area duct. Under these conditions the flow is "choked" and the Mach number is not independent of the other upstream variables. In this case, the back pressure to the device enters as an independent variable.

**The size of the liquid droplets produced by the atomization process is considered to be fixed by the other inlet conditions.

Finally, a review of the major assumptions in the theoretical analysis of the Aerothermopressor process is in order, for it is this analysis which is used in the interpretation of experimental results, and, in turn, the experimental results are analyzed to critically evaluate the theoretical model. These assumptions follow:

i) The flow is one-dimensional.

ii) A cloud of drops of uniform size are immediately produced by the atomizing process. The size of the droplets in this cloud is the volume-surface mean predicted by the correlation of Nukyama and Tanasawa (9). In the theoretical calculations made to date, either the number of drops in the cloud is held constant in the evaporation process, or the size of the droplet is fixed and the number varied to account for evaporation.*

iii) The heat and mass transfer between the liquid drops and the surrounding gas is assumed to obey the correlations of Runz and Marshall (10) with the Prandtl and Schmidt numbers constant.

iv) The well-known correlation between drag coefficient and Reynolds Number for solid spheres is used to evaluate the force interaction between the drops and the surrounding gas.

v) A reasonable estimate of the value of the duct-wall friction factor can be made.

---

*The effect on Aerothermopressor performance of the distribution of drop sizes produced by the atomizing process is now under study at the Massachusetts Institute of Technology by Mr. Alve Erickson, Instructor in Mechanical Engineering. Results of this study indicate that, in the zones of flow where the relative Reynolds Numbers for the droplets approach zero, the uniform drop size in a model cloud having the same liquid content and the same rate of evaporation as a real cloud containing a distribution of sizes remains nearly constant as evaporation proceeds.

vi) The deposit on, and re-entrainment of, water from the duct wall is insignificant.

vii) Certain property values, μ, C_p, k, K, h_{fg}, v, etc. are evaluated by methods explained by Gavril (4).

The view presented of the Aerothermopressor process and its theoretical analysis is not complete[2][4] nor original with the author. It is given as a convenient and necessary background for the evaluation of the experimental tests which are the substance of this report.

APPENDIX B

TEST APPARATUS

B.1 Main Test Equipment

Figure 1 shows in schematic form the layout of the major components of the facility used in the experimental testing of an Aerothermopressor with a 25 pound per second flow capacity. The purpose of most of the equipment pictured was to service and control the operation of the test Aerothermopressor and would not appear in a commercial installation. All large components were mounted on a structural steel frame outside the east wall of the Gas Turbine Laboratory of the Massachusetts Institute of Technology. The test section, together with measurement and control equipment, was housed in a temporary enclosure directly connecting with the Gas Turbine Laboratory.

Air was supplied to the test device by a positive displacement compressor (1)* in amounts up to about 27 pounds per second in steps of about 1.5 pounds per second. For flow control between the steps afforded by the compressor, blowoff through a flow control valve (4) was used. The pressure at which air was supplied was variable up to 20 psig. The upper limit was imposed by the design strength of the ducting and was insured by a safety relief valve (3). Two hydraulically controlled main valves (2) operated in unison so that air was

---

*Circled numbers correspond to those in Figure 1.

directed either to the Aerothermopressor or through a bypass to atmosphere. This feature provided for independent use of the air compressor, and further, the valves automatically acted to bypass air from the Aerothermopressor to the atmosphere in response to a number of safety devices installed to detect unsafe operation.

The supply air was heated by firing it with Number 2 fuel oil in a combustion chamber of commercial design (7). Provision was made to heat the air to any temperature in a range of 200° F to 1500° F; however, trouble with the refractory liner in the combustor prevented much operation at temperatures in excess of 1200° F.

The products of combustion were conducted to the inlet end of the Aerothermopressor through an insulated 304 stainless steel duct.

At the outlet end of the Aerothermopressor the flow passed through a system of quench-water sprays (11) which provided enough cooling to allow the downstream equipment to be constructed of mild steel for any operating condition of the Aerothermopressor.

An expansion joint (12) was installed at the downstream end of the Aerothermopressor to afford for the large thermal expansions encountered in operation (as much as 3 inches of axial displacement at the joint). Lastly, the flow passed into a water eliminator (14), through a hydraulically remote operated back pressure valve (15), and out through a sound muffler (16) to the atmosphere.

The water eliminator was provided to prevent carry over of water drops while allowing the gas to pass through. It accomplished this purpose by entraining the drops in a baffle-type separator, draining the collected water to a sump at the bottom of the eliminator, and pumping the collected water away by use of an automatic float level controlled sump pump(17).

Operation of the back pressure valve controlled the pressure at which gas was supplied to the Aerothermopressor.

For additional details regarding the specifications of the main test equipment reference can be made to the list at the end of this appendix.

B.2 Aerothermopressor Test Section

The experimental Aerothermopressor used in all tests is pictured in outline form in Figure 2. The essential constituents of the Aerothermopressor with a constant area evaporation section were an entrance nozzle, a straight cylindrical evaporation section, and a conical diffuser.

The inlet nozzle had an inside contour which reduced the diameter along an arc of a circle from 24 inches to 11 inches, and then continued downstream as an 11 inch diameter cylinder 6 inches long. The nozzle was formed by spinning a type 304 stainless steel tube originally 3/16 inches thick. The nozzle was fitted inside a heavy (3/8 inches thick) cone which served to strengthen it. Only the downstream end of the spun section was attached to the cone,

the flared end being free to allow for differential thermal expansions. Either end of the supporting cone was flanged, and pressure taps were located along the flared and cylindrical portions of the inlet nozzle. The whole nozzle assembly was covered with 6 inches of high-temperature insulation.

The constant area evaporation section was made by joining two cylindrical spool pieces 11 inches in inside diameter and, respectively, 42 and 36 inches long. They were rolled from 1/8 inch thick sheet and flanged at either end. Static pressure taps were spaced along the length of the evaporation section, and it was also fitted with a number of access ports to permit the introduction of special measuring probes. Blind plugs shaped to fit the inside contour of the cylindrical evaporation section were fitted to the access ports when no probes were in use.

The diffuser was a rolled cone, 222 1/8 inches long, 11 inches inside diameter at its small end, and $29\frac{3}{4}$ inside diameter at its large end, making an included cone angle of nearly 5°. It had flanges at either end, and its 1/8 inch thick wall was stiffened by two intermediately spaced rings welded on the outside. As with the evaporation section, the diffuser was provided with access ports and static pressure taps. The assembly of the Aerothermopressor was made by bolting the flanged sections together.

In order to produce an Aerothermopressor of variable

cross-sectional area, the simple constant-area Aerothermopressor was modified as shown in the bottom illustration of Figure 2. In this modification, provision was made to suspend concentrically located plugs within the Aerothermopressor from an overhead track and to traverse them axially. In all, four plugs were designed and constructed. They each had a similar streamlined shape which was a body of revolution formed by rotating a parabola about an axis perpendicular to its own axis of symmetry. All of these plugs had a nominal length of 84 inches, but each had a different maximum diameter. In particular, the diameters were sized to reduce the cross-sectional area of the 11 inch duct by respective maximums of 12, 16, 20 and 24 percent. The central portion of the plugs were spun to shape from 1/16 inch type 304 stainless steel sheet, welded and finished smooth. The ends of the plugs were machined pieces, fitted and contoured to match the central portion, and carried a single diamond-shaped airfoil support with clip which served to attach the plugs to the overhead track. These plug ends and attachments were made of hardened N-135 modified Nitralloy to offer maximum erosion resistance. The track on which the plugs were traversed had a simple T-bar form and was bolted to the duct wall. A track identical in form was also mounted in the bottom of the Aerothermopressor. It was designed to accommodate an axial and radial traversing stagnation pressure probe, but it was never used in the experiments reported in this work.

A photograph of the Aerothermopressor test section, together with some of its measuring instrumentation and operating controls, is shown in Figure 3. A geometric description of all the plugs which were constructed and a photograph of one of them appear in Figure 4.

Continuing upstream of the inlet nozzle was a spool piece 24 inches in inside diameter and 39 inches long. It contained a large port for access to the water injection nozzle which was mounted in this section. This piece was fitted with static pressure taps and provided for the introduction of temperature measuring probes and injection water. It was also covered with 6 inches of thermal insulation.

B.3 The Water Injection System

The water injection nozzle used in all tests is pictured in Figure 5, and shown in position within the Aerothermopressor in Figure 2. It was made up of a number (208) of small parallel tubes about 7 inches long arranged in 7 concentric rings for equal distribution over the area of an 11 inch diameter circle. The tubes were fed from airfoil-shaped distributor pipes which in turn were connected to a single axial header pipe. This water injector was mounted within and concentric with the entrance nozzle and upstream spool piece and, normally, with the exit plane of the water tubes coinciding with the entrance section of the 11 inch diameter duct. However, the axial position of the water injector could be located either upstream or downstream a

number of inches from this position. Up to 60 gallons per minute of filtered city water was pumped into this nozzle at pressures up to 155 psig by pump (10).

Water up to 6 gallons per minute could also be introduced into the boundary layer next to the duct wall in a region between the entrance nozzle and the cylindrical section (see Figure 2). This water oozed onto the wall through a porous stainless steel circular band about 1/8 inches thick and $\frac{3}{4}$ inches wide, whose 11 inch inside diameter matched the contour of the cylindrical duct. The band was fitted into a hollowed-out ring 1 inch between faces which was matched to, and bolted between, the adjacent flanges. The pump which supplied the injection nozzles also supplied water to the boundary layer.

All items making up the Aerothermopressor test section and water nozzle, unless otherwise specified, were made of type 304 stainless steel because of this material's resistance to high temperatures, corrosion, and erosion.

B.4 Design Criteria

Having completed a description of the design of the experimental Aerothermopressor, it might be illuminating to conclude by considering briefly how the major features of this device were determined.

The basic size of an Aerothermopressor, at least in its transverse dimensions, is set by its flow capacity. The availability of a 25 pound per second air supply, therefore, set the scale of the experimental device.

To illustrate this point, consider the design of the entrance nozzle. Theoretical and experimental results gained previous to the design of this device showed that for "best operation" an Aerothermopressor with a subsonic entry should have a Mach Number at the entrance to the evaporation section equal to the critical value or slightly below. Operation at entrance Mach Numbers above the critical are impossible so that the critical value could be established as an upper limit. Further, these results showed that the value of the critical Mach Number is not very sensitive to inlet conditions or duct size and a value of 0.75 could be taken as representative. For fixed values of the inlet stagnation pressure and temperature, and for the given values of Mach Number and flow rate, the diameter of the entrance to the evaporation section is determined. The range of values for the stagnation pressure and the stagnation temperature to be considered were those which one might encounter at the exhaust of a simple gas turbine power plant. In this range of stagnation pressures and temperatures, the diameter was chosen to insure critical Mach Number operation while using the full flow available from the compressors. These considerations gave a diameter of 11 inches, and this was fixed as the outlet diameter for the entrance nozzle.

The shape of the entrance nozzle was determined by these considerations: (1) it should be as short as possible in its axial dimension so that awkward parts of the water injection

system could be easily placed in a low-velocity region and (ii) it should be contoured to avoid separation of its boundary layer.

The length of the constant-area evaporation section was established by the rough criterion that it should be that length necessary to have the evaporative cooling and frictional effects in balance. If made longer, friction would be overpowering and produce losses in stagnation pressure. A length shorter than this would not exploit the possibilities of evaporative cooling. The length fixed by this criterion depends on the inlet conditions and, in this case of operation at the critical Mach Number, on the back pressure also. For the constant area evaporation section a length of about 7 feet was established as a compromise based on available theoretical analysis and experimental data. It was made in two sections to give some flexibility to this choice, but only experiments using the 7 foot length were made.

The plugs which provided the variable area evaporation sections were designed to approximate those area variations which were predicted by theory to give good performance. Four plugs were designed to give greater flexibility to the choice of area variations, and they were mounted so that they could be moved axially for the same reason.

It was recognized from the outset, that the use of internal plugs was not the ideal way of bettering Aerothermopressor performance through area control. The use of internal

plugs introduces certain parasitic losses such as additional wall friction losses, drag losses due to the presence of additional hardware within the duct needed to support and traverse the plugs, and to losses associated with the impingement of the injected water on the plugs and its reentrainment. The justification for use of internal area variation was that it would yield valuable technical information on variable area performance at a minimum expenditure of time and money.

The significant dimensions to be chosen for the diffuser were its cone angle and length. A good conventional subsonic conical diffuser has a 6°-7° included angle. A somewhat smaller cone angle is indicated for a diffuser which handles a flow in which liquid drops are present and evaporation is taking place. In this case, the smaller cone angle makes evaporative cooling more effective by having it occur at relatively higher Mach Numbers and it reduces the inefficiency associated with the decelleration of the liquid drops by reducing the relative velocity between them and the gas. Based on these considerations, a diffuser with a 5° included angle was designed.

The velocity at which one wishes to conduct and exhaust the flow to atmosphere and available space largely determine the length of a diffuser of fixed cone angle. A fairly arbitrary maximum value of 100 feet per second was imposed in the case of this design. With this value of velocity,

the problems associated with the mounting of auxiliary equipment in the downstream end of the Aerothermopressor (this equipment being peculiar to an experimental Aerothermopressor) were minimized. These considerations led to a diffuser 18 feet long.

The design of the water injection system was an attempt to meet the following requirements: (i) the injected water should produce a cloud of droplets in which the drops are of minimum size and uniformly distributed over the cross-section, and (ii) the parasitic losses associated with the flow of gas over the injection system should be as small as possible.

In accordance with requirement (i), the water was introduced at a number of points over the exit plane of the entrance nozzle into a high-speed zone of flow. The atomization which takes place with this arrangement produces tiny drops indeed, but lack of knowledge regarding the atomization process prevented a proper evaluation of this scheme. At any rate, it was consistent with the experimental results reported by Wadleigh[3].

To meet requirement (ii) the water was introduced through long parallel axial tubes which placed the bulky portions of the system into the low-speed zone of flow upstream of the entrance nozzle. Further, the pipe systemswhich fed these tubes and which constituted the bulky portion of the injection system were streamlined to reduce drag.

It might be noted that the terms entrance nozzle, evaporation section, and diffuser, have been used principally to identify different parts of the Aerothermopressor. In conventional gas flow systems, we can readily identify the particular geometric configuration bounding the flow with the changes taking place in its state. Unfortunately, the fact that events taking place in the Aerothermopressor are complex makes this difficult, and we identify the various sections only by the main objectives which they serve. For instance, the main purpose of the entrance nozzle is to accelerate the flow; however, the flow continues to accelerate to a considerable extent downstream of its exit due to the drag imposed by the injected water. Although evaporation takes place at all locations downstream of the injection station, the evaporation section is identified as that region in which the predominate influence is that of evaporative cooling. Although the flow may decelerate and the pressure rise in a substantial portion of the evaporation section, the diffuser is identified by the fact that the major purpose of area variation is to recover pressure efficiently. In short, no fine line of demarcation can be drawn between these sections; and, indeed, identification of them in an Aerothermopressor having a continuously varying cross-section would be difficult and arbitrary.

B.5 Major Equipment Specifications

Following is a list of the major equipment making up the experimental Aerothermopressor test facility. Some specifications pertinent to each item are included. The number preceding the listing of each item corresponds to that identifying the same piece in Figure 1.

1 - Two identical Cooper-Bessemer, 2-stage horizontal opposed-piston reciprocating compressors. Each has 3 first-stage and 2 second-stage cylinders, with piston displacements of 7750 and 3710 CFM, respectively. Each compressor motor is rated at 900 H.P. The compressors may be operated staged or unstaged either as compressors or vacuum pumps.

2 - Two 12 inch flanged List 44 rising stem gate valves with 7 in. diameter bronze mounted 150 psig hydraulic cylinder. One valve mounted with roller and face stock. Both valves manufactured by Ludlow Valve Mfg. Co.

3 - 6 inch cast iron body only of No. 700D diaphragm control valve with double seated A-2 type disc made by Minneapolis Honeywell Regulator Co., and fitted with a Rivett Lathe and Grinder, Inc. hydraulic cylinder, rod and flange mounted model 151-SS-3 inch bore x 2 inch stroke, double acting, for oil service.

4 - 8 inch N.P.T. bolted type Safety Head-Assembly No.1 with aluminum rupture disk and type B copper vacuum support made by Black, Sivalls and Bryson, Inc. Ratings: 20-50 psig, 220° F maximum temperature.

5 - Badger Mfg. Co. 12 inch expansion joint, 3 corrugations, non-equalizing type with sleeve, seamless copper with 125 lb. cast iron vanstone flanges, 16 inches face to face. Rated to accommodate $\frac{1}{4}$ inch lateral deflection and $\frac{1}{2}$ inch axial compression with maximum force of 500 pounds.

6 - R-S Products 16 inch butterfly wafer valve, Type B8705-A, with electric A.T.C. No. 36B506 110 v-60 cycle operator.

7 - Todd Shipyard Corp. Todd Thermo Contra Flow Combustion Chamber and System, Drawing TC-0782, capable of heating 25 pounds per second of air in 1500° F at a pressure up to 20 psig and firing up to 2000 pounds of number 2 fuel oil per hour.

8 - See Article B.2.

9 - See Article B.3.

10 - Worthington Corp. model $1\frac{1}{2}$ DONL-72, standard fitted end suction vertically split case Monobloc centrifugal pump driven by a 20 H.P. 3600 RPM 3 phase 220/440 volt 60 cycle motor capable of pumping 60 G.P.M. at 160 psig maximum.

11 - 22 model 1158 F and 1 6J-$\frac{1}{2}$ inch type 303 stainless steel spray nozzles manufactured by the Spray Engineering Co. to handle 100 G.P.M. of water at 60 psig maximum.

12 - 30 inch 1.0 x 32 inch face to face Fallea Bros. Figure No. 8 non-equalizing type 304 stainless steel expansion joint with 10 corrugations and $1\frac{1}{4}$ inch thick carbon steel Vanstone flanges for air, water vapor, and water

droplet service from 0 to 20 psig, 60° F to 400° F, and 0 to 4 5/8 inch axial movement.

13 - Allis Chalmers Type SS-E water pump with P-319 impeller and a 1750 R.P.M. 440 V 3 phase 50 H.P. motor drive.

14 - Peerless Mfg. Co. single bank top outlet type mist extractor with special housing designed to handle flow 0-25 pounds per second, 0 to 20 psig, and temperatures up to 300° F.

15 - R-S Products Corp. 20 inch heavy duty butterfly wafer valve fitted with 4 inch x 12 inch cylinder for use with 150 psig hydraulic oil.

16 - Size 20 BR6 Hi-Velocity discharged silencer manufactured by the Maxim Silencer Co.

17 - Intersoll-Rand Co. 2-RV-7½ H.P. Motor Pump with 220 volt 3 phase 60 cycle 3450 RPM standard open motor to service 180 GPM water at 81 feet total head.

APPENDIX C

DEFINITION AND DETERMINATION OF SYSTEM PROPERTIES

In the effort to gain further understanding of the Aerothermopressor process, sufficient measurements were made to evaluate the following characteristics of the Aerothermopressor system: (i) inlet mass flow rate of gas; (ii) inlet stagnation temperature; (iii) upstream stagnation pressure; (iv) inlet stagnation pressure and entrance nozzle loss; (v) inlet Mach Number; (vi) inlet specific humidity of gas; (vii) outlet stagnation pressure; (viii) lengthwise distribution of static pressure, stagnation pressure and Mach Number; (ix) radial distribution of stagnation pressure and Mach Number at selected stations; (x) mass flow rate of injected water; and (xi) velocity of injected water.

Because of the complexity of the natural flow through the Aerothermopressor, careful consideration must be given to the definition of its properties. The real flow through the Aerothermopressor is at least two-dimensional (axially symmetric), yet it is most difficult to deal theoretically with this complication. Accordingly, in many instances it has been convenient to force the real flow into correspondence with its one-dimensional theoretical model by considering only certain average properties of the natural flow. In defining these average properties such as inlet stagnation pressure, inlet stagnation temperature, inlet Mach Number, etc., thought has

been given to the comparisons which were to be made between them and their counterparts in the theoretical one-dimensional model of the real flow. Definitions of these average properties along with some others of interest are given in the following articles.

To properly evaluate the experimental results, account must be taken of the methods employed to evaluate the characteristics of the Aerothermopressor system. For this reason, a detailed description of these methods has also been presented.

C.1 Mass Flow Rate of Gas

The mass flow rate of gas, w, entering the Aerothermopressor was equal to the mass flow rate of air supplied by the compressors plus the mass flow rate of fuel entering the combustion chamber.

The fuel-air ratios encountered in experiments never exceeded 1½ percent, which proved to be less than the uncertainty involved in measuring their flow. Nevertheless, the fuel flow was metered by a Shutte and Koerting Fig. 1891 Universal Rotameter and included in the mass flow computations.

The mass flow rate of air supplied by the compressors was measured using a sharp-edged orifice. The pressure upstream of this orifice and the pressure drop across it were read on a mercury-in-glass and a water-in-glass manometer, respectively. The temperature in advance of the orifice

was taken by a Foxboro Company gas thermometer and its reading corrected by assuming a recovery factor of 0.65. The orifice was calibrated by making mass flow measurements using pitot probe traverses through Port No. 1* in the evaporation section.

An analysis of the errors involved in the calibration process and in the reading of the orifice temperature and pressures indicated that the maximum error in the determination of the mass flow was within $\pm$ 6 percent. Also the scatter of points on the calibration plot fell within this range.

C.2 Inlet Stagnation Temperature

The inlet stagnation temperature, T_{o_1}, refers to the stagnation temperature of the gas, as conventionally defined, at the entrance to the evaporation section. The measurement of temperature was actually taken in the straight section upstream of the entrance nozzle by means of a five-shielded chromel-alumel thermocouple probe manufactured by Aerotech Specialties Company and a Leeds and Northrup K2 potentiometer. The velocity at the measurement point was so low that no correction for "velocity error" was required. Temperature traverses taken across the duct axis for a range of flow rates and temperatures of interest showed that a probe located 8.5 inches from the center line of the duct would record a

---

*Refer to Table VII.

temperature within $\pm$ 10° F of the mass flow averaged temperature.* It was assumed that the inlet stagnation temperature appropriate to a one-dimensional flow corresponded to the temperature measured with the probe in this location. Instrument errors, reading errors, and errors caused by the non-uniformity of the temperature distribution combined to yield a maximum uncertainty in this temperature measurement of $\pm$ 17°.

C.3 Upstream Stagnation Pressure

The upstream stagnation pressure, p_{oo}, refers to the conventionally defined stagnation pressure of a gas in a region of the duct upstream of the entrance nozzle and water injection system. This quantity was not measured directly, but computed on the basis of a one-dimensional flow at this location having the measured properties of static pressure, stagnation temperature, and mass flow rate. It was further assumed in this computation that the entering gas was air with a ratio of specific heats, k, equal to 1.4. As the difference between the computed stagnation pressure and the measured static pressure in this region upstream of the entrance nozzle never exceeded 1 percent of the static pressure, the assumptions of the computation were of little consequence. The upstream stagnation pressure was easily determined within 0.15 inches of mercury.

---

*The temperature which, for a one-dimensional flow, would give the same flux of enthalpy across the section as in the real flow.

C.4 Inlet Stagnation Pressure and Entrance Nozzle Losses

The inlet stagnation pressure, p_{o_1} is of interest because it enters the theoretical computations as a fixed entrance condition. For the purposes of this work we define the inlet stagnation pressure of the gas as that value of the stagnation pressure which, for a one-dimensional flow, would give the same flux of stagnation pressure across the inlet of the evaporation section as the real flow. In other words it is an average stagnation pressure based on mass flow rate. This definition is fairly arbitrary and can be particularly criticized for treating the stagnation pressure as an extensive property. However, it is of interest to note the computed values of the stagnation pressure based on this definition differed very slightly from computed values of the stagnation pressure which, for a one-dimensional flow, would give the same entropy flux as the actual stream. This definition of inlet stagnation pressure takes account of the two-dimensional nature of the flow at the inlet to the evaporation section in a particular manner.

Values of the inlet stagnation pressure were obtained as a result of the following calibration procedure. First, while operating the Aerothermopressor "dry" (without water injection) total pressure traverses were taken for a number of flow conditions at Port No. 1 using the probe described in (11). Stagnation pressures were computed from this data in accordance

with their definition.* The Mach Numbers corresponding to these stagnation pressures and the measured static pressures at this location were also computed. Next these values of stagnation pressure and Mach Number were corrected to apply to the entrance of the evaporation section by assuming a one-dimensional, adiabatic, flow with friction between this section and the probe location with a wall friction factor equal to .004. Lastly, the percentage loss in stagnation pressure between the upstream and inlet sections, $p_{oo}-p_{o_1}/p_{oo}$, was correlated with inlet Mach Number, as shown in Figure 6.

This figure was regarded as a calibration curve from which p_{o_1} could be obtained from properties measured upstream of the inlet section, and it was applied even in the cases of operation with water injection. Here the assumption was made that water injected downstream at Section 1 would not significantly alter the behavior of the flow

---

*Assuming a flow having axial symmetry and a uniform stagnation temperature and static pressure across the plane of measurement, the stagnation pressure becomes

$$p_o = \frac{\int_{r_i}^{r_o} p_{or}[1 + \frac{K-1}{2} M_r^2]^{\frac{1}{2}} M_r \, rdr}{\int_{r_i}^{r_o} [1 + \frac{K-1}{2} M_r^2]^{\frac{1}{2}} M_r \, rdr} \qquad (C.1)$$

M_r was evaluated from measured data, an assumed value if $K = 1.4$, and the equation

$$\frac{p_{or}}{p} = [1 + \frac{K-1}{2} M_r^2]^{K/K-1} \qquad (C.2)$$

p_o was then computed using graphical evaluation of the integrals in equation C.1.

upstream of this section. p_{oo} was determined as outlined in Article C.1, and the inlet Mach Number, M_1, was obtained from measured upstream properties as described in Article C.5.

C.5 Inlet Mach Number

The inlet Mach Number, M_1, when used in this work in connection with measured results, refers to that value of Mach Number consistent with a one-dimensional flow of a perfect gas through the inlet to the evaporation section having the measured values of the following properties: inlet stagnation pressure, inlet stagnation temperature, and gas flow rate. This definition of inlet Mach Number in combination with the experimental results shown plotted in Figure 6 led directly to the functional relationship illustrated in Figure 30. The use of Figure 30, together with the measured upstream properties, w, T_{oo}, p_{oo}, was the most direct method employed to determine M_1; however, difficulties were encountered with this method. The value of M_1 determined in this way was found sensitive to the errors involved in the evaluation of the parameter, $w/A_1/\sqrt{T_{oo}}/p_{oo}$, particularly at higher values of M_1. For instance, a 5 percent uncertainty in the determination of $w/A_1/\sqrt{T_{oo}}/p_{oo}$ at M_1 equal to 0.7 results in an uncertainty in the evaluation of M_1 of almost 12 percent. Because the uncertainty in the determination of the gas flow rate, w, was about 5 percent, the subsequent evaluation of M_1 by this technique led to large errors at the higher values of M_1. However, for low values of the inlet

Mach Number, this method of evaluation was used with good results.

For the purpose of getting a more accurate determination of the inlet Mach Number, the entrance nozzle was calibrated. In this calibration the inlet Mach Numbers were obtained in the manner described in Article C.4 while operating the Aerothermopressor without water injection at a number of flow conditions. These values were then correlated with the static pressure measured at tap number 7,* p_7, in the entrance nozzle and the upstream stagnation pressure, p_{oo}, as shown by the crossed data points in Figure 31.

Unfortunately a single curve would not suffice to show the functional relationship between p_7/p_{oo} and M_1 for all conditions of operation of the Aerothermopressor. Variations in the specific heat ratio of the entering gas, Reynolds Number variations, and changes in the geometry of the entrance nozzle due thermal effects all influenced this functional relationship. The ratio of specific heats of the incoming gases varied in the range 1.40 to 1.35 depending primarily on the inlet temperature. The duct-diameter Reynolds Numbers based on conditions at the inlet to the evaporation section varied in the range 1×10^6 to 3×10^6 for all test conditions. The changes which took place in the geometry of the entrance nozzle for any particular set of

---

*Refer to Table VII.

operating conditions were difficult to determine. It is obvious that changes did take place, for, in all "hot" runs with water injection, the exit to the entrance nozzle was kept approximately at room temperature from the cooling effect of the boundary layer water while the upstream portions were red hot. Assuming a free thermal expansion, the cross-sectional area of the nozzle in the region of tap number 7 increased by approximately 2% at worse conditions.

In an effort to account for the above mentioned variations, it was assumed that the effect of changing Reynolds Number was negligible and that small changes in area ratio and specific heat ratio would effect the real flow between the cross-section at tap number 7 and the inlet to the evaporation section in the same manner as they would a one-dimensional isentropic flow between these same sections. The influences of area variation and specific heat variation on the relationship between p_7/p_{oo} and M_1 were computed in accordance with these assumptions and are shown plotted in Figure 31. This figure was used to evaluate M_1 from measured values of p_7 and p_{oo}. It was particularly useful in obtaining the higher values of M_1. In all cases of water injection, the assumption was made that this did not change the behavior of fluid flow upstream of the injection plane and, hence, the calibration remained valid.

It was difficult to assess the uncertainty in M_1 determined by this last method. The thermal distortion of the

entrance nozzle was a major source of error. This nozzle was calibrated before the experiments with a constant area evaporation section and again before the experiments with area variation. Some change in calibration was noted, and Figure 31, which represents the first calibration, was altered. Throughout the period of operation reported upon, the evaluation of M_1 for reproduced experiments was repeatable within $\pm$ 6 percent. It is estimated that the uncertainty in a single value of M_1 lies within this same range.

C.6 Outlet Stagnation Pressure

The outlet stagnation pressure, p_{03}, refers to the stagnation pressure of the gas phase leaving the diffuser. This quantity was obtained in either of two ways: it was measured directly with a special pitot probe (11) connected to a mercury-in-glass manometer, or it was computed on the basis of a one-dimensional flow at the exit to the diffuser having the properties of measured static pressure, estimated stagnation temperature, and estimated mass flow rate. The stagnation temperature was obtained from the application of the energy equation to the fluid system between the upstream and exit sections of the Aerothermopressor. It was assumed that either the injected water evaporated completely or saturation was reached at the exit. The mass flow rate at the exit was computed to be that measured at the inlet plus the mass of water evaporated. Certain other assumptions were involved in the determination of the properties of the fluid stream

at the exit of the diffuser, but, as the difference between the stagnation pressure and the static pressure at this location never exceeded 0.6 percent, their influences were not important.

C.7 Static Pressures and Stagnation Pressure Traverses

Fifty static pressure taps were spaced along the length of the test section at the locations given in Table VII. They were connected to a mercury manometer board to permit measurement of the static pressure distribution along the test section.

Even the measurement of static pressure, usually so simple and commonplace, presented some difficulties. As water was usually streaming along the duct wall over the static pressure tap hole, provision had to be made to prevent any water which might enter the pressure conducting system from adversely effecting the accuracy of the reading. A satisfactory solution to this problem was obtained by the following construction. The pressure tap holes were made small (0.040 inches in diameter) and located on the horizontal axis of the duct. These holes communicated to the larger (3/16 inches I.D., 5 to 8 inches long) pressure taps which ended at a water trap. The pressure was communicated from the trap to the manometer board through water-free flexible lines.

At high Mach Numbers, particularly in transonic and supersonic regions of the flow, the static pressure

distribution appeared quite irregular. The construction of the test section and pressure taps was blamed for this irregularity. The test section was fabricated from sheet which meant there were unavoidable irregularities along its surface and in its cross-section. Its various sections were flanged and bolted together producing discontinuities at the joints. The pressure taps were brazed or welded to the duct walls, and, although pains were taken to smooth the inside surface of the duct in the region of these taps, local distortions were present. Finally, carbon deposits from the combustion process gave some trouble. It might be noted that tests carried out on the small scale Aerothermopressor[3] having a honed inside wall showed no irregularities in the static pressure distribution.

Steady conditions of operation were obtained except in a narrow range of inlet Mach Numbers slightly below the critical value and in zones of flow having compression shocks. For steady operation the static pressure could be easily read to within .05 inches of mercury. The deviation of any particular pressure reading from a smooth faired curve of the pressure distribution was as much as 1.5 inches of mercury in the supersonic flow regions.

The test section was provided with fourteen horizontally mounted access ports to permit the introduction of special measuring probes. The axial locations of these ports are given in Table VII. In this work, probes were introduced

through the ports and traversed horizontally across the duct diameter measuring stagnation pressure. The stagnation pressure probes were especially designed, as described in reference 11, to measure the total pressure of the gas phase of a stream containing water droplets. The measurements of stagnation pressure were made on a mercury-in-glass manometer which could be read to within .05 inches.

These probes performed, on the whole, quite adequately. However, some difficulties were encountered in their use. The size of these probes proved to be a handicap. In all cases they altered the flow conditions somewhat, and, in some cases, a great deal. In certain critical cases their introduction choked the flow at the probe location or produced drag losses which greatly modified the flow conditions. They were too large to get accurate information within the boundary layer close to the wall. When placed in transonic or supersonic flows they sometimes fluttered to the extent that they could not be introduced into the stream more than 5 or 6 inches. Erosion of the probe head due to impinging water droplets and particles from the refractory liner of the combustion chamber was a continual source of trouble. To prevent errors caused by water entering the probe stem it was found necessary to periodically blow it free with auxiliary high pressure air while taking readings.

The stagnation pressure traverses were analyzed to give the radial distribution of Mach Number, at the various port

locations. To evaluate the Mach Numbers* from the measured static pressure and stagnation pressure data, the assumption was made in all cases that the specific heat ratio, K, was equal to 1.4. In the actual flow K varied between 1.40 and 1.35. Assuming K equal to 1.4 introduced a maximum error in the computed Mach Number of 2 percent, and in most cases less than 1 percent.

C.8 Properties of the Injected Water

As explained previously, water was introduced into the test section through the water injection system and the boundary layer water ring. The mass flow rate was the only measured property of the water. The total flow rate of

---

*In recognition of the non one-dimensional nature of the real flow, an average Mach Number was defined as that single value which would give the same mass flow rate as the radial distribution of Mach Numbers. Assuming a flow with axial symmetry and having a uniform stagnation temperature and static pressure across the plane of measurement, this definition led to the expression

$$M\left[1 + \frac{K-1}{2} M^2\right]^{\frac{1}{2}} A = 2\pi \int_{r_1}^{r_o} \left[1 + \frac{K-1}{2} M_r^2\right]^{\frac{1}{2}} M_r \, r\,dr \qquad (C.3)$$

M_r was evaluated from measured data, an assumed value of $K \cong 1.4$, and the equation

$$\frac{p_{or}}{p} = \left[1 + \frac{K-1}{2} M_r^2\right]^{K/K-1} \qquad (C.4)$$

The average value, M, was then computed from equation C.3 using graphical integration.

water was metered by a Shutte and Koerting Series No. 90 Universal Rotameter, and that portion of it going to the boundary layer water ring was separately measured by a calibrated sharp-edged orifice. The velocity of the injected water, V_ℓ, could be deduced knowing its mass flow rate and the exit area of the water injection tubes (.324 in.^{2}). The temperature of the injected water, T_ℓ, was unknown. Its temperature was raised from a nominal city water temperature of 40° F to 70° F while flowing in the water injection system up to the injection point. The inlet temperature of the injected water could be estimated by using Figure 32. This figure resulted from heat transfer calculations applied to the water injection system within the Aerothermopressor. The results shown on Figure 32 can be regarded as only approximate because of crudities in the heat transfer calculations.

C.9 Inlet Specific Humidity and Water-Air Ratio

The amount of water entering the Aerothermopressor in the vapor form was dependent on the humidity of the air entering the compressors and on the water vapor formed as a result of the combustion process. During operation the specific humidity of the entering air was obtained from the local U. S. Weather Bureau at least every four hours. The amount of water formed in the combustion process was computed from a material balance and the measured fuel flow rate. 1.42 pounds of water were formed for every pound of fuel burned.

The water-gas ratio, Ω_o, commonly referred to as the water-air ratio, was simply computed from the values of the mass flow rate of gas and the mass flow rate of injected water obtained, as outlined in Articles C.1 and C.8. In computing this ratio, the water introduced into the boundary layer was excluded. No effect of the boundary layer water on Aerothermopressor performance could be detected experimentally.

APPENDIX D

DETERMINATION OF APPARENT WALL FRICTION FACTOR AND SPECIFIC HUMIDITY

D.1 Analysis and Results

Let section 1 be the inlet plane of the Aerothermopressor. At this plane all the water is injected, and the state of the flowing liquid-gas system is considered known. At section 2 downstream,(sometimes referred to as the measurement plane) the static pressure and Mach Number are known. The problem is to determine the amount of water which has evaporated and the apparent friction factor between the two stations.

The analysis of this type of problem and the methods for solution have been well established[3][4]. Accordingly, in this section only an outline of the analysis will be given, and equations resulting from this analysis will be presented in a developed form. However, the numerical procedures underlying the results of Articles 5.1 and 5.3 will be illustrated in sufficient detail to be repeated.

In the analysis of this problem, the so-called "discontinuity" analysis, one simply relates the unknown properties at the measurement plane to the known conditions at the inlet plane by the simultaneous application of the continuity, momentum, and energy equations to a control volume which conforms to the boundaries of the fluid system included between these planes.

The following assumptions are made for this analysis:

(i) The flow is steady, one-dimensional, and adiabatic.

(ii) The duct cross-section is either circular or annular.

(iii) The gas, either air or an air-water vapor mixture, obeys the semi-perfect gas rules. The air-water vapor mixture follows the rules stemming from the Gibbs-Dalton Law.

(iv) The entering gas is dry air.

(v) The water is all injected axially, and the volume of liquid is negligible compared with that of the gas phase.

(vi) The water droplet temperature is 140° F.

(vii) The water droplet and gas velocities are identical at the measurement plane.

Under these conditions the energy equation becomes

$$\bar{C}_{pa}(T_{o1}-T_2) + \Omega_o\left(\frac{V_{\ell 1}}{V_1}\right)^2 \frac{R_a T_1}{2} k_1 M_1^2 = \tag{D.1}$$

$$(1+\omega\frac{W_a}{W_v})(\frac{1+\Omega_o}{1+\omega})\frac{R_a T_2}{2} k_2 M_2^2 + \omega[\bar{C}_{pv}(T_2-T_\ell) + h_{fg}]$$

where

$$\bar{C}_{pa} \equiv \frac{1}{T_{o1}-T_2}\int_{T_2}^{T_{o1}} C_{pa}\, dT \tag{D.2}$$

$$\bar{C}_{pv} \equiv \frac{1}{T_2-T_{\ell 2}}\int_{T_{\ell 2}}^{T_2} C_{pv}\, dT \tag{D.3}$$

The continuity equation is

$$\frac{p_2 A_2}{p_1 A_1} = \sqrt{\frac{k_1 M_1^2 T_2}{k_2 M_2^2 T_1} (1+\omega)(1+\omega \frac{W_a}{W_v})} \qquad (D.4)$$

and the momentum equation is

$$-\int_1^2 A dp - \int_1^2 f \frac{k p M^2}{2} \pi (D_o + D_i) dz = \left(1 + \frac{\Omega_o - \omega}{1+\omega}\right) k_2 M_2^2 p_2 A_2 - (1+\Omega_o \frac{V_{\ell_1}}{V_1}) k_1 M_1^2 p_1 A_1 \qquad (D.5)$$

As seen from equation D.5, the momentum equation introduces two integral expressions relating to the history of the process between sections 1 and 2. For convenience, we define two additional quantities which express these integrals in terms of the end conditions. First

$$\bar{f} \frac{\ell}{D} \equiv \frac{\frac{\pi}{2} \int_1^2 f k p M^2 (D_o + D_i) \, dz}{p_1 A_1 k_1 M_1^2 + p_2 A_2 k_2 M_2^2} \qquad (D.6)$$

Where D is taken as the arithmetic mean hydraulic diameter between sections 1 and 2. And second

$$\mathbb{P} \equiv \frac{\int_1^2 \frac{A dp}{p_1 A_1} + 1}{\frac{p_2 A_2}{p_1 A_1}} \qquad (D.7)$$

The above terms, $\bar{f} \ell/D$ and $\mathbb{P}$ were first defined by Gavril[4]. We select equation D.6 to define an "apparent mean friction factor." It is defined such that the numerical

values of $\bar{f}$ will approximate those of the conventionally measured pipe-wall friction factors. $\mathbb{P}$ is introduced to account for the axial component of the pressure force on a variable area evaporation section. $\mathbb{P} = 1$ for a constant area duct.

Combining equations D.1 to D.7 we get the following useful relations

$$\frac{T_2}{T_1} = \frac{\frac{k_2 M_2^2}{k_1 M_1^2}\left[1 + k_1 M_1^2\left(1 + \Omega_o \frac{V_{\ell 1}}{V_1} - \bar{f}\frac{\ell}{D}\right)\right]^2}{(1+\omega)(1+\omega\frac{W_a}{W_v})\left[\mathbb{P} + k_2 M_2^2\left(\frac{1+\Omega_o}{1+\omega} + \bar{f}\frac{\ell}{D}\right)\right]^2} \tag{D.8}$$

$$k_2 M_2^2 = \frac{-B \pm \sqrt{B^2 - 4AC}}{2C} \tag{D.9}$$

where

$$A \equiv a\mathbb{P}^2 \tag{D.10}$$

$$a \equiv \frac{k_1 M_1^2 (1+\omega)(1+\omega\, W_a/W_v)}{\left[1+k_1 M_1^2\left(1+\Omega_o \frac{V_{\ell 1}}{V_1} - \bar{f}\frac{\ell}{D}\right)\right]^2}\left[\bar{C}_{pa}\frac{T_{o1}}{T_1} - \omega\frac{h_{fg}-\bar{C}_{pv}T_\ell}{T_1} + \Omega_o\left(\frac{V_{\ell 1}}{V_1}\right)^2 \frac{k_1 M_1^2 R_a}{2}\right] \tag{D.11}$$

$$B \equiv 2a\mathbb{P}\left(\frac{1+\Omega_o}{1+\omega} + \bar{f}\frac{\ell}{D}\right) - (\bar{C}_{pa} + \omega\,\bar{C}_{pv}) \tag{D.12}$$

$$C \equiv a\left(\frac{1+\Omega_o}{1+\omega} + \bar{f}\frac{\ell}{D}\right)^2 - \frac{1+\Omega_o}{1+\omega}\left(1+\omega\frac{W_a}{W_v}\right)\frac{R_a}{2} \tag{D.13}$$

and

$$\frac{p_2 A_2}{p_1 A_1} = \frac{1 + k_1 M_1^2\left(1 + \Omega_o \frac{V_{\ell 1}}{V_1} - \bar{f}\frac{\ell}{D}\right)}{\mathbb{P} + k_2 M_2^2\left(\frac{1+\Omega_o}{1+\omega} + \bar{f}\frac{\ell}{D}\right)} \tag{D.14}$$

Choosing section 2 to correspond to the selected stations at which static pressure and Mach Number were measured, equations D.8 through D.14 were sufficient to determine the value of ω and $\bar{f}$ appropriate to these same stations. Using the data from Experiments Number 541221-1, 541223-1, and 550621-1, the following operations necessary to the solution were carried out. First, for Port Number 9 at the end of the evaporation section

(i) Values for $\bar{f}\,\ell/D$, $\mathbb{P}$, and ω were selected. $\bar{f}\,\ell/D$ was selected with the knowledge that $\bar{f}$ probably had a value close to that of a conventional pipe-wall friction factor. $\mathbb{P} = 1$ for a constant area duct. In any other case, (550621-1) $\mathbb{P}$ could be evaluated from the measured static pressure distribution. A value of ω was selected to correspond to the expected value in the region of Port 9. The theoretical calculations corresponding to the experiments aided materially in this selection.

(ii) A value of T_2 was guessed. Again, the theoretical calculations aided in this guess.

(iii) Equation D.9 was solved for $K_2 M_2^2$.

(iv) Equation D.8 was used to check the assumed value of T_2. Iteration could be used at this point if necessary, repeating steps (i) through (iv) until the guessed at and solved for value of T_2 converged. In practice, the original value chosen for T_2 was often sufficiently accurate to make iteration unnecessary.

(v) Equation D.9 was solved for M_2.

(vi) Equation D.14 was solved for p_2/p_1.

For the case of the constant area evaporation section, steps (i) through (vi) were repeated for different values of ω and $\bar{f}\,\ell/D$ resulting in a family of curves as illustrated in Figure 33 for Run No. 541223-1. The solution of the problem results when the chosen value of ω and $\bar{f}\,\ell/D$ gives the measured values p_2/p_1 and M_2. This condition is shown by the open circles on Figure 33 corresponding to properties of Port 9. The result is $\bar{f}\,\ell/D = 0.03$ and $x = \frac{\omega}{\Omega_0} = 0.565$. As $\ell/D = 7.03$ for this station, $\bar{f}$ becomes 0.00426. As Ω_0 for this run was 0.20, ω becomes 0.113. The inlet specific humidity, $\omega_1 = 0.019$, was added to this value giving $\omega = 0.132$. This is the value shown plotted in Figure 25. The above procedure amounts to a simultaneous solution of equations D.8, D.9, and D.14 using trial and error methods.

The foregoing steps could be repeated in their entirety for all measurement stations. Rather than do this, however, the assumption was made that $\bar{f} = 0.00426$ throughout the evaporation section. Then, with measured values of p_2/p_1 for each port location, the corresponding value of x could be taken directly from Figure 33 as shown. Similarly, the measured values of M_2 could be used to determine x. As the measurement of p_2/p_1 was considered more reliable than the measurement of M_2, the value of x determined by it was selected to plot on Figure 25. It is worth noting, however,

that the values of x determined by using measured values of either M_2 or p_2/p_1 do not differ a great deal.

The procedure described above was repeated for the case of constant area Run Number 541223-1 with the result $\bar{f} = 0.00426$ and the humidities shown in Figure 25. The reasons for adopting this procedure to determine the specific humidity are described in the following article.

For the case of the variable area evaporation section (Run No. 550621-1) $\mathbb{P}$ varied with ω. This fact made a trial and error solution more cumbersome, but, in principle, could be handled by the methods previously described. In practice, reasonable and consistent values of ω and $\bar{f}\,\ell/D$ could not be obtained for the variable area case throughout the evaporation section because of the uncertainties involved in the evaluation of $\mathbb{P}$ from the measured data.

D.2 Evaluation

The reliability of the evaluation of $\bar{f}$ and ω by the discontinuity analysis depends to a great extent on the precision of the measurements. The determination of $\bar{f}\,\ell/D$ is particularly sensitive as can be illustrated by observations made on Figure 33. At Port 9, the measured values of p_2/p_1 and M_2 were 1.028 and 0.680, respectively, and a solution resulting from the discontinuity analysis gave $x = 0.565$ and $\bar{f}\,\ell/D = 0.03$. If on the other hand the measured value of M_2 had been 0.700 , the solution would have been $\bar{f}\,\ell/D = 0$ and $x = 0.40$. Under the circumstances, the fact that all

three experiments gave computed values of $\bar{f}\,\ell/D$ for Port 9 equal to 0.03 must be viewed as accidental. Nevertheless, the fact that the three computations of $\bar{f}\,\ell/D$ did correspond and that subsequent calculations of ω based on this value gave reasonable results, lends weight to the conclusion that the computed value of the apparent friction factor is not greatly in error.

The use of an assumed value of $\bar{f}$ and measured values of either p_2/p_1 or M_2 to determine ω in effect eliminates a measured quantity in favor of an assumption. A close examination of Figure 33 will show that at many port locations an exact solution to the discontinuity problem using measured data would involve a considerable change in the values of $\bar{f}\,\ell/D$ and ω from the ones indicated. The solutions using measured values of both M_2 and p_2/p_1 gave results showing large random fluctuations in $\bar{f}\,\ell/D$ and ω with z. In other words, results based entirely on measured data could not be made to conform to the requirements of the discontinuity analysis, of a uniformly increasing ω with z, and a reasonably stable $\bar{f}$. Again we look to uncertainties in the measurements as the major cause of trouble, for it is seen from Figure 33 that very slight alterations in the measured quantities would produce conformity.

To illustrate this point further, if we assume values for $\bar{f}$ and K_2 and have measured values of p_2 and M_2, the momentum equation (eq. D.14) should suffice to determine ω.

However, sample calculations of ω made on this basis showed, for instance, that a one percent error in M_2 could lead to a 15 percent error in ω. Accordingly, in order to minimize the uncertainties due measurement errors, the procedure as described above was adopted to determine ω.

As noted previously the evaluation of x based on M_2 or p_2/p_1 did not differ greatly, which fact gives support to the method of evaluation and the results stemming from it. The value of ω obtained by the method described is fortunately, not sensitive to the assumed value for $\bar{f}$. This is particularly true at forward regions of the evaporation section where the influence of friction is small.

In any case where the data for a particular port gave results inconsistent with those of neighboring ports, it was discarded. Results for ports numbers 7 and 8 do not appear in Figure 33 for this reason. The difficulties associated with getting accurate measurements in the unsettled flow regime immediately downstream of the shock was accepted as the cause of the incompatible results.

The uncertainties inherent in the assumptions of the discontinuity analysis are believed minor relative to those due measurement. The assumption that $V_l/V = 1$ produces inaccuracies in the computed results particularly in the forward end of the evaporation section and in shock regions. If $V_l/V > 1$ then the true value of ω is greater than that computed on the assumption $V_l/V = 1$. Computations show that,

for the same values of p_2/p_1 and $\bar{f}\ell/D$, the percentage error in ω is somewhat less than the percentage error involved in the assumed value of V_ℓ/V. As the theoretical calculations corresponding to the experiments used in this study show that the value of V_ℓ/V at all ports (except No. 6 for 541223-1) were within 5 percent of unity, little error results from the assumption $V_\ell/V = 1$.

The assumption that the droplet temperature was 140° F appears to be a good one. In all cases, the complete theoretical analysis indicated values of T_ℓ at all ports within 30° of this value. Further the results of the discontinuity analysis are insensitive to the assumed value of T_ℓ.

In conclusion, the reliability with which $\bar{f}$ and ω were determined depended more upon the precision of the measurements than upon the uncertainties inherent to the assumptions of the discontinuity analysis. The uncertainty involved in any single computation of $\bar{f}$ and ω using measured values of p_2 and M_2 is large. Only by assuming a value for the apparent friction factor and discarding a measured quantity could consistent values of ω be obtained. Although the latter procedure had limitations, the results obtained from it were considered reasonable and useful to the purposes of the investigation.

APPENDIX E

ESTIMATION OF STAGNATION PRESSURE LOSSES

This appendix is presented in support of Article 6.2.

E.1 Entrance Nozzle Loss

The losses due to wall friction in the entrance nozzle and to the aerodynamic drag of the injector system are obtained by methods explained in Article 2.1. Entering Figure 6 with the measured inlet Mach Number of Run Number 550621-1, $M_1 = 0.73$, we get a percentage stagnation pressure loss of about 2.5 percent.

E.2 Wall Friction Loss

The loss of stagnation pressure in the evaporation section due to friction can be expressed by

$$\int_0^{\ell} \frac{dp_o}{p_o} = \ell n \frac{p_{o2}}{p_{o1}} = - \int_0^{\ell} 2K M^2 f \frac{dz}{D} \cong \frac{p_{o2}-p_{o1}}{p_{o1}} \qquad (E.1)$$

where D is taken to be the appropriate hydraulic diameter.

To make the comparison of Article 6.2, the Mach Number distribution, $M = f(z)$, is taken in each case to be that measured in Run Number 550621-1. The hydraulic diameter as a function of z, $D = f(z)$ is known for the experimental unit. The hydraulic diameter for the unit with external area variation is computed to give the area variation of the experimental device. In this, we assume the area variation and the Mach Number distribution in the unit having clean design are the same as those present in the experimental unit. This

condition cannot truly be realized; but, as the variations in the hydraulic diameter in the evaporation section of the unit having external area variation are small, the assumption of equal area variation to determine this hydraulic diameter has but a minor influence on the computation of frictional loss. f for the experiment is taken equal to the average value measured in dry tests with the tracks in place (.0046). f for the clean unit is chosen equal to the average value measured in dry tests without the tracks (.0037). k is taken equal to 1.37, an average value in the evaporation section determined by theoretical computations (Tape No. 120-75-226).

With the foregoing information, the integral of equation E.1 is evaluated graphically with the following results.

For the experimental unit:

$$\frac{p_{o_2}-p_{o_1}}{p_{o_1}} \cong -2k f \int_0^{\ell} M^2 \frac{dz}{D} = -2\,(1.37)(.0046)(10.16) = -12.8\%$$

For the extrapolation to a device of clean aerodynamic design:

$$\frac{p_{o_2}-p_{o_1}}{p_{o_1}} \quad -2k f \int_0^{\ell} M^2 \frac{dz}{D} = -2\,(1.37)(.0037)(7.83) = -8.0\%$$

E.3 Diffuser Loss

The difference between the fractional change in stagnation pressure in the diffuser of the experimental unit and that in the unit of clean design is estimated to be equal to that

difference which would be computed from the results of dry tests made on the experimental Aerothermopressor before and after the mounting of the plugs.

The diffuser with internal complications has a measured average "dry" diffuser efficiency of 82 percent. With an entrance Mach Number equal to 0.55 determined from Run Number 550621-1, Figure 7 gives a basic diffuser loss of 3.6 percent.

The efficiency of the diffuser belonging to the unit of clean design is taken equal to 90 percent, an average value measured in the experimental device before the mounting of the plugs. With this efficiency and the same entrance Mach Number, Figure 7 gives a loss of 2.0 percent.

E.4 Loss Associated with Water Impingement

The erosion of the nose sections of the plugs makes evident the fact that water impinges on them. What happens to the water which is deposited on the plug is not clear, but one can imagine it running along the surface, accumulating in certain regions, and being re-entrained in the main stream. That it cannot be continually drained from the plug without re-entrainment is certain, for an adequate drainage path does not exist. The amount of water which is deposited and the regions of re-entrainment are not known, but in the following estimate it is assumed that the water droplet trajectories are straight lines and all deposited water is re-entrained slightly downstream from the maximum diameter of the plug.

From the table of influence coefficients, Table IV, we obtain

$$\int \frac{dp_o}{p_o} = \int_{y=0}^{y=1} -\frac{KM^2}{2}\left[2 - \frac{K-1\ M^2\ y}{1 + \frac{K-1}{2} M^2}\right] \frac{w_\ell}{w} \frac{dV_\ell}{V} \cong \frac{\Delta p_o}{p_o} \qquad (E.2)$$

The amount of water deposited on the plug in a length, dz, is equal to

$$dw_\ell = \frac{w(\Omega_o + \omega_1 - \omega)}{2\ D_o^2} D_i \frac{dD_i}{dz} dz$$

where D_o in this case designates the duct diameter and D_i the plug diameter.

The total amount of water deposited over the forward half of the plug becomes

$$\frac{w_\ell}{w} = \int_{5\text{ in}}^{47\text{ in}} \frac{(\Omega_o + \omega_1 - \omega)}{D_o^2} D_i \frac{dD_i}{dz} dz \qquad (E.3)$$

The integral of equation E.3 is evaluated graphically after substituting $\omega = f(z)$ from the theoretical computations of Tape No. 120-75-226. This evaluation gives $w_\ell/w = .026$.

The stagnation pressure loss is then computed from equation E.2 by assuming $K = 1.37$, V = constant, and a constant Mach Number of unity. The gas properties are chosen to correspond closely to those present immediately downstream of the maximum plug diameter for Run Number 550621-1, and are held constant to facilitate the

calculations. In this estimate, a more complex computation is not believed to be warranted. The result is $\Delta p_o/p_o$ = - 3.1 percent.

The computed loss of 3.1 percent can probably be regarded as an upper limit to the true loss. The assumption that the water trajectories are straight lines very likely leads to a greater water deposit on the plug than actually takes place. Likewise, the assumption that all deposited water re-entrains in a zone of flow having a Mach Number as high as unity results in a predicted stagnation pressure loss that is probably too large.

BIOGRAPHICAL NOTE

Arthur Adams Fowle was born in Boston, Massachusetts, on January 2, 1924.

His primary and secondary schooling was received in Woburn, Massachusetts. He entered the Massachusetts Institute of Technology in 1941, but left after a year and a half of study for military service.

From 1943 to 1946 he served the United States Army Air Force as weather and operations officer in the continental United States and North Africa.

In 1946 he returned to M.I.T. to receive the degree of Bachelor of Science in 1948. One year of study in the Graduate School of Mechanical Engineering, together with work as Research Assistant in the Gas Turbine Laboratory followed. He obtained a degree of Master of Science in Mechanical Engineering in 1949.

From 1949 to 1952 he worked at the Ultrasonic Corporation of Cambridge, Massachusetts, in various engineering capacities.

In 1952 he became Assistant Professor of Mechanical Engineering at M.I.T. Since this time he has served as consultant to Arthur D. Little, Inc. and the Crosby Steam Gage and Valve Co.

He is a co-author of:

"The Aerothermopressor - A Device for Improving the Performance of a Gas Turbine Power Plant," with A. H. Shapiro, H. R. Wadleigh, and B. D. Gavril, Report submitted under O.N.R. Contract N5ori-07878, M.I.T., D.I.C. 5-6985, March 1955. Also to be published Trans. A.S.M.E.

"Design, Application, Performance, and Limitations of Sonic Type Flocculators and Collectors," with E. P. Neumann and C. R. Soderberg, Jr. Proceedings of the U. S. Technical Conference on Air Pollution, McGraw-Hill Book Co., Inc., New York, 1952.

LIST OF REFERENCES

1. Shapiro, A. H., "The Dynamics and Thermodynamics of Compressible Fluid Flow." Ronald Press, New York, 1953

2. Shapiro, A. H., Wadleigh, K. R., Gavril, B. D., and Fowle, A. A., "The Aerothermopressor - A Device for Improving the Performance of a Gas Turbine Power Plant." Report, Submitted under O.N.R. Contract N5ori-07878, M.I.T., D.I.C. 5-6985, March 1955. Also to be published Trans. A.S.M.E.

3. Wadleigh, K. R., "An Experimental Investigation of a Small-Scale Aerothermopressor - A Device for Increasing the Stagnation Pressure of a High-Temperature, High-Velocity Gas Stream by Evaporative Cooling." Sc.D. Thesis, Department of Mechanical Engineering, M.I.T., Cambridge, Mass., 1953.

4. Gavril, B. D., "A Theoretical Investigation of the Thermodynamic and Dynamic Effects of Water Injection into High-Velocity, High-Temperature Gas Streams." Sc.D. Thesis, Department of Mechanical Engineering, M.I.T., Cambridge, Mass., 1954.

5. Shapiro, A. H., and Hawthorne, W. R., "The Mechanics and Thermodynamics of Steady, One-Dimensional Gas Flow." Journal of Applied Mechanics, Trans. A.S.M.E., Vol. 14, No. 4, 1947.

6. Gisvold, P. A., and Matheson, J. C., "Small-Scale Constant-Area Test of an Aerothermopressor." Naval Eng. Thesis, Dept. of Naval Architecture and Marine Eng., M.I.T., Cambridge, Mass., 1952.

7. Hawkins, R. A., and Mowell, L. V., "The Design, Construction, and Preliminary Test of the Aerothermopressor." Naval Eng. Thesis, Dept. of Naval Architecture and Marine Eng., M.I.T., Cambridge, Mass., 1949.

8. Templeton, O. A., and Wish, J. R., "Theory and Operation of the 'Aerothermoprex.'" Naval Eng. Thesis, Dept. of Naval Architecture and Marine Eng., M.I.T., Cambridge, Mass., 1949.

9. Nukyama, S., and Tanasawa, Y., "An Experiment on the Atomization of Liquid by Means of an Air Stream." Trans. S.M.E. Japan, Vol. 4, Reports 1-6, 1938.

10. Ranz, W. E., and Marshall, W. R., Jr., "Evaporation from Drops." Chemical Engineering Progress, Vol. 48, Nos. 3 and 4, 1952.

11. Carpenter, J. W., and Martin, W. L., "Construction and Preliminary Test of a Traversing Stagnation Pressure Probe for a Large Scale Aerothermopressor." Naval Eng. Thesis, Dept. of Naval Architecture and Marine Eng., M.I.T., Cambridge, Mass., 1954.

12. Keenan, J. H., and Kaye, J., "Gas Tables." John Wiley & Sons, Inc., New York, 1948.

13. Keenan, J. H., and Keyes, F. G., "Thermodynamic Properties of Steam." John Wiley and Sons, Inc., New York, 1936.

14. McAdams, W. H., "Heat Transmission," McGraw-Hill Book Co., Inc., New York, 1942.

TABLE I

DRY DUCT-WALL FRICTION FACTOR FOR CONSTANT AREA EVAPORATION SECTION

RUN NO.	INLET MACH NO.	INLET DIAMETER REYNOLDS NO.	WITH OR WITHOUT TRACKS	FRICTION FACTOR
541109-1	0.547	2.94×10^6	WITHOUT	0.00380
541110-1	0.738	2.25×10^6	WITHOUT	0.00372
541110-2	0.750	2.06×10^6	WITHOUT	0.00360
541115-2	0.699	2.13×10^6	WITHOUT	0.00368
550406-1	0.285	1.73×10^6	WITH	0.00429
550406-2	0.540	2.82×10^6	WITH	0.00456
550406-3	0.745	2.00×10^6	WITH	0.00485
550425-7	0.310	1.83×10^6	WITH	0.00500
550425-8	0.420	2.37×10^6	WITH	0.00462
550425-9	0.555	2.88×10^6	WITH	0.00445
550426-1	0.310	1.86×10^6	WITH	0.00466
550426-2	0.423	2.34×10^6	WITH	0.00460
550426-3	0.545	2.87×10^6	WITH	0.00456

AVERAGE FRICTION FACTOR WITHOUT TRACKS = 0.0037
AVERAGE FRICTION FACTOR WITH TRACKS = 0.0046

TABLE II

DIFFUSER EFFICIENCIES

RUN NO.	BEFORE OR AFTER MODIFICATION	PLUG NO.	PLUG POSITION Z(IN)	MACH NO. AT DIFFUSER INLET	DIFFUSER EFFICIENCY
551109-1	BEFORE	NONE	–	0.575	90
551110-1	BEFORE	NONE	–	0.900	88
551115-2	BEFORE	NONE	–	0.784	93
550426-1	AFTER	1	85.0	0.311	85
550426-2	AFTER	1	85.0	0.431	82
550426-3	AFTER	1	85.0	0.590	82
550426-6	AFTER	1	43.5	0.354	87
550426-5	AFTER	1	43.5	0.502	86
550426-4	AFTER	1	43.5	0.728	82
550426-7	AFTER	1	5.0	0.331	85
550426-8	AFTER	1	5.0	0.452	82
550426-9	AFTER	1	5.0	0.631	81
550425-7	AFTER	2	85.0	0.323	82
550425-8	AFTER	2	85.0	0.433	82
550425-9	AFTER	2	85.0	0.597	80
550425-6	AFTER	2	43.5	0.389	83
550425-5	AFTER	2	43.5	0.546	83
550425-4	AFTER	2	43.5	0.770	85
550425-1	AFTER	2	5.0	0.330	87
550425-2	AFTER	2	5.0	0.449	82
550425-3	AFTER	2	5.0	0.609	80

NOTE: PLUG POSITION DENOTES LOCATION OF NOSE OF PLUG DOWNSTREAM FROM INLET TO EVAPORATION SECTION.

TABLE III

EXPERIMENTS WITH A CONSTANT AREA EVAPORATION SECTION

RUN NO.	T_{01} °R	P_{00} IN. HG.	P_{01} IN. HG.	M_1	Ω_0	ω_1	$\frac{P_{03}-P_{00}}{P_{00}}$	$\frac{P_{03}-P_{01}}{P_{01}}$	SHOCK AT Z (IN.)
541123- 3	1239	41.22	40.69	.45	.10	.015	−.017	−.004	−
541123- 2	1232	41.00	40.45	.46	.17	.015	−.013	+.000	−
541123- 4	1242	41.04	40.51	.45	.37	.015	−.013	+.000	−
541123- 6	1417	41.13	40.58	.46	.11	.019	−.016	−.002	−
541123- 5	1422	40.93	40.38	.46	.22	.019	−.007	+.006	−
541123- 7	1419	41.01	40.46	.46	.43	.019	−.009	+.004	−
541123-10	1660	40.88	40.35	.45	.21	.024	−.006	+.007	−
541123- 9	1670	41.07	40.44	.45	.35	.024	−.002	+.013	−
541123- 8	1630	41.08	40.45	.45	.46	.024	−.003	+.013	−
541216- 9	1270	41.97	41.09	.64	.08	.024	−.027	−.006	−
541216- 8	1268	42.16	41.30	.63	.16	.015	−.008	+.012	−
541216- 7	1247	41.88	41.05	.62	.30	.014	−.018	+.002	−
541216- 3	1470	41.72	40.84	.65	.15	.019	−.003	+.019	−
541216- 2	1495	41.73	40.81	.67	.24	.020	−.002	+.024	−
541216- 4	1495	41.72	40.76	.69	.32	.020	−.008	+.030	−
541216- 6	1655	41.77	40.85	.67	.15	.023	−.011	+.011	−
541216- 5	1655	41.77	40.85	.67	.27	.023	+.006	+.028	−
541218-16	1652	41.37	40.57	.61	.41	.028	−.006	+.014	−
541218- 2	1287	38.80	37.86	.74	.08	.020	−.034	−.010	10
541218- 3	1288	38.88	37.93	.73	.19	.020	−.004	+.020	10
541218- 4	1289	39.33	38.36	.74	.32	.020	−.018	+.006	10
541218- 8	1459	41.17	40.14	.74	.08	.024	−.041	−.017	10
541218- 9	1464	41.22	40.13	.78	.18	.025	+.007	+.033	10
541218-10	1480	41.72	40.63	.78	.30	.024	−.005	+.022	10
541218-14	1662	43.44	42.38	.74	.19	.028	−.002	+.023	10
541218-13	1660	43.51	42.39	.77	.30	.028	+.010	+.036	10
541218- 1	1295	38.85	37.85	.77	.08	.020	−.059	−.036	53
541216-12	1273	39.60	38.53	.79	.20	.015	−.039	−.012	53
541216-11	1271	39.80	38.78	.76	.29	.015	−.049	−.024	53
541218- 7	1455	41.25	40.20	.76	.08	.024	−.071	−.049	53
541218- 6	1460	41.23	40.16	.77	.19	.024	−.033	−.007	53
541218- 5	1463	41.47	40.42	.76	.30	.024	−.030	−.005	53
541218-12	1658	43.57	42.44	.77	.19	.028	−.034	−.008	53
541218-11	1654	43.59	42.46	.77	.30	.028	−.020	−.006	53
541221- 1	1420	40.37	39.72	.47	.22	.019	−.005	+.011	−
541230- 3	1413	40.73	40.09	.46	.45	.022	−.010	+.006	−
23- 1 541230- 1	1463	41.09	40.10	.74	.20	.018	−.029	−.005	55
541230- 2	1466	41.22	40.24	.73	.32	.021	−.036	−.013	62

TABLE IV - INFLUENCE COEFFICIENTS

	$\frac{dA}{A}$	$\frac{dQ-\frac{w_\ell}{w}dh_\ell}{c_pT_o}$	$\frac{dw}{w}$	$4f\frac{dz}{D}$	$\frac{w_\ell}{w}\frac{dV_\ell}{V}$	$\frac{dW}{W}$	$\frac{dk}{k}$
$\frac{dM^2}{M^2}$	$-\frac{2\left(1+\frac{k-1}{2}M^2\right)}{1-M^2}$	$\frac{(1+kM^2)\left(1+\frac{k-1}{2}M^2\right)}{1-M^2}$	$-\frac{(1+kM^2)\left(1+\frac{k-1}{2}M^2\right)}{1-M^2}\left[\frac{h_v-h_\ell+\frac{V^2}{2}(1-y^2)}{c_pT_o}\right]+\frac{2\left(1+\frac{k-1}{2}M^2\right)}{1-M^2}\left[1+(1-y)kM^2\right]$	$\frac{kM^2\left(1+\frac{k-1}{2}M^2\right)}{1-M^2}$	$\left(\frac{kM^2}{1-M^2}\right)\times\left[2\left(1+\frac{k-1}{2}M^2\right)-\frac{k-1}{k}\left(1+kM^2\right)y\right]$	$-\frac{1+kM^2}{1-M^2}$	-1
$\frac{dV}{V}$	$-\frac{1}{1-M^2}$	$\frac{1+\frac{k-1}{2}M^2}{1-M^2}$	$-\frac{1+\frac{k-1}{2}M^2}{1-M^2}\left[\frac{h_v-h_\ell+\frac{V^2}{2}(1-y^2)}{c_pT_o}\right]+\frac{1+(1-y)kM^2}{1-M^2}$	$\frac{kM^2}{2(1-M^2)}$	$\frac{kM^2-(k-1)M^2y}{1-M^2}$	$-\frac{1}{1-M^2}$	0
$\frac{dp}{p}$	$\frac{kM^2}{1-M^2}$	$-\frac{kM^2\left(1+\frac{k-1}{2}M^2\right)}{1-M^2}$	$\frac{kM^2\left(1+\frac{k-1}{2}M^2\right)}{1-M^2}\left[\frac{h_v-h_\ell+\frac{V^2}{2}(1-y^2)}{c_pT_o}-2+\frac{1+(k-1)M^2}{1+\frac{k-1}{2}M^2}y\right]$	$-\frac{kM^2\left[1+(k-1)M^2\right]}{2(1-M^2)}$	$-\frac{kM^2}{1-M^2}\left[1+(k-1)M^2(1-y)\right]$	$\frac{kM^2}{1-M^2}$	0
$\frac{dT}{T}$	$\frac{(k-1)M^2}{1-M^2}$	$\frac{(1-kM^2)\left(1+\frac{k-1}{2}M^2\right)}{1-M^2}$	$-\frac{(1-kM^2)\left(1+\frac{k-1}{2}M^2\right)\left[\frac{h_v-h_\ell+\frac{V^2}{2}(1-y^2)}{c_pT_o}\right]+(k-1)M^2\left[1+kM^2(1-y)\right]}{1-M^2}$	$-\frac{k(k-1)M^4}{2(1-M^2)}$	$-\frac{(k-1)M^2}{1-M^2}\left[y+kM^2(1-y)\right]$	$\frac{(k-1)M^2}{1-M^2}$	0
$\frac{dT_o}{T_o}$	0	1	$-\frac{h_v-h_\ell+\frac{V^2}{2}(1-y^2)}{c_pT_o}$	0	$-\frac{(k-1)M^2y}{1+\frac{k-1}{2}M^2}$	$\frac{\frac{k-1}{2}M^2}{1+\frac{k-1}{2}M^2}$	$\frac{M^2/2}{1+\frac{k-1}{2}M^2}$
$\frac{d\theta_o}{\theta_o}$	0	$\frac{1+\frac{k-1}{2}M^2}{\alpha}$	$-\frac{1+\frac{k-1}{2}M^2}{\alpha}\left[\frac{h_v-h_\ell+\frac{V^2}{2}(1-y^2)}{c_pT_o}\right]-\frac{\frac{k-1}{2}M^2\left(1+\frac{w_\ell}{w}\right)y^2}{\alpha}$	0	0	$\frac{\frac{k-1}{2}M^2\left(1+\frac{w_\ell}{w}y^2\right)}{\alpha}$	$\frac{\frac{M^2}{2}\left(1+\frac{w_\ell}{w}y^2\right)}{\alpha}$
$\frac{dp_o}{p_o}$	0	$-\frac{k}{2}M^2$	$\frac{k}{2}M^2\left[\frac{h_v-h_\ell+\frac{V^2}{2}(1-y^2)}{c_pT_o}-2(1-y)\right]$	$-\frac{k}{2}M^2$	$-\frac{kM^2}{2}\left[2-\frac{(k-1)M^2y}{1+\frac{k-1}{2}M^2}\right]$	$\frac{\frac{k}{2}M^2}{1+\frac{k-1}{2}M^2}$	$\left(\frac{k}{k-1}\frac{M^2}{2}\right)\Big/\left(1+\frac{k-1}{2}M^2\right)-\frac{k}{(k-1)^2}\ln\left(1+\frac{k-1}{2}M^2\right)$
$\frac{dP_o}{P_o}$	0	$-\frac{k}{2}M^2$	$\frac{+\frac{k}{2}M^2\left(1+\frac{k-1}{2}M^2\right)\left(1+\frac{w_\ell}{w}y^2\right)}{\alpha}\left[\frac{h_v-h_\ell+\frac{V^2}{2}(1-y^2)}{c_pT_o}\right]-\frac{kM^2}{2\alpha}\left(1+\frac{w_\ell}{w}\right)y^2-kM^2(1-y)$	$-\frac{k}{2}M^2$	$-kM^2(1-y)$	$\frac{\frac{kM^2}{2}\left(1+\frac{w_\ell}{w}y^2\right)}{\alpha}$	$\frac{k}{(k-1)^2}\left[\frac{\alpha-1}{\alpha}-\ln\alpha\right]$

Definitions:

$y \equiv V_\ell/V$

$\alpha \equiv \theta_o/T \equiv 1+\left(1+\frac{w_\ell}{w}y^2\right)\frac{k-1}{2}M^2$

$T_o/T \equiv 1+\frac{k-1}{2}M^2$

$\beta \equiv \frac{h_v-h_\ell}{c_pT_o}+\frac{\frac{k-1}{2}M^2}{1+\frac{k-1}{2}M^2}(1-y^2)$

$p_o/p \equiv (T_o/T)^{\frac{k}{k-1}}$

$P_o/p \equiv (\theta_o/T)^{\frac{k}{k-1}}$

Note: The table summarizes the algebraic relations between the variables of the left-hand column and the variables of the top row, and is to be interpreted in the manner,

$$\frac{dM^2}{M^2} = -\frac{2\left(1+\frac{k-1}{2}M^2\right)}{1-M^2}\frac{dA}{A}+\frac{(1+kM^2)\left(1+\frac{k-1}{2}M^2\right)}{1-M^2}\frac{dQ-\frac{w_\ell}{w}dh_\ell}{c_pT_o}+\ldots \text{ etc.}$$

TABLE V - BEHAVIOR OF STREAM PROPERTIES UNDER INFLUENCE OF AREA CHANGE, EVAPORATION, WALL FRICTION, AND DROPLET DRAG

		Area increase produces[a]	Evaporation produces[b]	Wall friction produces[c]	Liquid acceleration produces[d]
Mach Number, M	subsonic	decrease	decrease[h]	increase	increase[e]
	supersonic	increase	increase[h]	decrease	decrease[e]
Gas Velocity, V	subsonic	decrease	decrease[h]	increase	increase[e]
	supersonic	increase	increase[h]	decrease	decrease[e]
Pressure, p	subsonic	increase	increase[h]	decrease	decrease[e]
	supersonic	decrease	decrease[h]	increase	increase[e]
Temperature, T	subsonic	increase	decrease[h]	decrease	decrease[e]
	supersonic	decrease	increase[h]	increase	increase[e]
Gas Stagnation Temperature, T_o	subsonic	nil	decrease	nil	decrease[f]
	supersonic	nil	decrease	nil	decrease[f]
Mixture Stagnation Temperature, θ_o	subsonic	nil	decrease	nil	nil[g]
	supersonic	nil	decrease	nil	nil[g]
Gas Stagnation Pressure, p_o	subsonic	nil	increase[h]	decrease	decrease[e]
	supersonic	nil	increase[h]	decrease	decrease[e]
Mixture Stagnation Pressure, P_o	subsonic	nil	increase[h]	decrease	decrease[g]
	supersonic	nil	increase[h]	decrease	decrease[g]

Notes:
(a) Opposite effects for area decrease.
(b) Opposite effects for condensation.
(c) Opposite effects are impossible.
(d) When $y < 1$, $dV_\ell > 0$; when $y > 1$, $dV_\ell < 0$
(e) Dependent upon magnitude of y for liquid deceleration.
(f) Opposite effect for liquid deceleration.
(g) Same effect for liquid deceleration.
(h) Based on β only, and generally correct for β in excess of two; otherwise effects are indeterminate.

TABLE VI

EXPERIMENTS WITH VARIABLE AREA EVAPORATION SECTION

RUN NO.	PLUG AT Z (IN.)	PLUG NO.	T_{01} °R	P_{00} IN. HG.	P_{01} IN. HG.	M_1	Ω_0	ω_1	$\frac{P_{03}-P_{00}}{P_{00}}$	$\frac{P_{03}-P_{01}}{P_{01}}$	SHOCK AT Z (IN.)
550414-1	1	5.0	1448	41.69	40.63	.75	.27	.026	+.025	+.051	–
550414-2	1	10.0	1455	41.70	40.64	.76	.27	.025	+.015	+.042	–
550415-3	1	20.0	1438	41.36	40.47	.66	.24	.027	–.022	–.000	–
550414-3	1	20.0	1448	38.91	37.96	.74	.29	.025	–.010	+.015	–
550415-4	1	43.5	1436	41.25	40.36	.66	.24	.027	–.021	+.001	–
550414-4	1	43.5	1451	38.87	37.92	.74	.29	.025	–.047	–.023	–
550415-1	1	85.4	1427	40.50	39.46	.76	.20	.026	–.035	–.010	51
550513-1	2	5.0	1446	39.04	38.63	.39	.30	.022	–.018	–.008	–
550513-2	2	5.0	1456	38.53	37.64	.70	.22	.021	–.025	–.000	–
550512-1	2	5.0	1458	42.02	40.98	.74	.27	.021	+.025	+.051	51
550513-3	2	10.0	1463	39.00	38.11	.69	.22	.021	–.029	–.007	–
550512-2	2	10.0	1473	42.20	41.15	.75	.27	.021	+.018	+.044	51
550513-4	2	20.0	1458	38.33	37.41	.72	.22	.015	–.043	–.019	–
550512-3	2	20.0	1477	42.16	41.11	.75	.27	.021	–.003	+.022	61
550513-5	2	43.5	1467	38.61	37.70	.70	.22	.021	–.034	–.011	–
550422-4	2	43.5	1505	38.83	37.82	.77	.30	.025	–.076	–.051	10
550513-6	2	85.6	1451	42.17	41.37	.60	.24	.020	–.009	+.010	–
550512-5	2	85.4	1485	42.22	41.17	.75	.27	.021	–.046	–.022	51
550405-4	3	.90	1455	41.05	40.54	.44	.24	.020	–.002	+.010	–
550405-1	3	.90	1628	38.09	37.29	.65	.27	.024	–.019	+.003	51
550405-3	3	41.0	1455	41.83	41.31	.43	.24	.020	+.001	+.014	–
550404-5	3	43.5	1480	45.03	44.07	.66	.28	.020	–.204	–.187	88
550404-4	3	50.0	1460	43.93	42.92	.70	.27	.020	–.283	–.266	99
550404-3	3	55.1	1460	42.90	41.83	.74	.26	.019	–.266	–.248	36 & 99
550404-2	3	59.7	1460	42.82	41.77	.73	.26	.019	–.264	–.246	65 & 99
550405-2	3	82.0	1450	41.25	40.73	.44	.24	.021	–.007	+.006	–
550405-5	3	82.0	1460	41.27	40.25	.74	.20	.021	–.025	–.003	51
550621-1	2	5.0	1515	40.92	40.00	.73	.26	.029	.022	.047	52

NOTE: PLUG POSITION DESIGNATED BY DISTANCE OF NOSE FROM PLANE ON INJECTION

TABLE VII

AXIAL LOCATION OF MEASURING STATIONS

PORT NO.	PORT LOCATION Z(IN)	STATIC PRESSURE TAP NO.	TAP LOCATION Z(IN)	STATIC PRESSURE TAP NO.	TAP LOCATION Z(IN)	STATIC PRESSURE TAP NO.	TAP LOCATION Z(IN)
0	-41.00	1	-42.81	21	46.75	43	190.00
1	9.37	2	-18.56	22	51.63	44	207.83
2	17.87	3	-12.56	23	54.25	45	220.25
3	26.37	4	-9.56	24	58.13	46	221.38
4	34.87	5	-6.15	25	62.25	47	243.63
5	43.37	6	-5.25	26	66.13	48	261.75
6	51.94	7	-3.54	27	70.81	49	279.88
7	60.44	8	0.25	28	74.13	50	297.88
8	68.94	9	4.00	29	78.13		
9	77.44	10	2.25	30	82.13		
10	89.62	10a	5.13	31	88.25		
11	156.62	10b	8.19	32	96.38		
12	223.64	11	9.50	33	100.00		
13	290.62	12	12.13	34	106.25		
THERMO-COUPLE 5-SHIELDED	LOCATION Z(IN)	13	16.13	35	112.31		
	-26.19	14	20.13	36	118.13		
		15	24.13	37	126.38		
		16	28.07	38	124.25		
		17	32.13	39	142.13		
		18	36.13	40	153.25		
		19	40.13	41	166.25		
		20	44.13	42	178.00		

NOTES

1. Z IS POSITIVE MEASURED DOWNSTREAM FROM THE INLET TO THE EVAPORATION SECTION.
2. ALL LOCATIONS ACCURATE TO ± 0.07 IN.

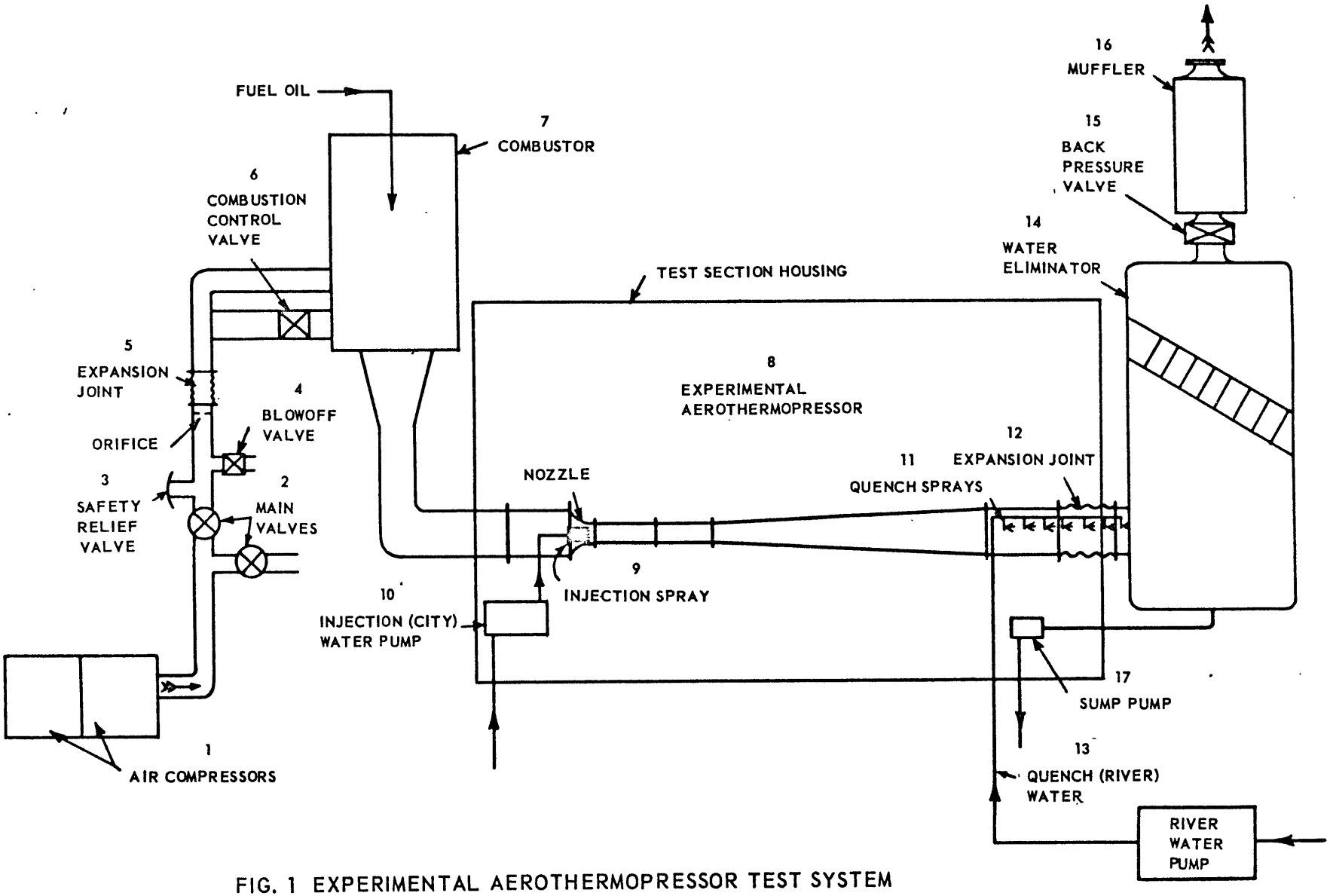

FIG. 1 EXPERIMENTAL AEROTHERMOPRESSOR TEST SYSTEM

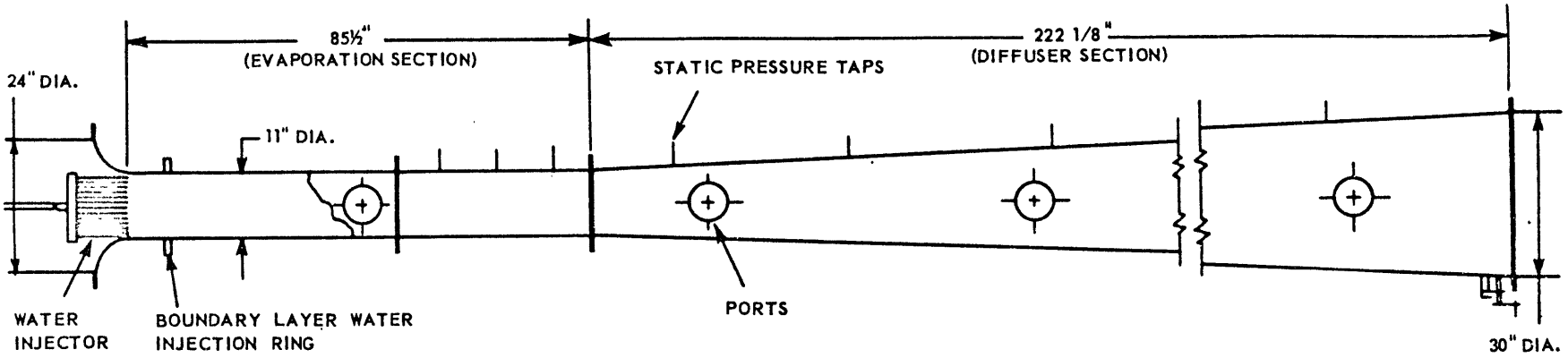

25 POUND PER SECOND AEROTHERMOPRESSOR
WITH 11 INCH CONSTANT DIAMETER
EVAPORATION SECTION

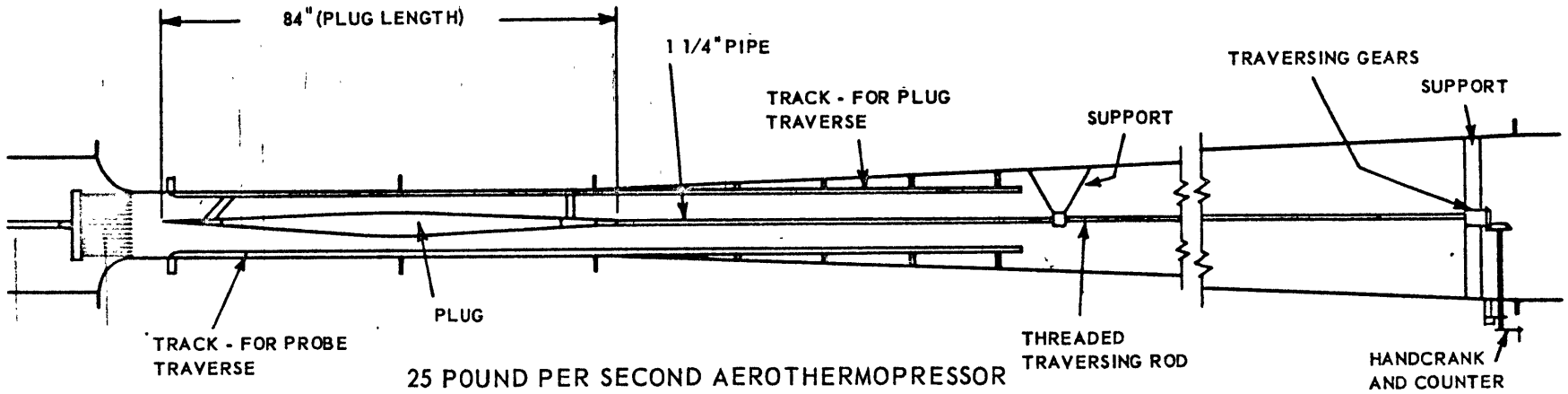

25 POUND PER SECOND AEROTHERMOPRESSOR
AS MODIFIED FOR AREA VARIATION BY USE OF
INTERNAL PLUGS

FIG. 2 AEROTHERMOPRESSOR TEST SECTIONS

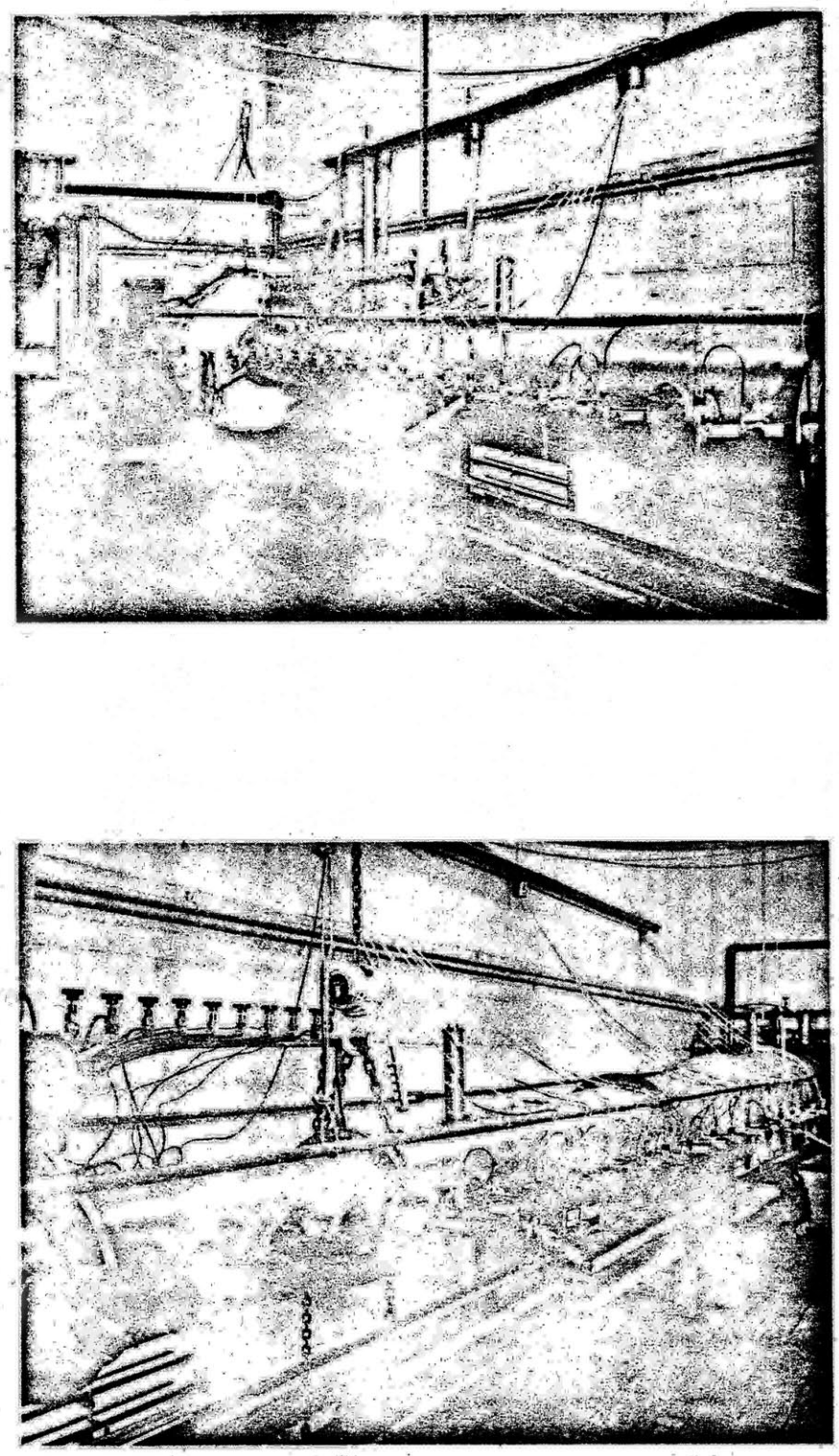

FIG. 3 AEROTHERMOPRESSOR TEST SECTION.

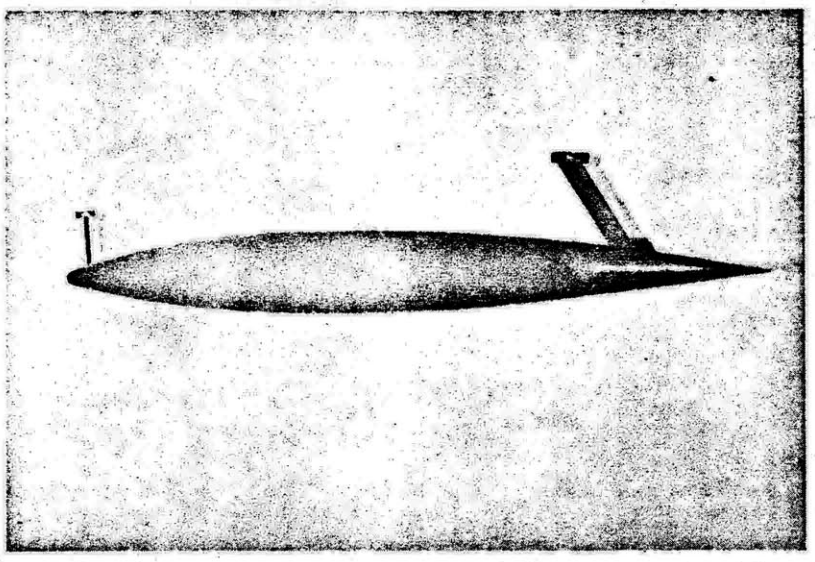

PLUG DESIGN

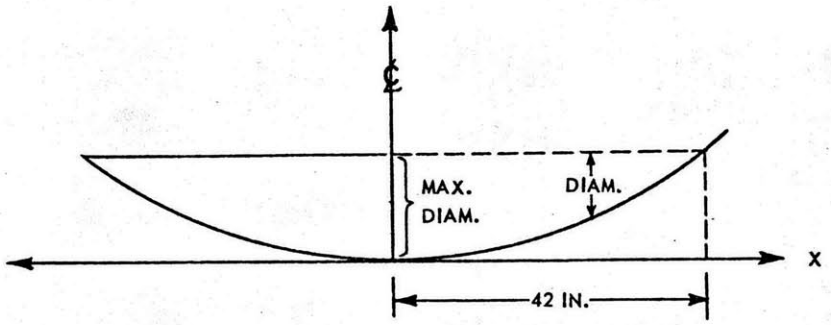

DESIGN FORMULA FOR ALL PLUGS: DIAMETER AT X = MAXIMUM DIAMETER $- aX^2$

PLUG NO.	MAXIMUM DIAMETER(IN)	LENGTH (IN)	a (1/IN)	MAXIMUM PERCENT AREA REDUCTION
1	3.82	84	0.00217	12
2	4.40	84	0.00249	16
3	4.93	84	0.00280	20
4	5.40	84	0.00306	24

FIG. 4 INTERNAL PLUG DESIGN

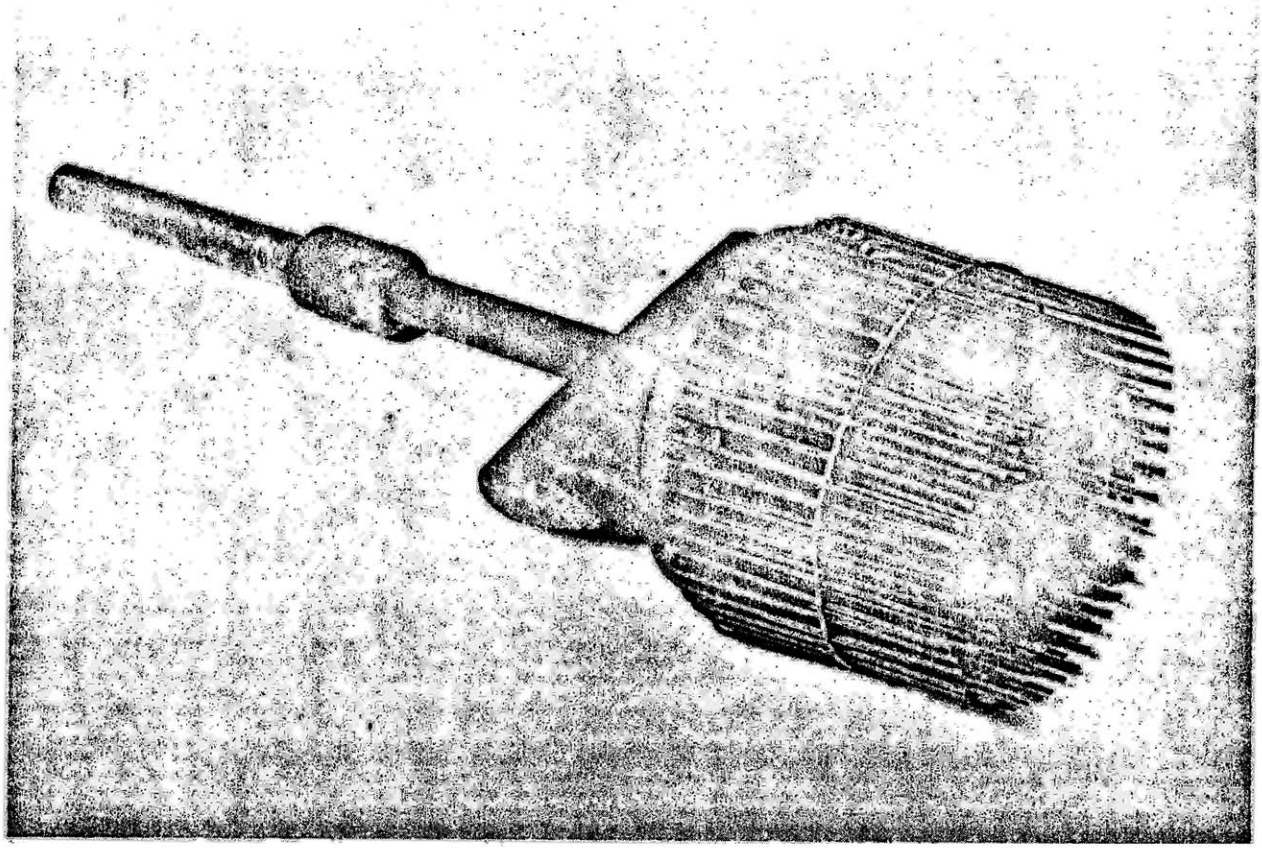

FIG. 5 WATER INJECTION SYSTEM

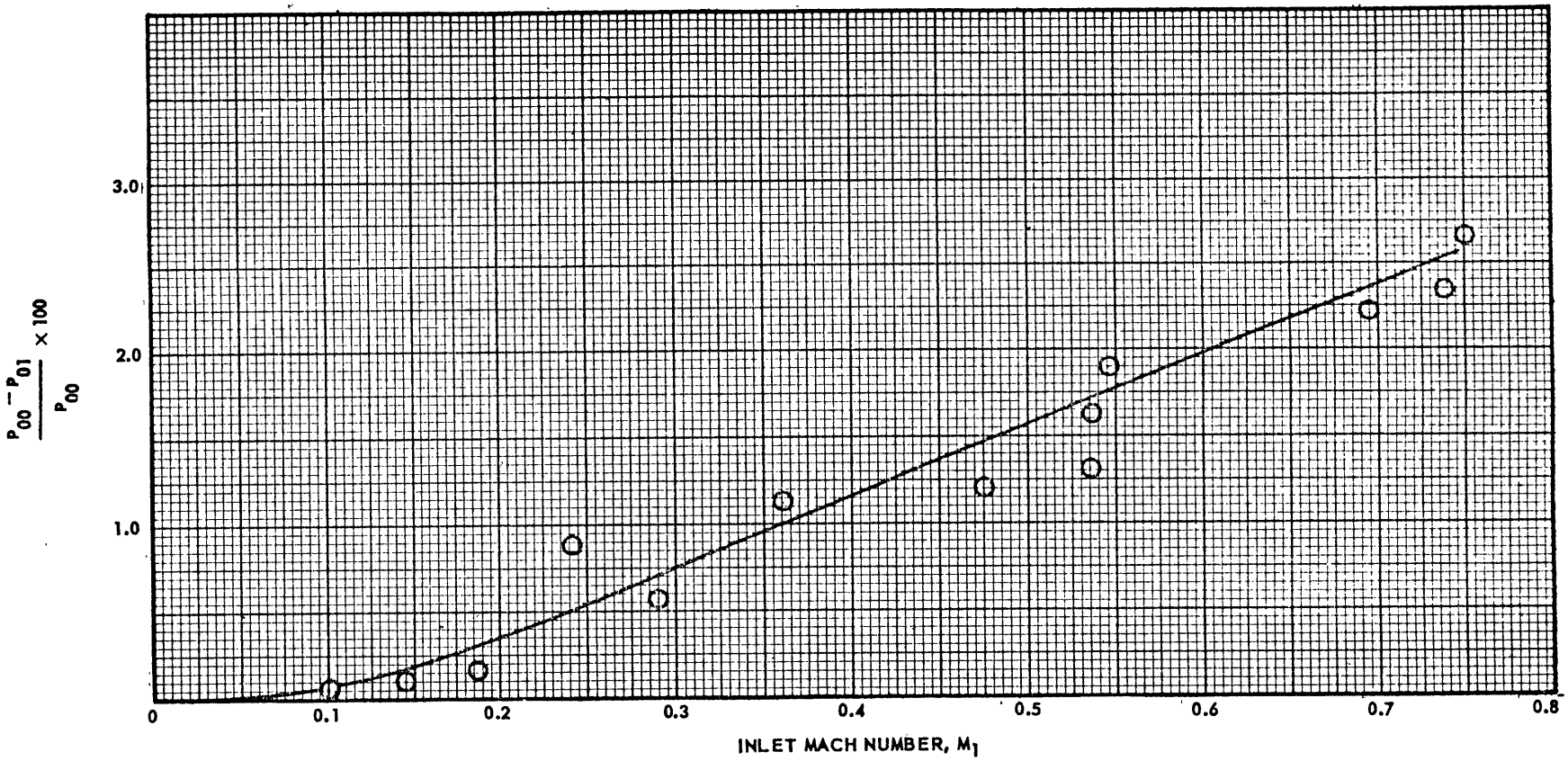

FIG. 6 STAGNATION PRESSURE LOSS IN ENTRANCE NOZZLE

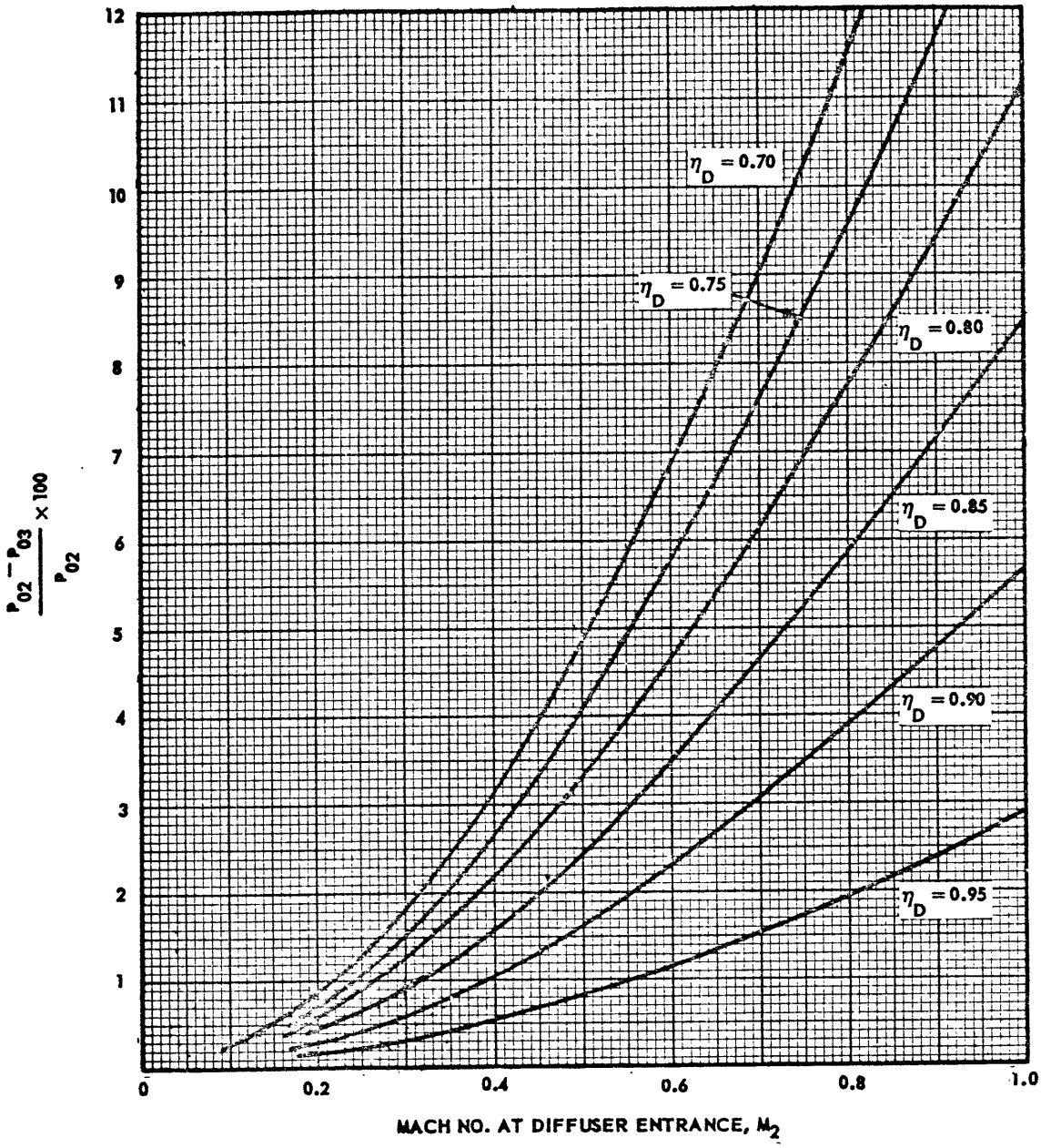

FIG. 7 STAGNATION PRESSURE LOSS VS. DIFFUSER EFFICIENCY

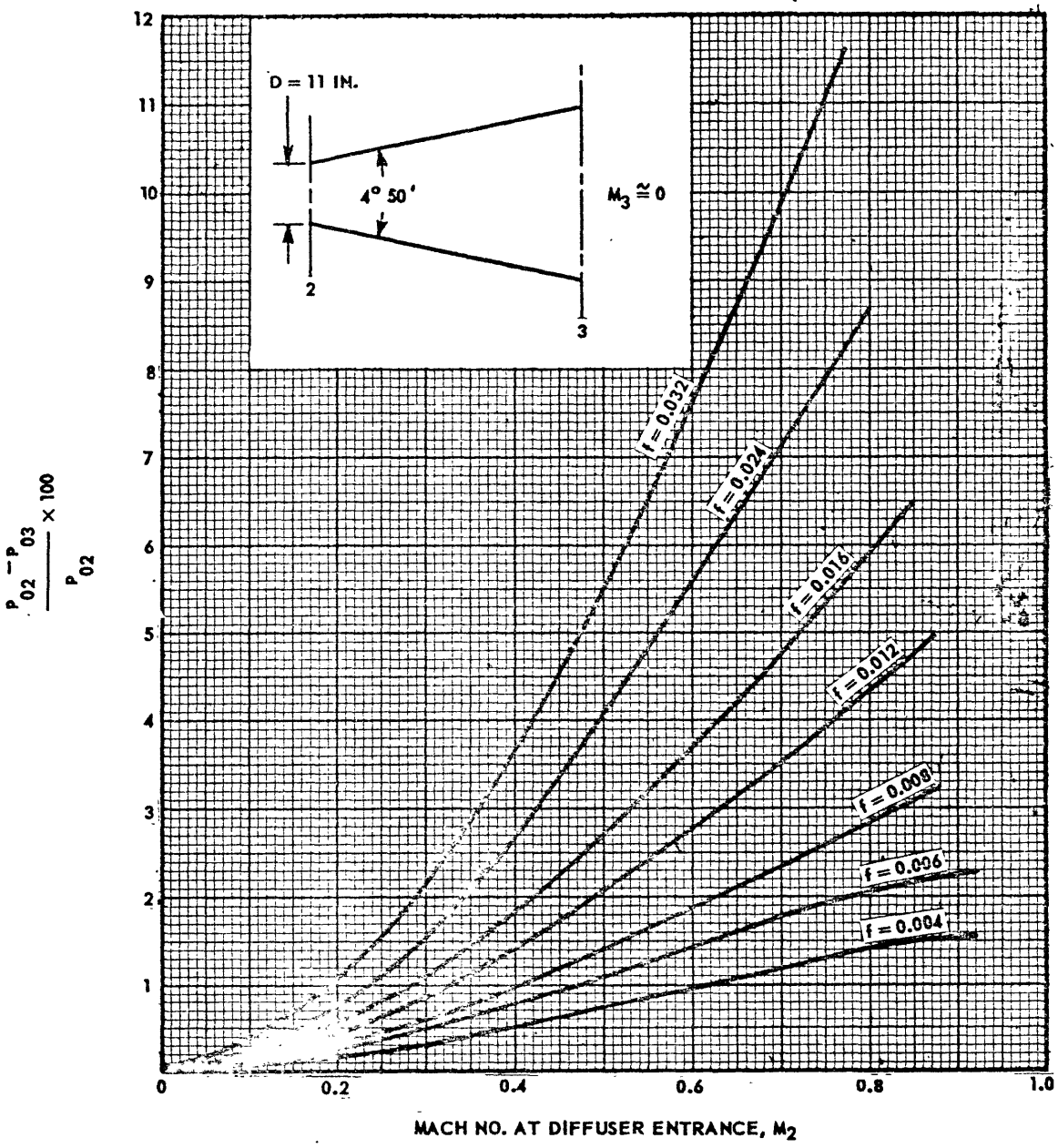

FIG. 8 LOSSES IN CONICAL DIFFUSER DUE WALL FRICTION ONLY

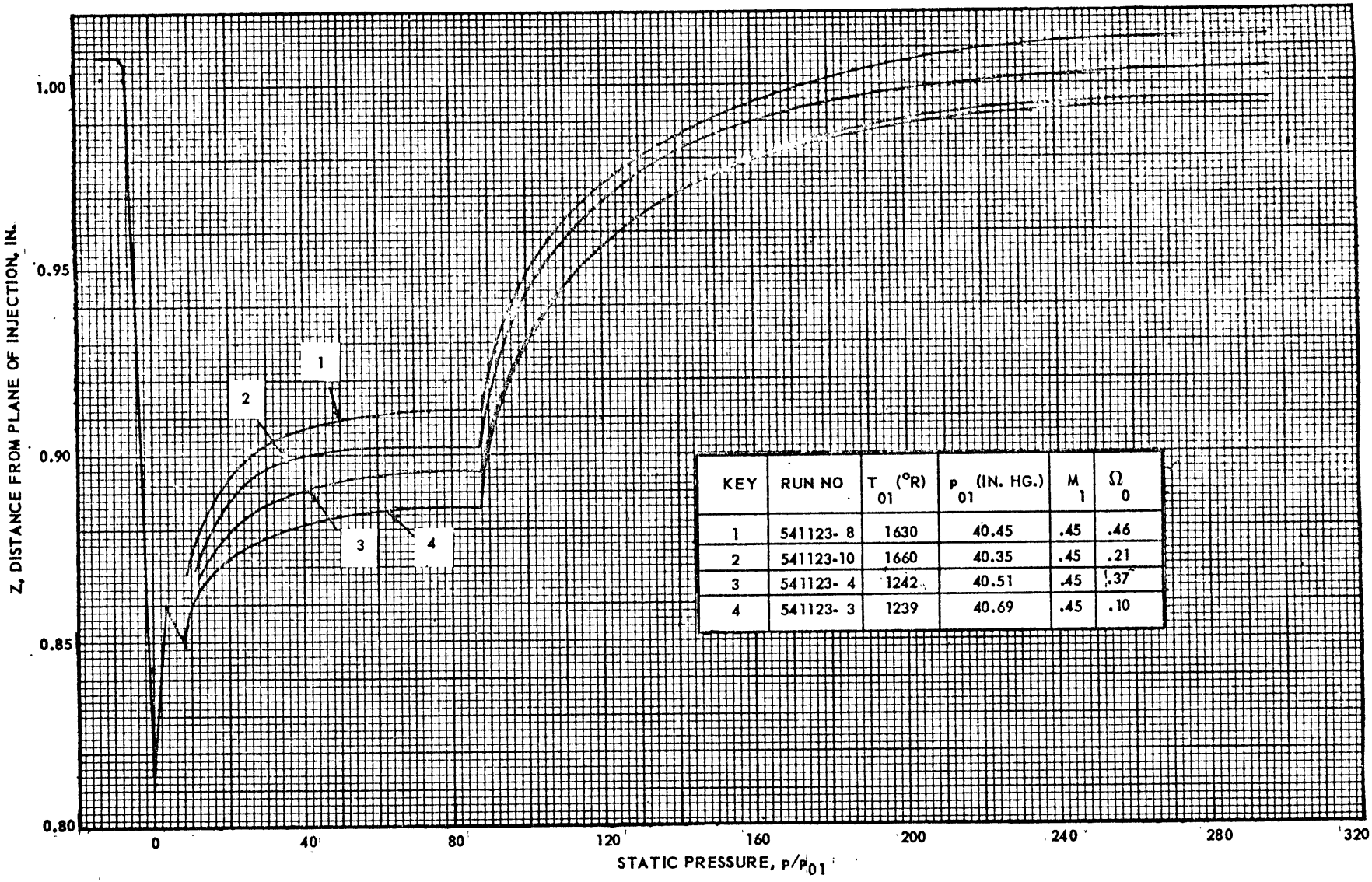

KEY	RUN NO	T_{01} (°R)	p_{01} (IN. HG.)	M_1	Ω_0
1	541123- 8	1630	40.45	.45	.46
2	541123-10	1660	40.35	.45	.21
3	541123- 4	1242	40.51	.45	.37
4	541123- 3	1239	40.69	.45	.10

FIG. 9 STATIC PRESSURE VARIATION WITH LENGTH: AEROTHERMOPRESSOR OPERATION WITH A CONSTANT AREA EVAPORATION SECTION WITH RATHER LOW SUBSONIC FLOWS

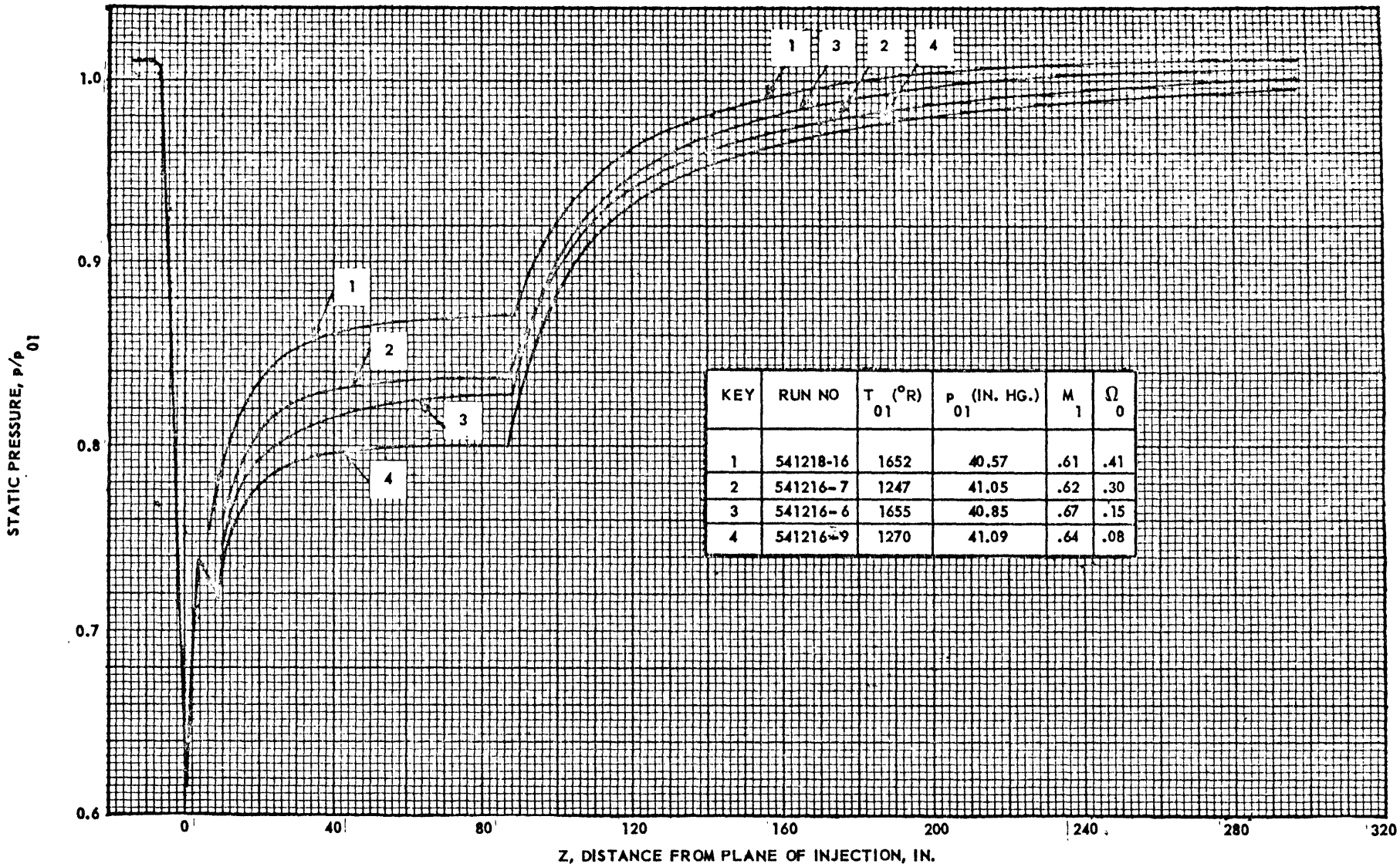

KEY	RUN NO	T_{01} (°R)	p_{01} (IN. HG.)	M_1	Ω_0
1	541218-16	1652	40.57	.61	.41
2	541216-7	1247	41.05	.62	.30
3	541216-6	1655	40.85	.67	.15
4	541216-9	1270	41.09	.64	.08

FIG. 10 STATIC PRESSURE VARIATION WITH LENGTH: AEROTHERMOPRESSOR OPERATION WITH A CONSTANT AREA EVAPORATION SECTION WITH MODERATE SUBSONIC FLOWS.

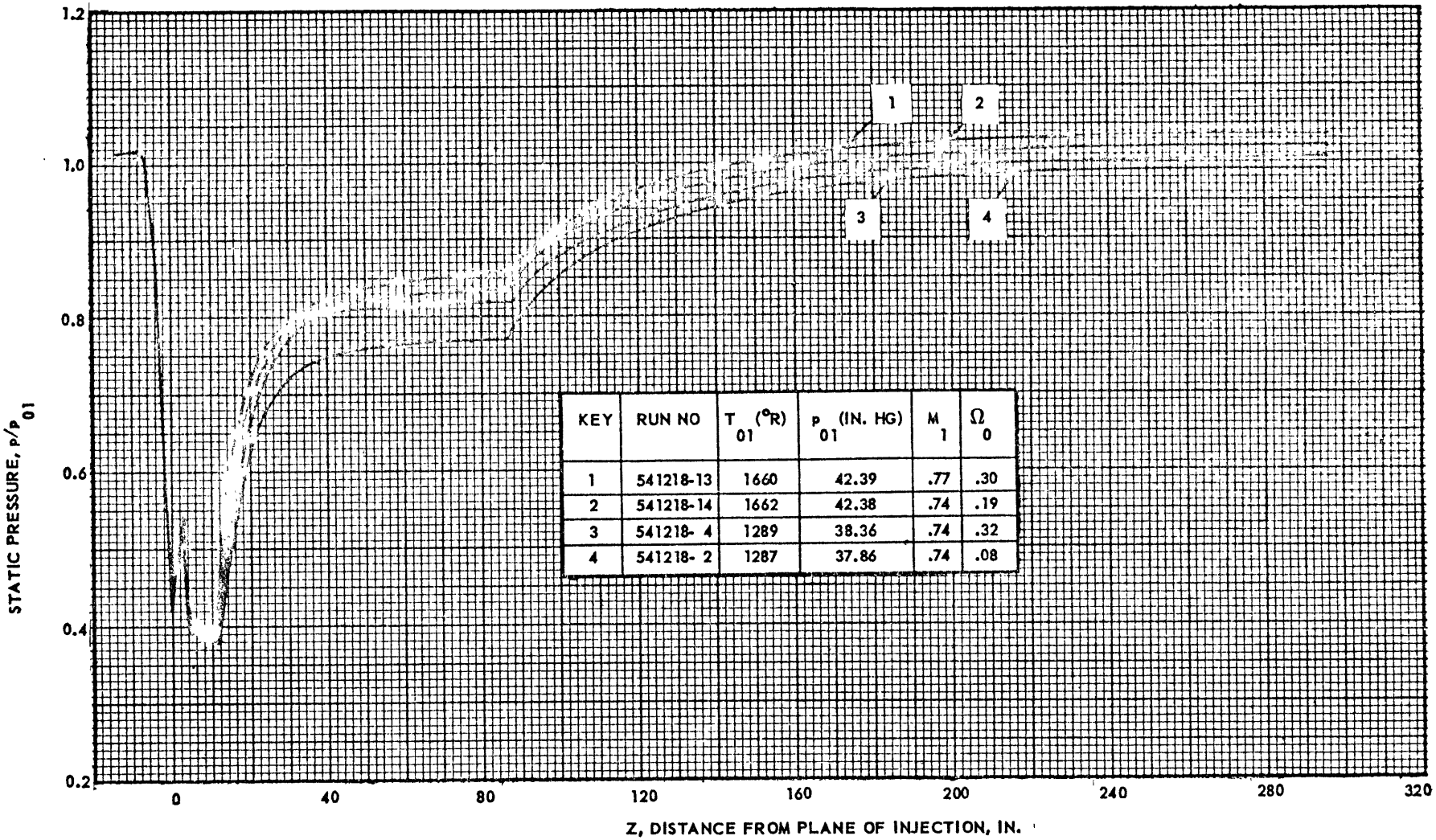

KEY	RUN NO	T_{01} (°R)	p_{01} (IN. HG)	M_1	Ω_0
1	541218-13	1660	42.39	.77	.30
2	541218-14	1662	42.38	.74	.19
3	541218- 4	1289	38.36	.74	.32
4	541218- 2	1287	37.86	.74	.08

FIG. 11 STATIC PRESSURE VARIATION WITH LENGTH: AEROTHERMOPRESSOR OPERATION WITH A CONSTANT AREA EVAPORATION SECTION WITH A CRITICAL INLET MACH NO., SUPERSONIC FLOW AND A "WEAK" SHOCK.

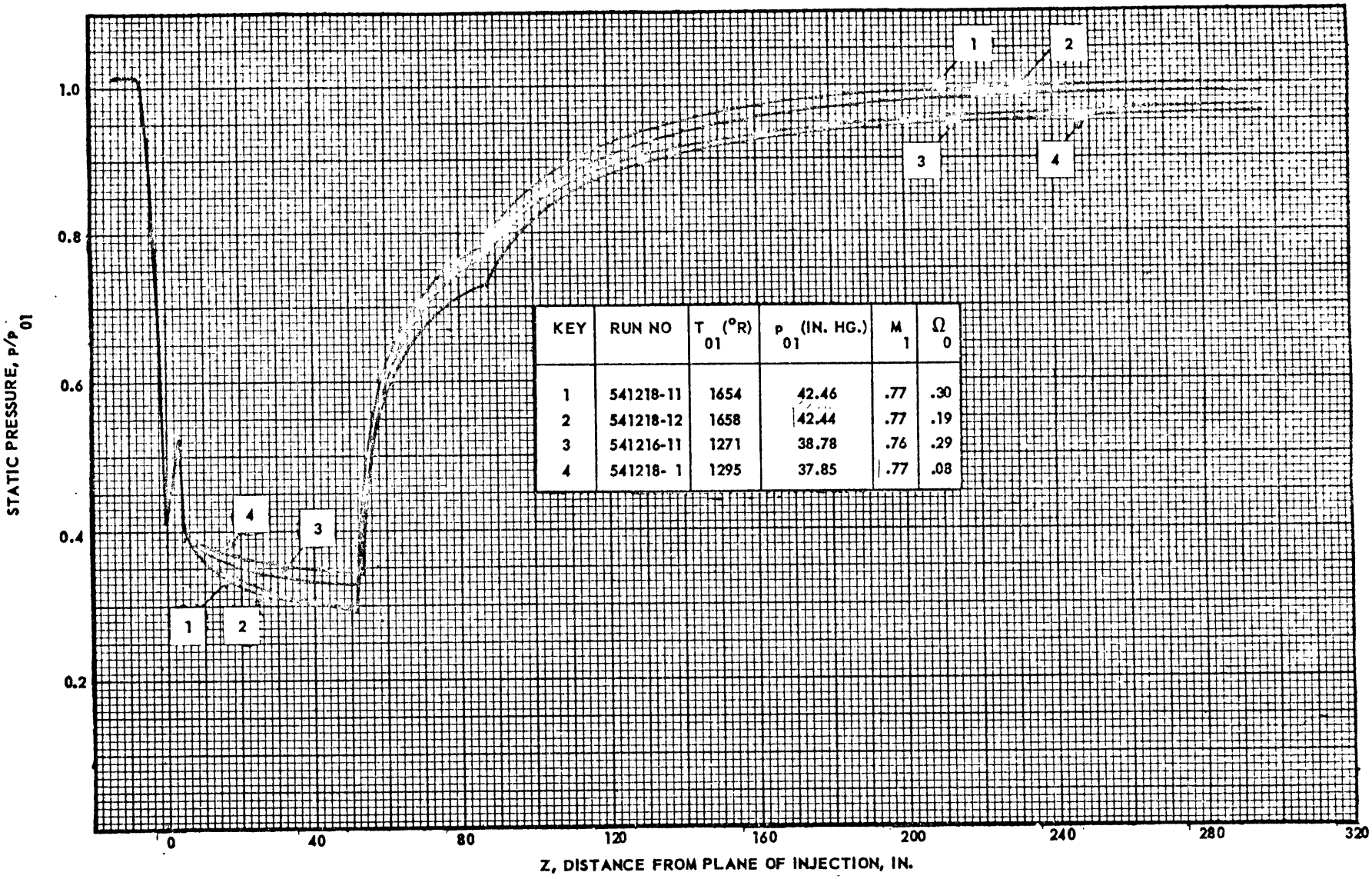

KEY	RUN NO	T_{01} (°R)	p_{01} (IN. HG.)	M_1	Ω_0
1	541218-11	1654	42.46	.77	.30
2	541218-12	1658	42.44	.77	.19
3	541216-11	1271	38.78	.76	.29
4	541218- 1	1295	37.85	.77	.08

FIG. 12 STATIC PRESSURE VARIATION WITH LENGTH: AEROTHERMOPRESSOR OPERATION WITH A CONSTANT AREA EVAPORATION SECTION WITH A CRITICAL INLET MACH NO., SUPERSONIC FLOW AND A "STRONG" SHOCK.

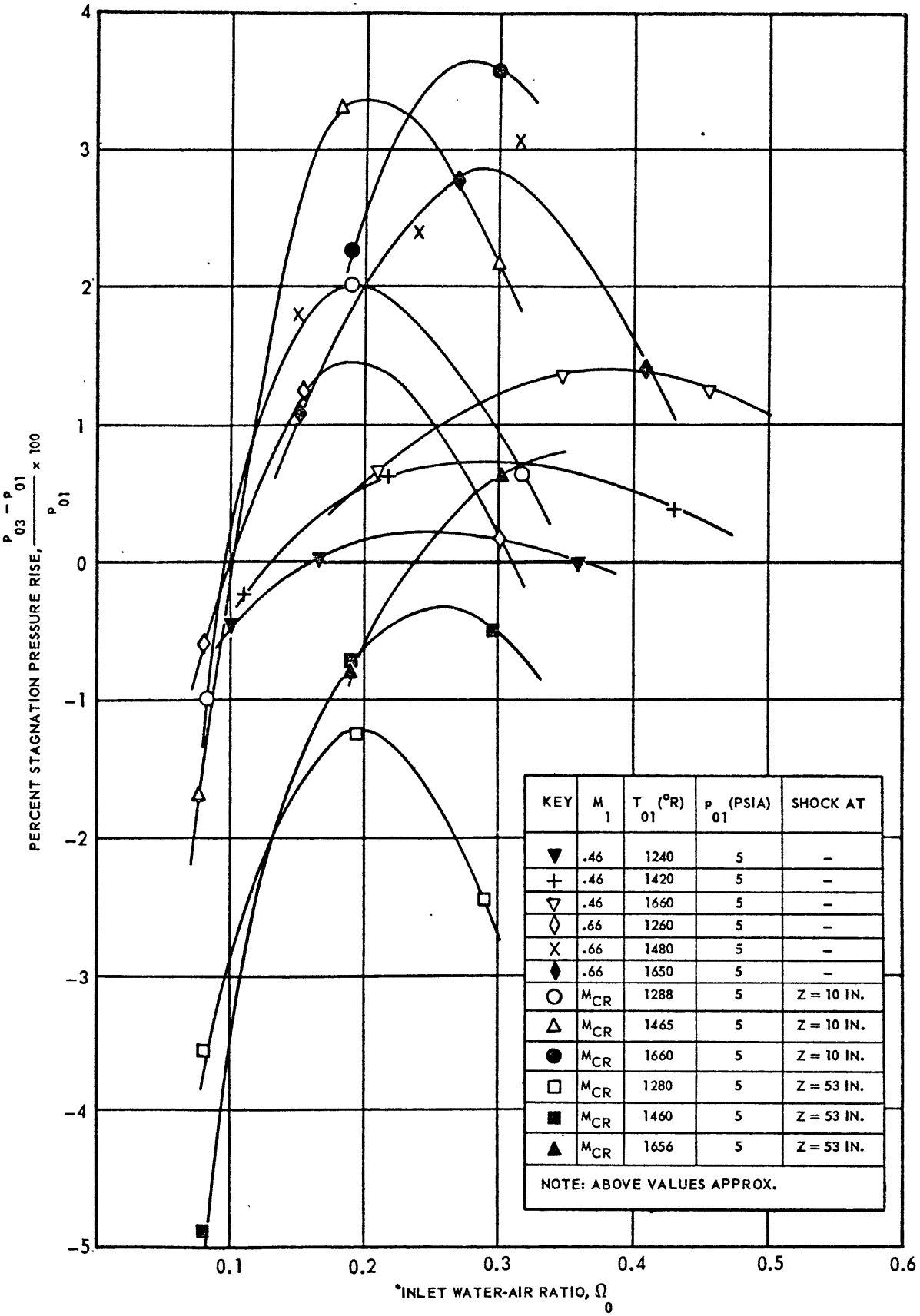

FIG. 13 AEROTHERMOPRESSOR PERFORMANCE WITH CONSTANT AREA EVAPORATION SECTION

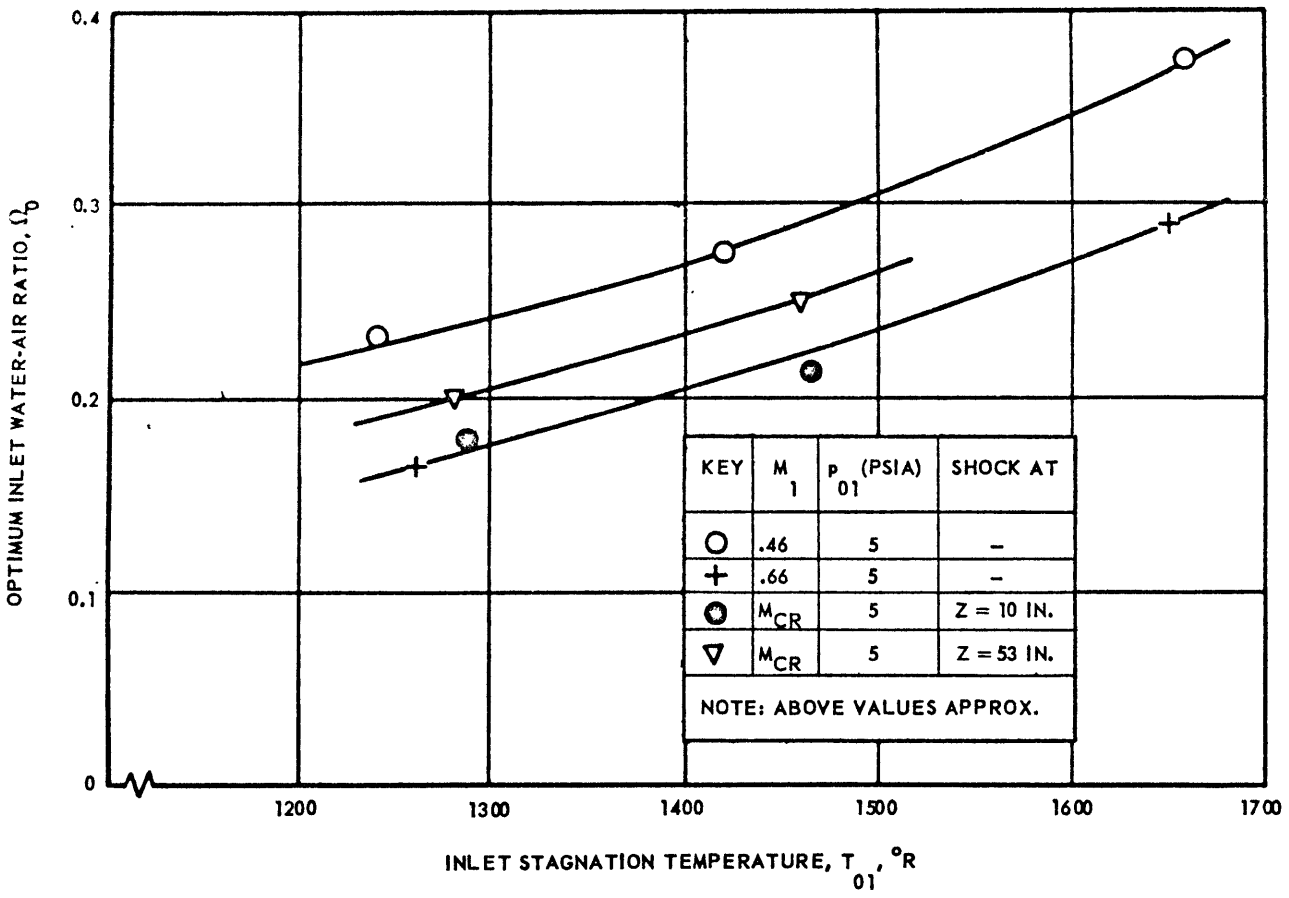

FIG. 14 WATER-AIR RATIO FOR OPTIMUM CONSTANT AREA AEROTHERMOPRESSOR PERFORMANCE

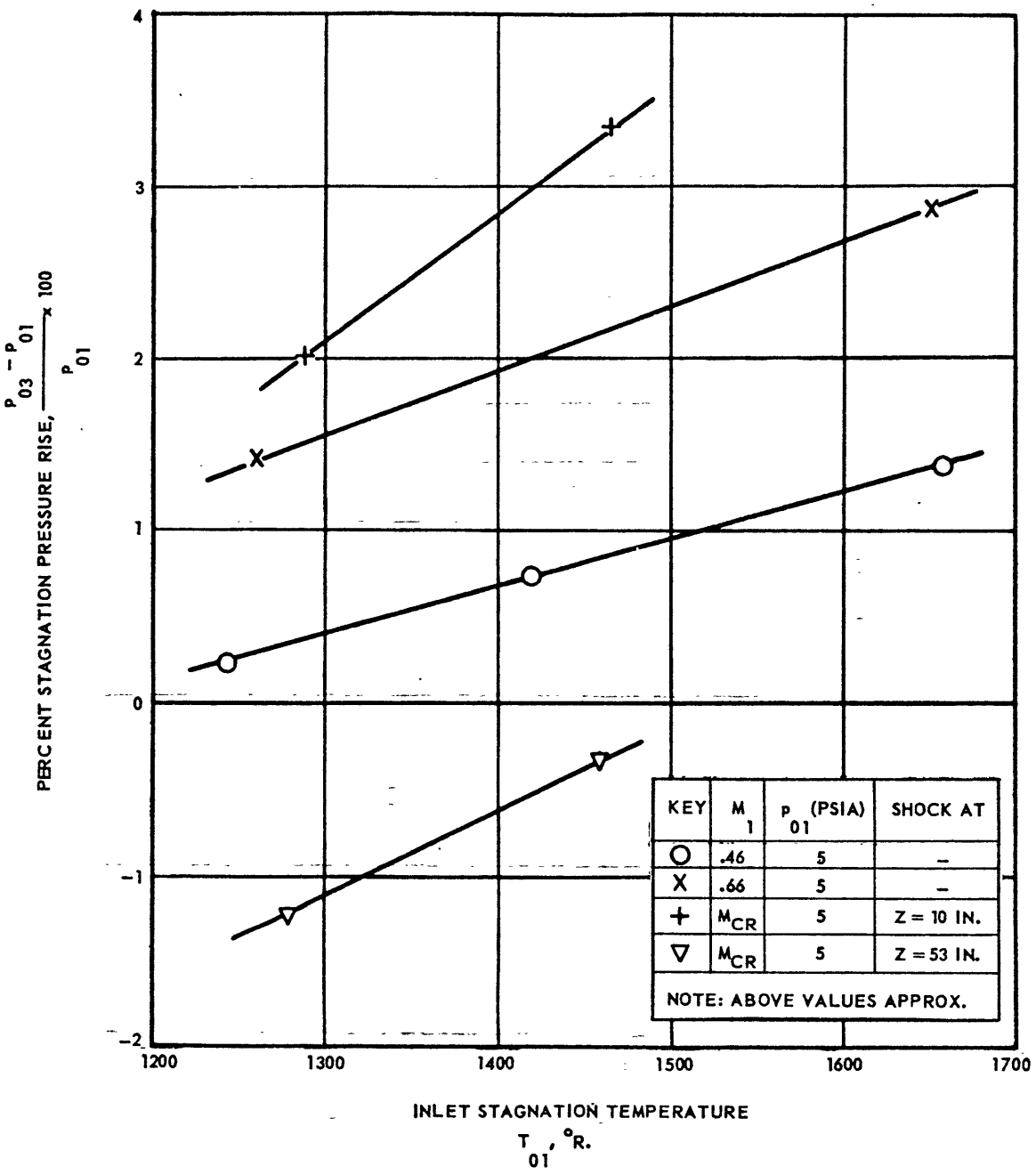

FIG. 15.. EFFECT OF INLET STAGNATION TEMPERATURE ON OPTIMUM CONSTANT AREA AEROTHERMOPRESSOR PERFORMANCE

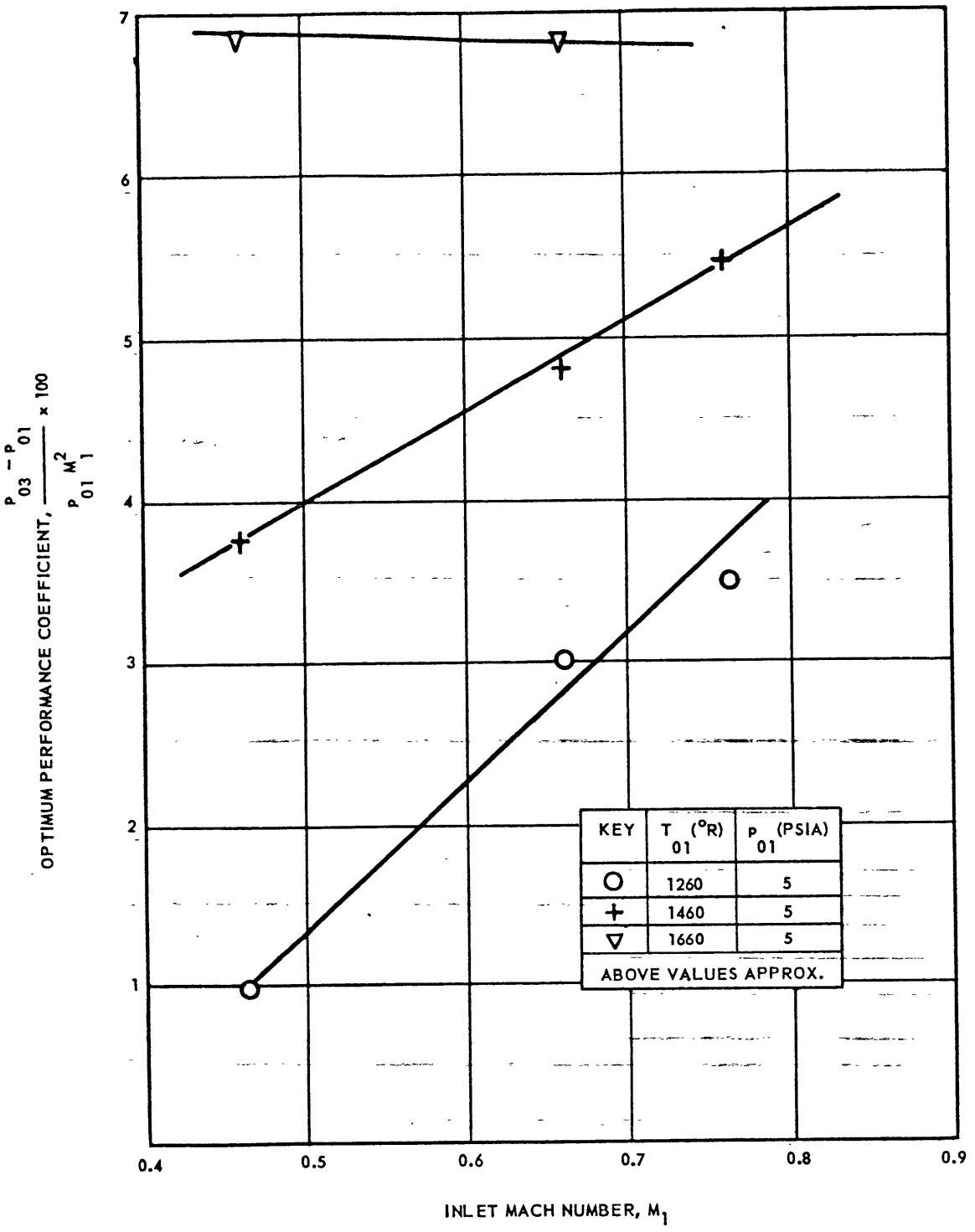

FIG. 16 EFFECT OF INLET MACH NO. ON OPTIMUM CONSTANT AREA AEROTHERMOPRESSOR PERFORMANCE

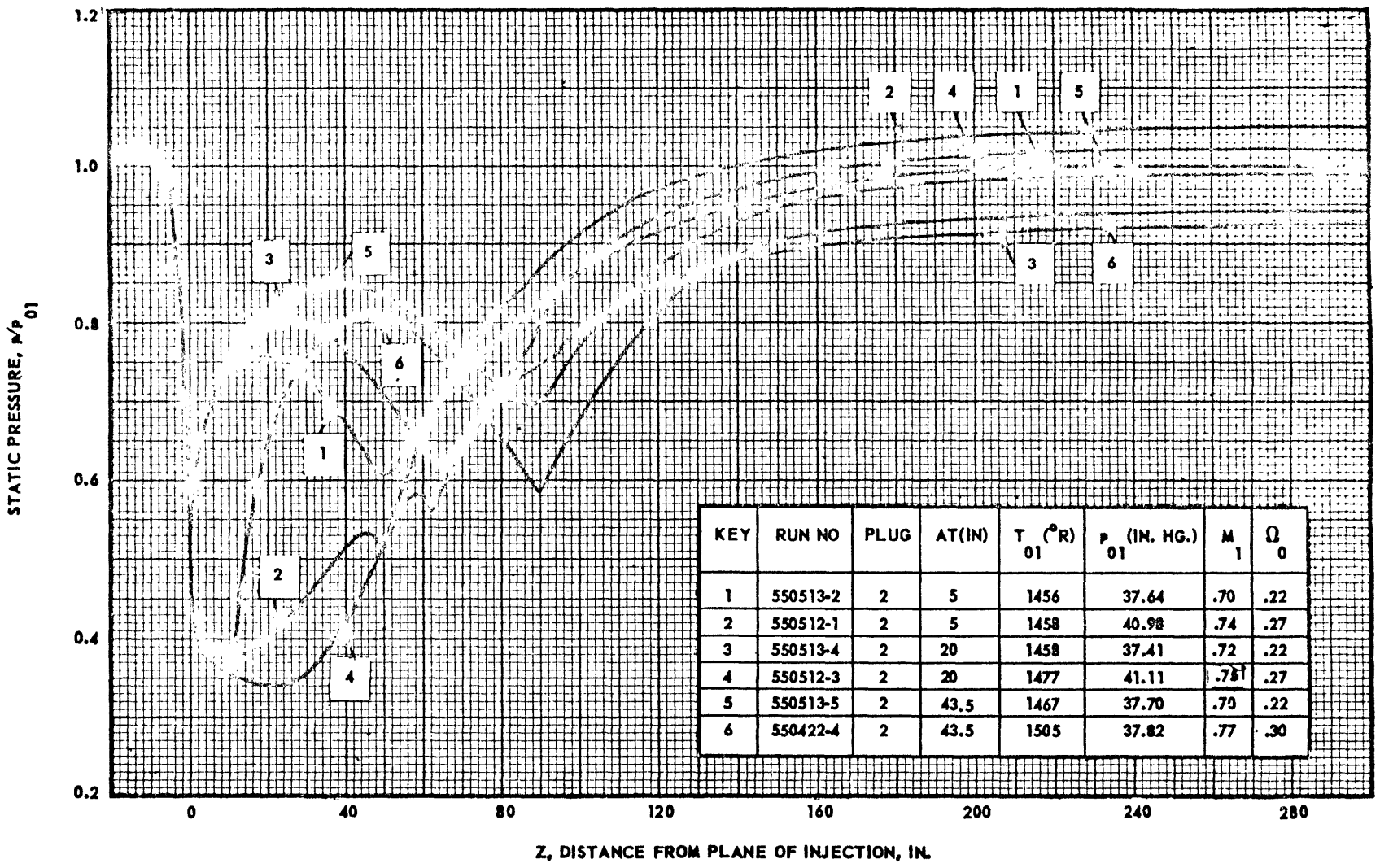

KEY	RUN NO	PLUG	AT(IN)	T_{01} (°R)	P_{01} (IN. HG.)	M_1	Ω_0
1	550513-2	2	5	1456	37.64	.70	.22
2	550512-1	2	5	1458	40.98	.74	.27
3	550513-4	2	20	1458	37.41	.72	.22
4	550512-3	2	20	1477	41.11	.75	.27
5	550513-5	2	43.5	1467	37.70	.70	.22
6	550422-4	2	43.5	1505	37.82	.77	.30

FIG. 17 STATIC PRESSURE VARIATION WITH LENGTH: AEROTHERMOPRESSOR OPERATION WITH VARIABLE AREA EVAPORATION SECTIONS PROVIDED BY PLUG NO 2.

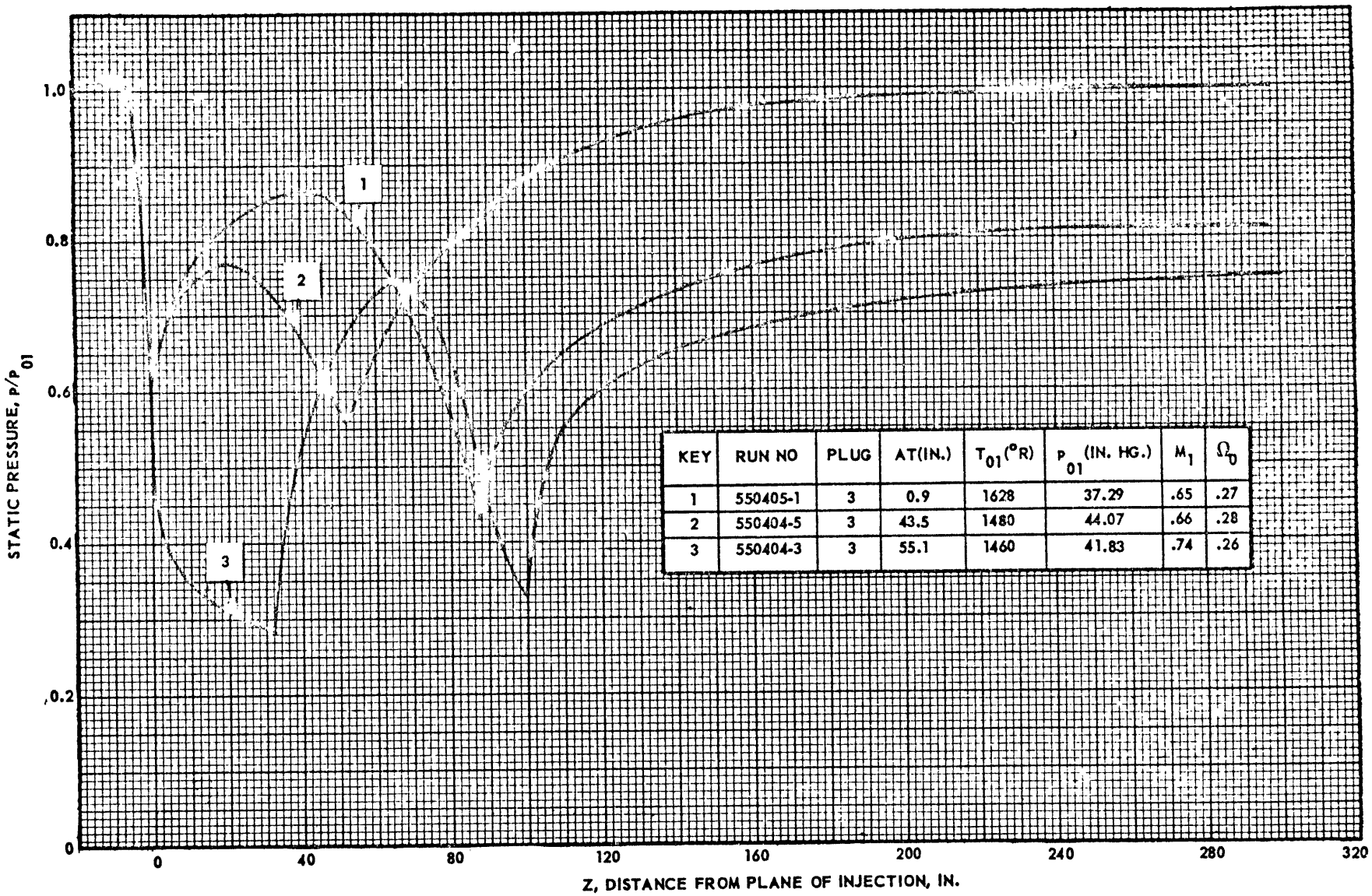

KEY	RUN NO	PLUG	AT(IN.)	T_{01}(°R)	p_{01} (IN. HG.)	M_1	Ω_0
1	550405-1	3	0.9	1628	37.29	.65	.27
2	550404-5	3	43.5	1480	44.07	.66	.28
3	550404-3	3	55.1	1460	41.83	.74	.26

FIG. 18 STATIC PRESSURE VARIATION WITH LENGTH: AEROTHERMOPRESSOR OPERATION WITH VARIABLE AREA EVAPORATION SECTIONS PROVIDED BY PLUG NO. 3.

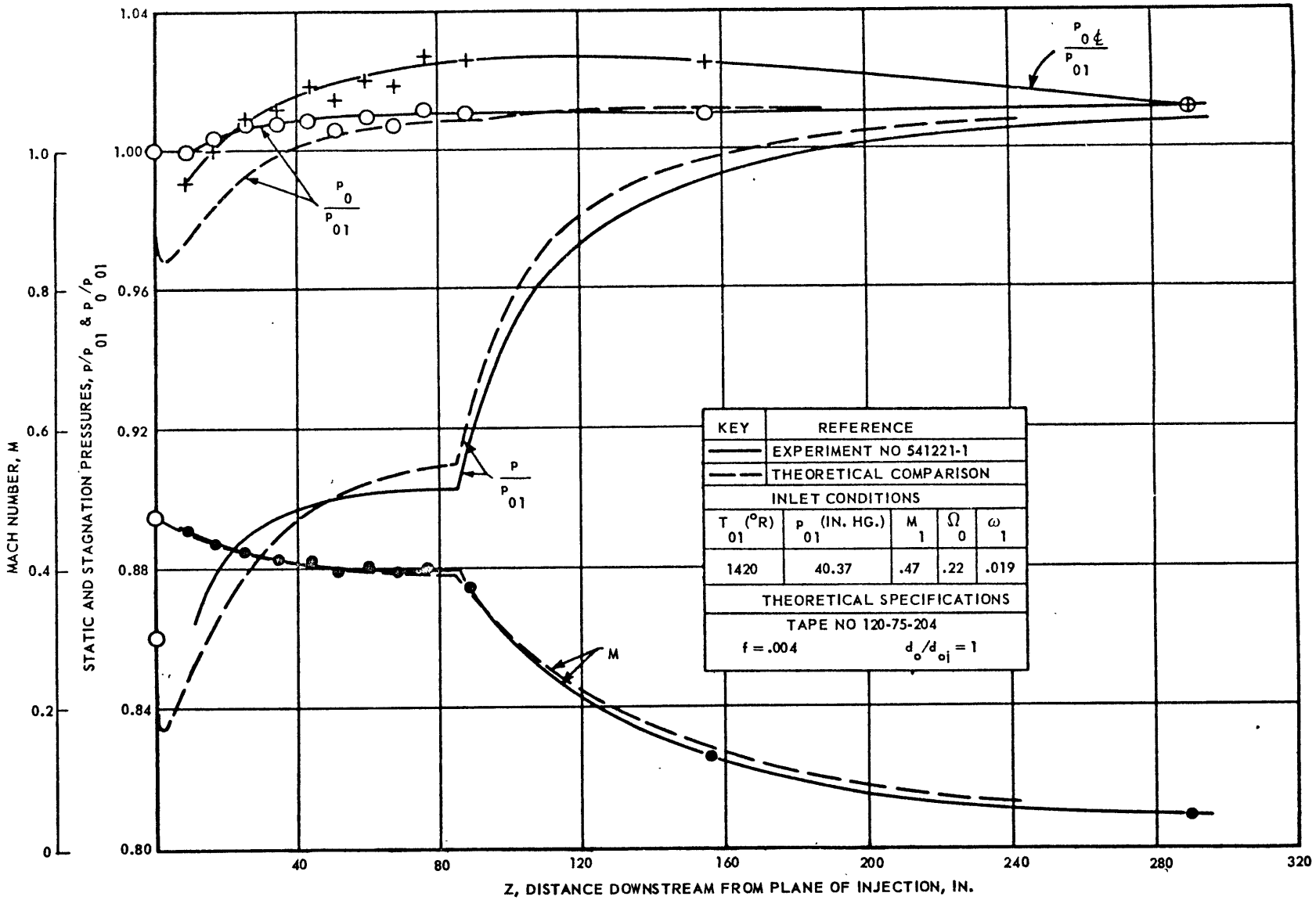

FIG. 19 COMPARISON OF THEORETICAL AND EXPERIMENTAL RESULTS

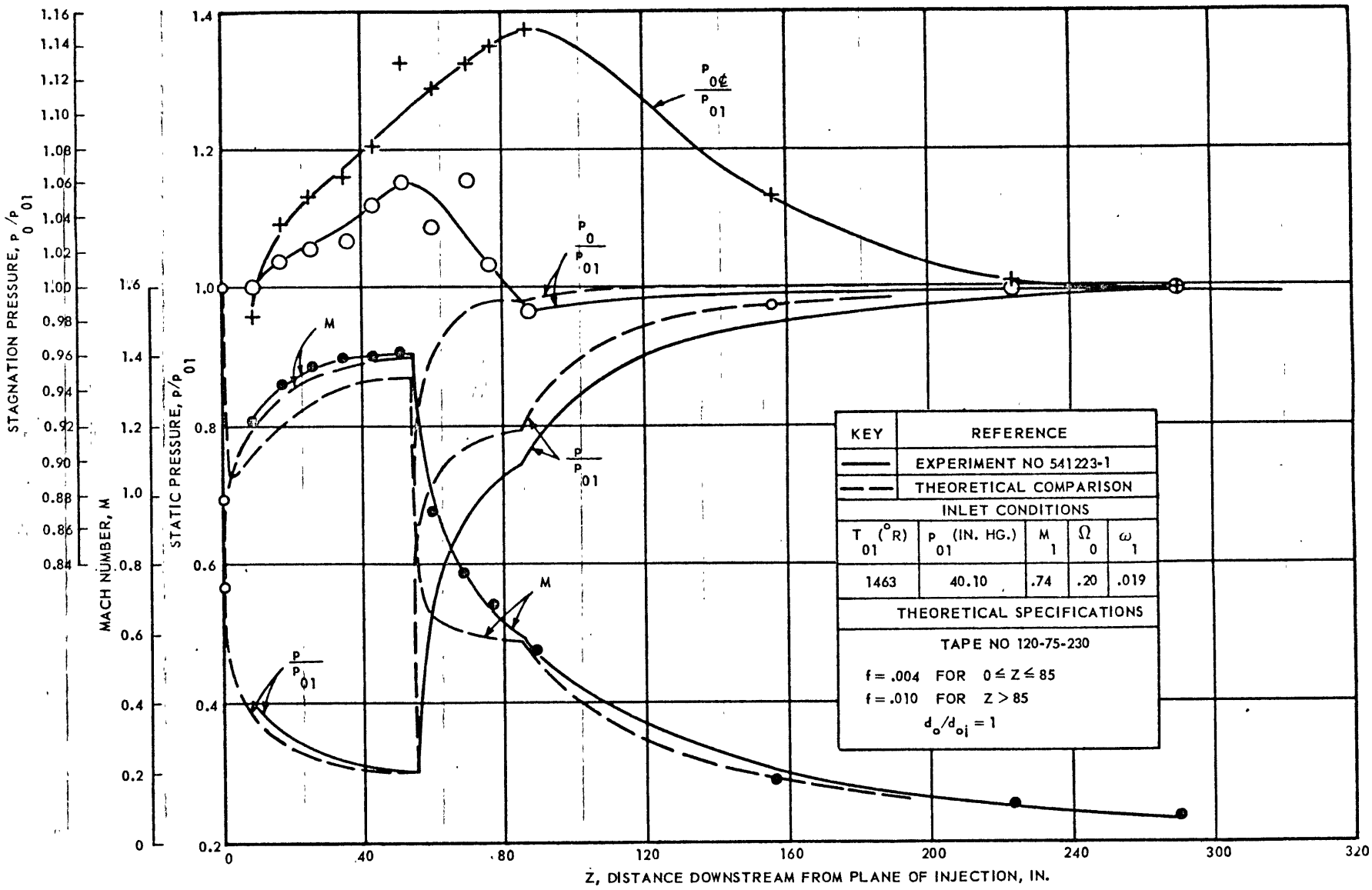

FIG. 20 COMPARISON OF THEORETICAL AND EXPERIMENTAL RESULTS

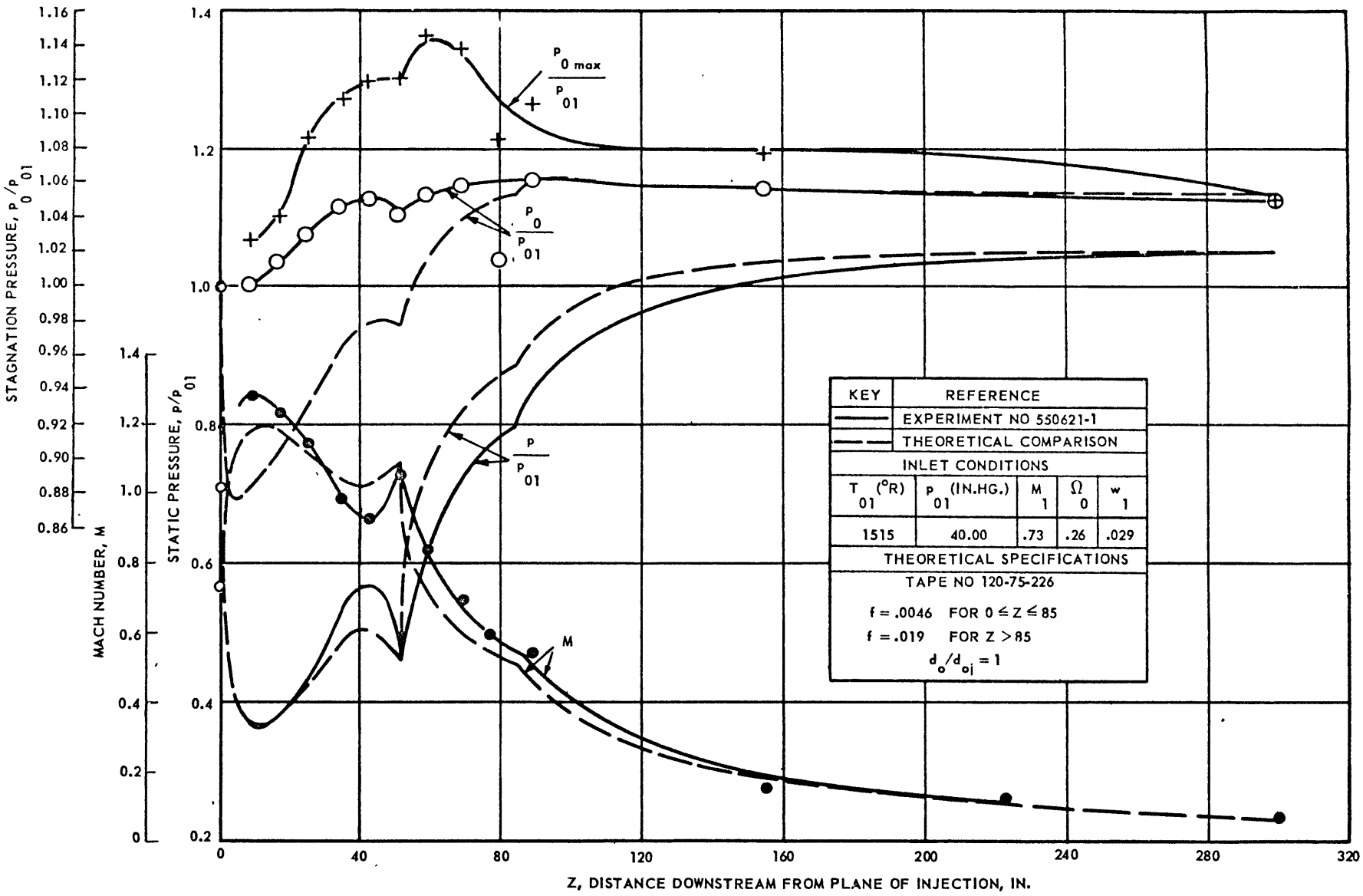

FIG. 21 COMPARISON OF THEORETICAL AND EXPERIMENTAL RESULTS

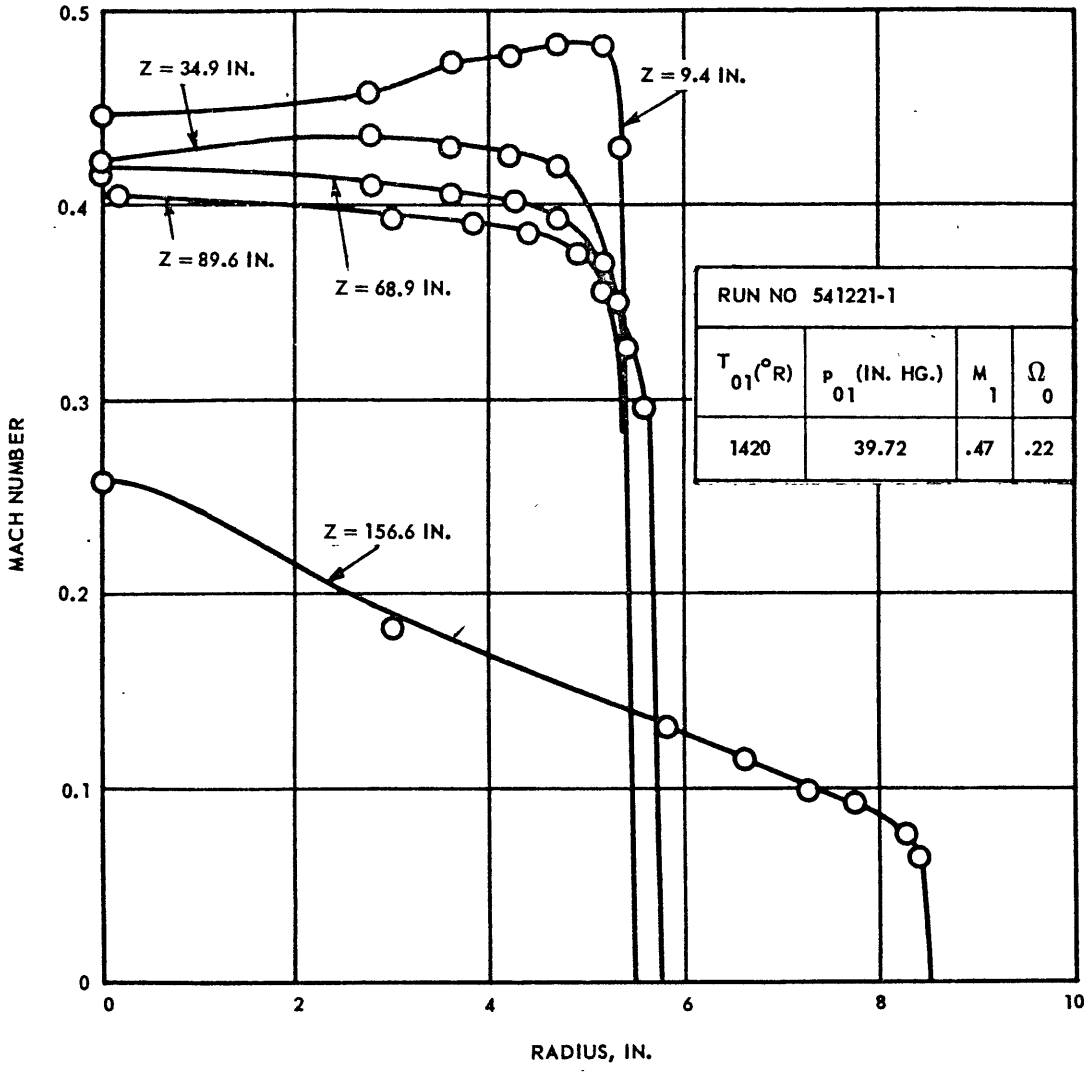

FIG. 22 MACH NUMBER PROFILES

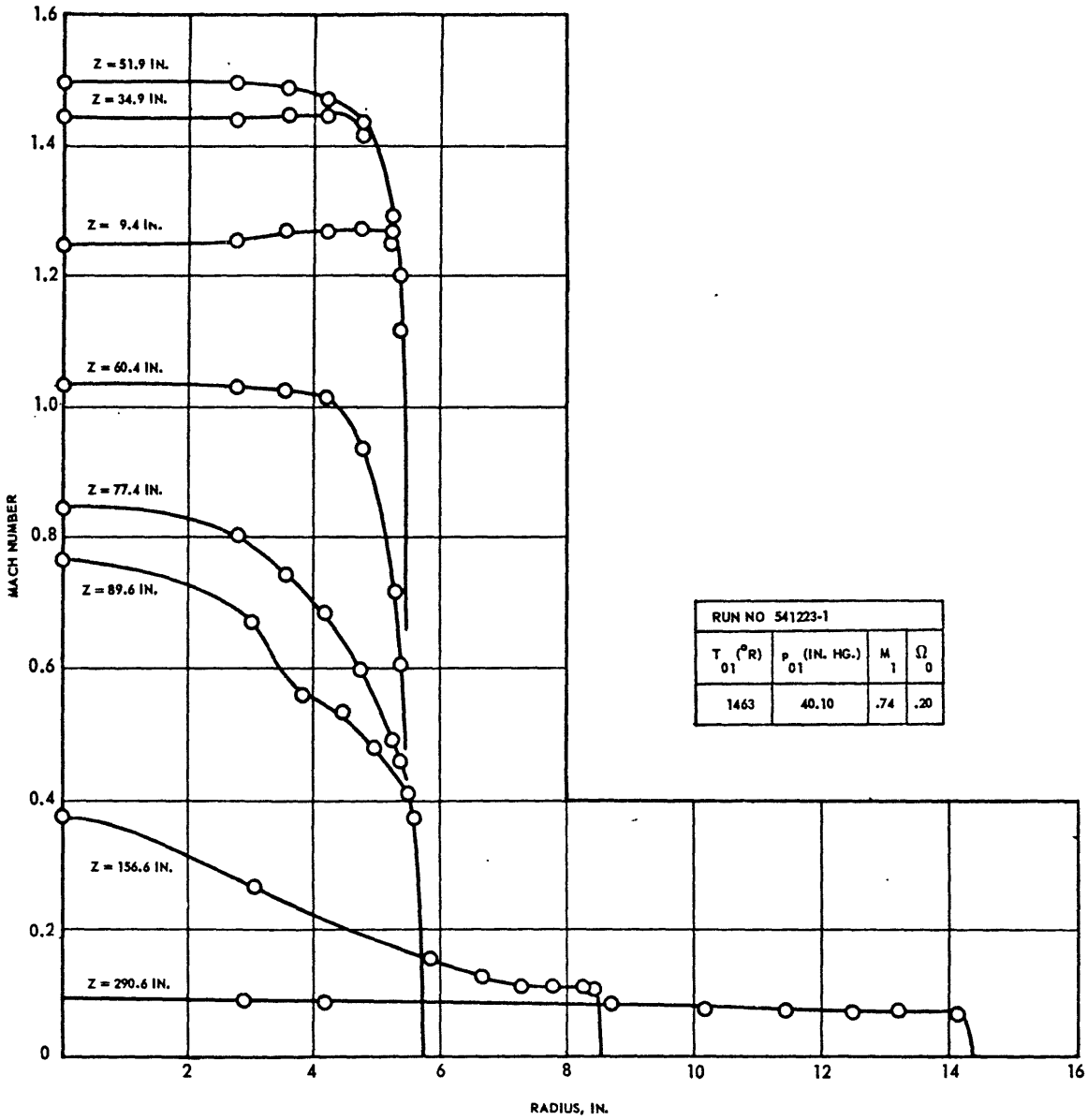

FIG. 23 MACH NUMBER PROFILES

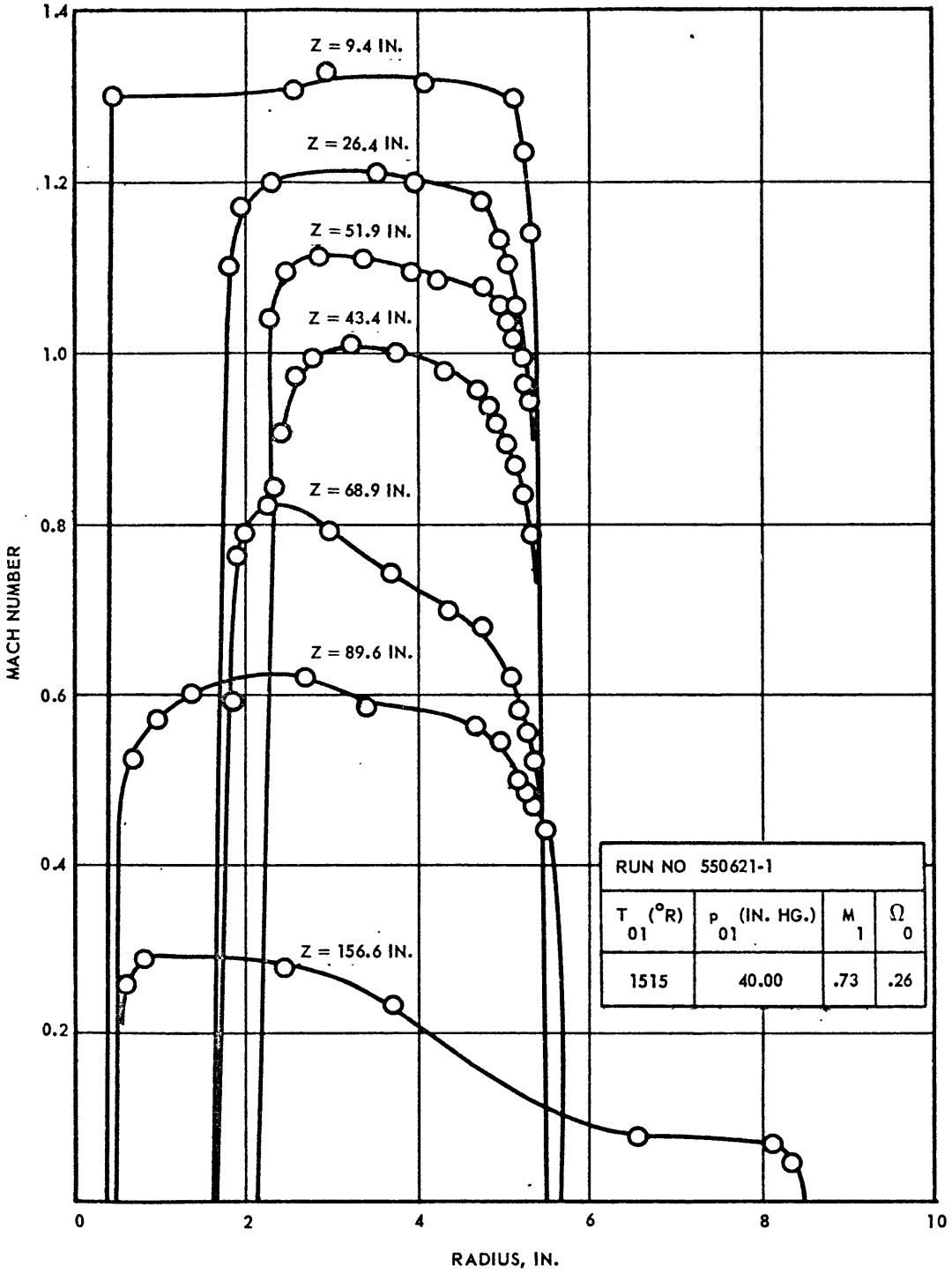

FIG. 24 MACH NUMBER PROFILES

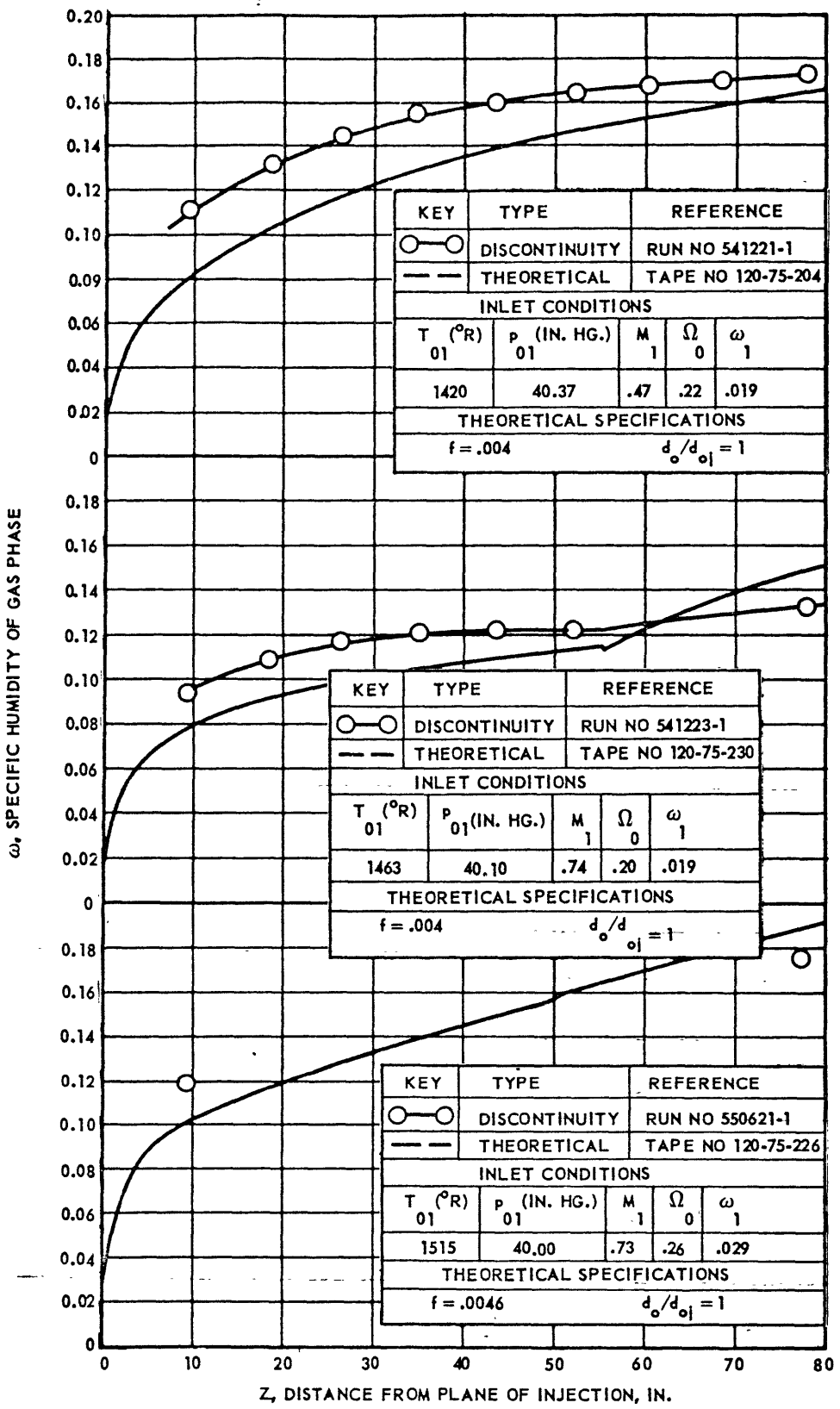

FIG. 25 COMPARISON OF THE SPECIFIC HUMIDITIES DETERMINED FROM MEASURED DATA AND A DISCONTINUITY ANALYSIS TO THOSE DETERMINED BY A COMPLETELY THEORETICAL ANALYSIS.

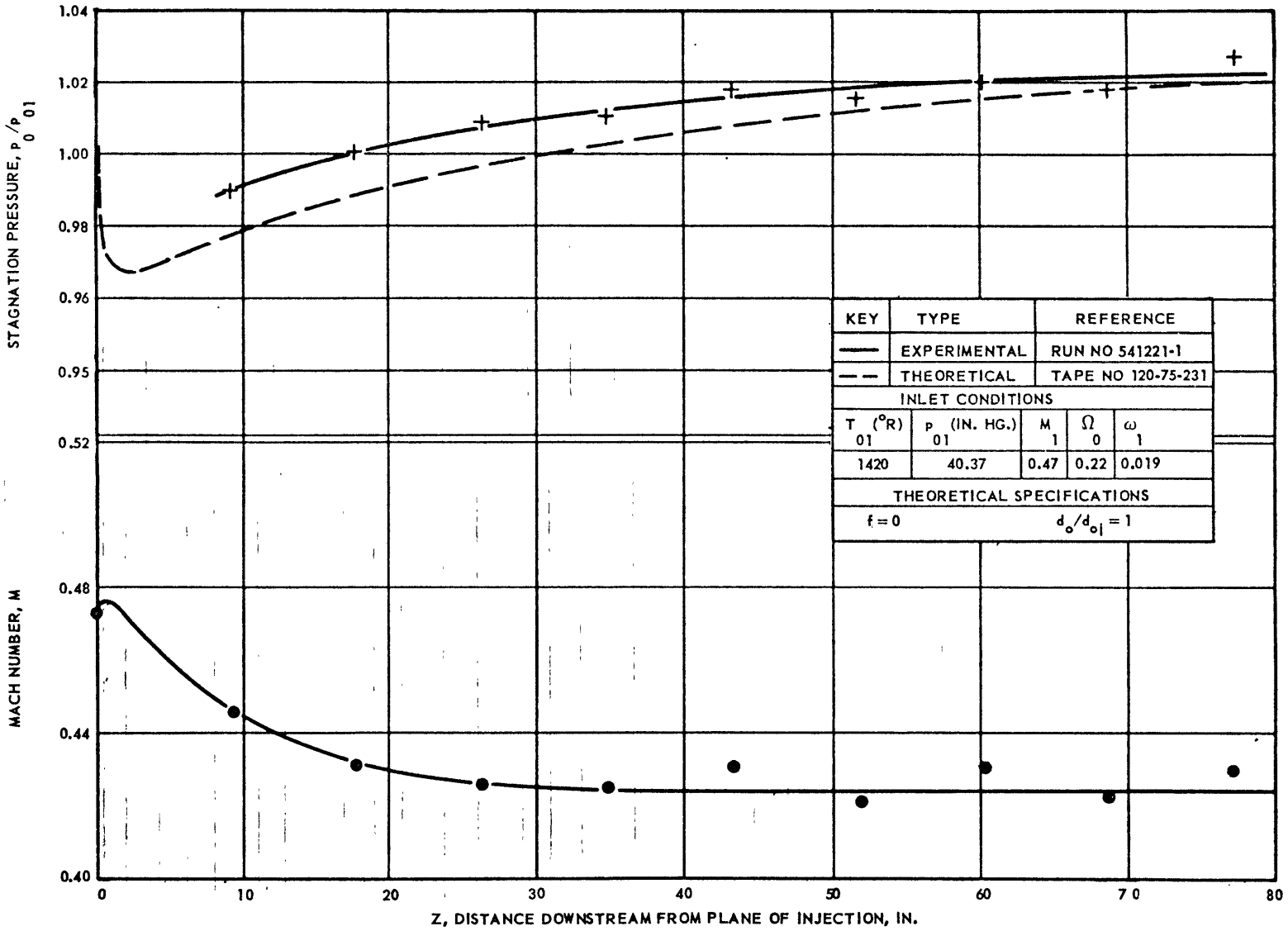

FIG. 26 COMPARISON OF THEORETICAL AND EXPERIMENTAL RESULTS PERTAINING TO THE CORE FLOW.

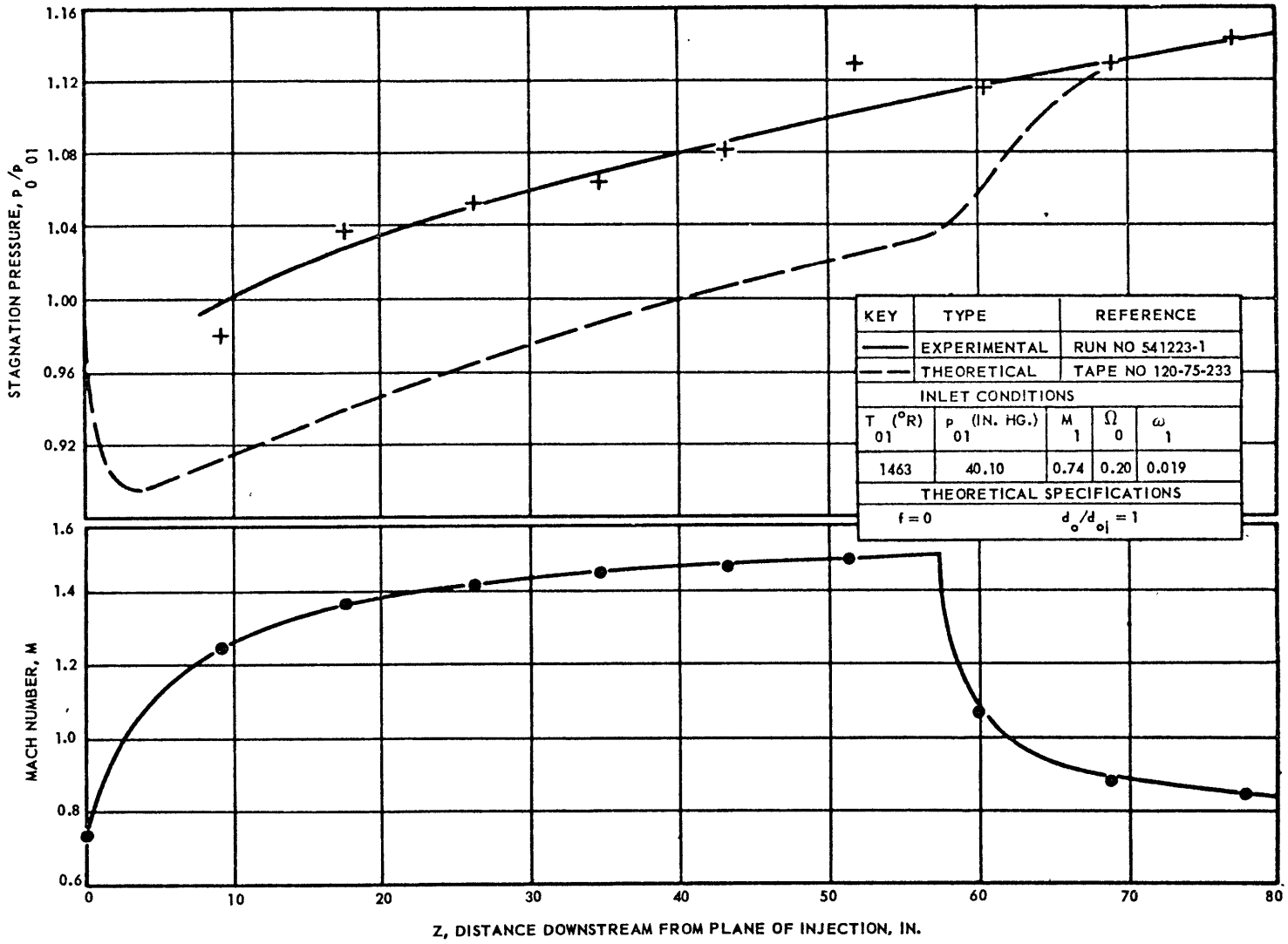

FIG. 27 COMPARISON OF THEORETICAL AND EXPERIMENTAL RESULTS PERTAINING TO THE CORE FLOW.

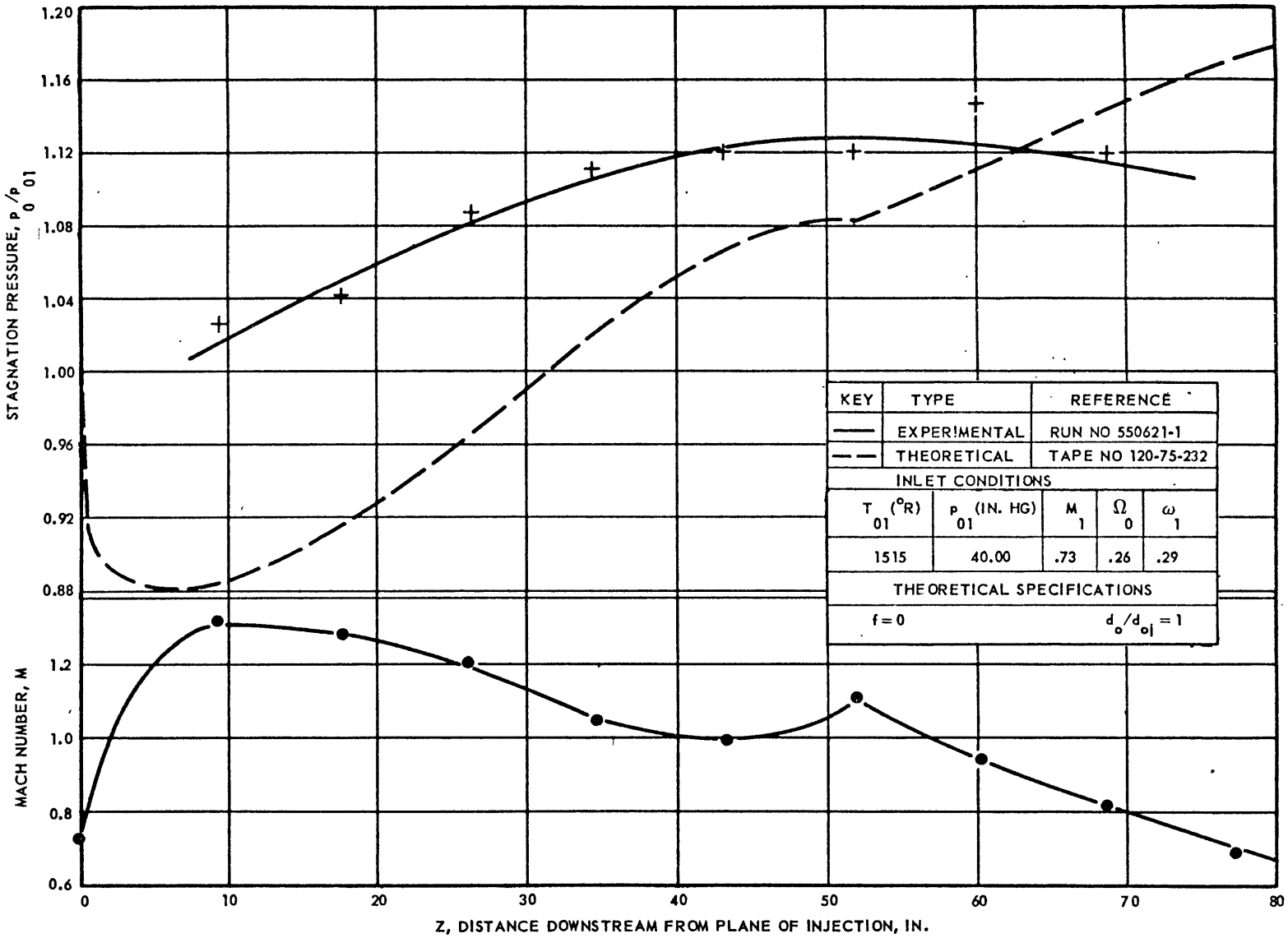

FIG. 28 COMPARISON OF THEORETICAL AND EXPERIMENTAL RESULTS PERTAINING TO THE CORE FLOW.

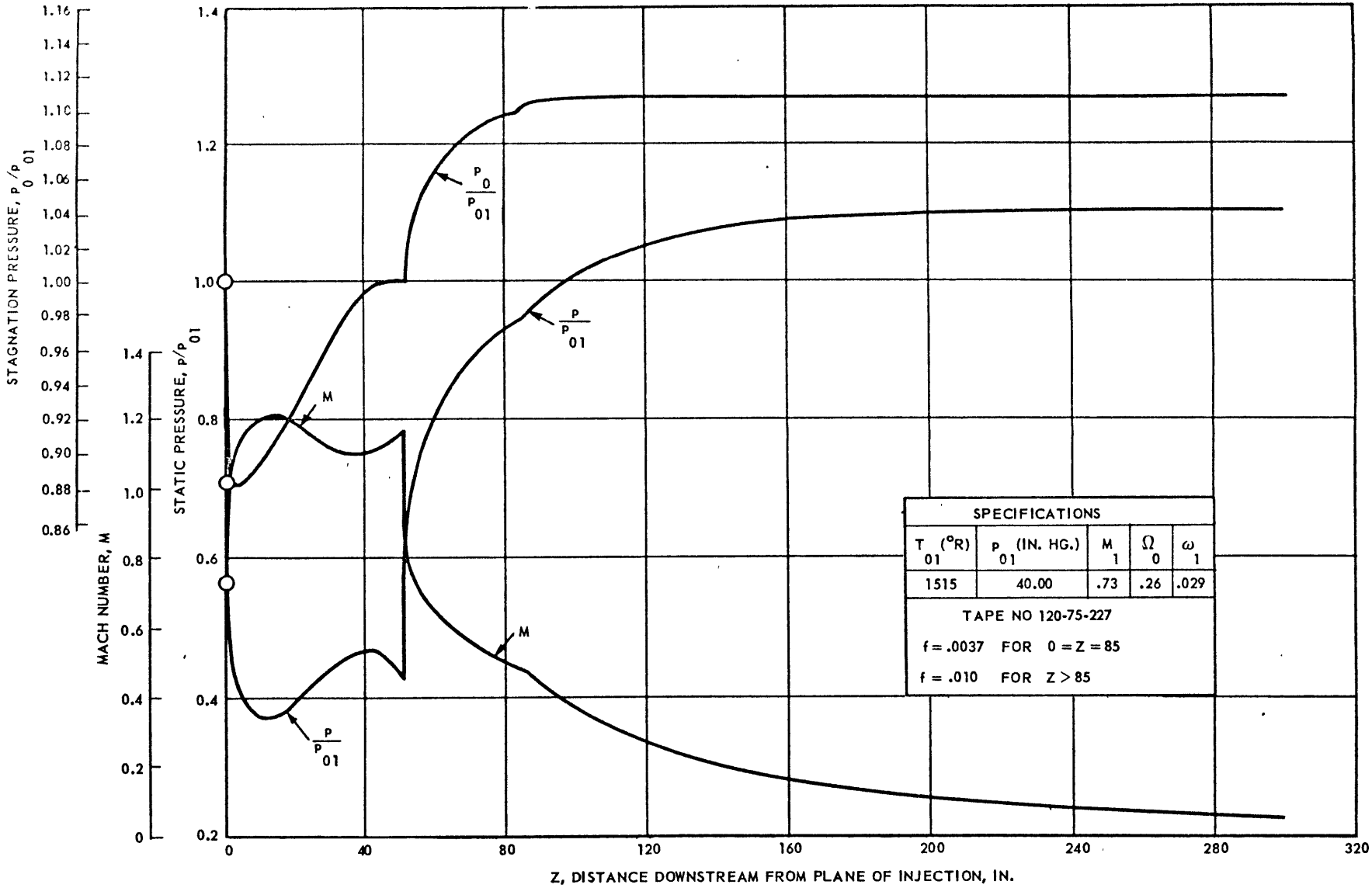

FIG. 29 THEORETICAL PERFORMANCE OF AEROTHERMOPRESSOR WITH EVAPORATION SECTION HAVING EXTERNAL AREA VARIATION.

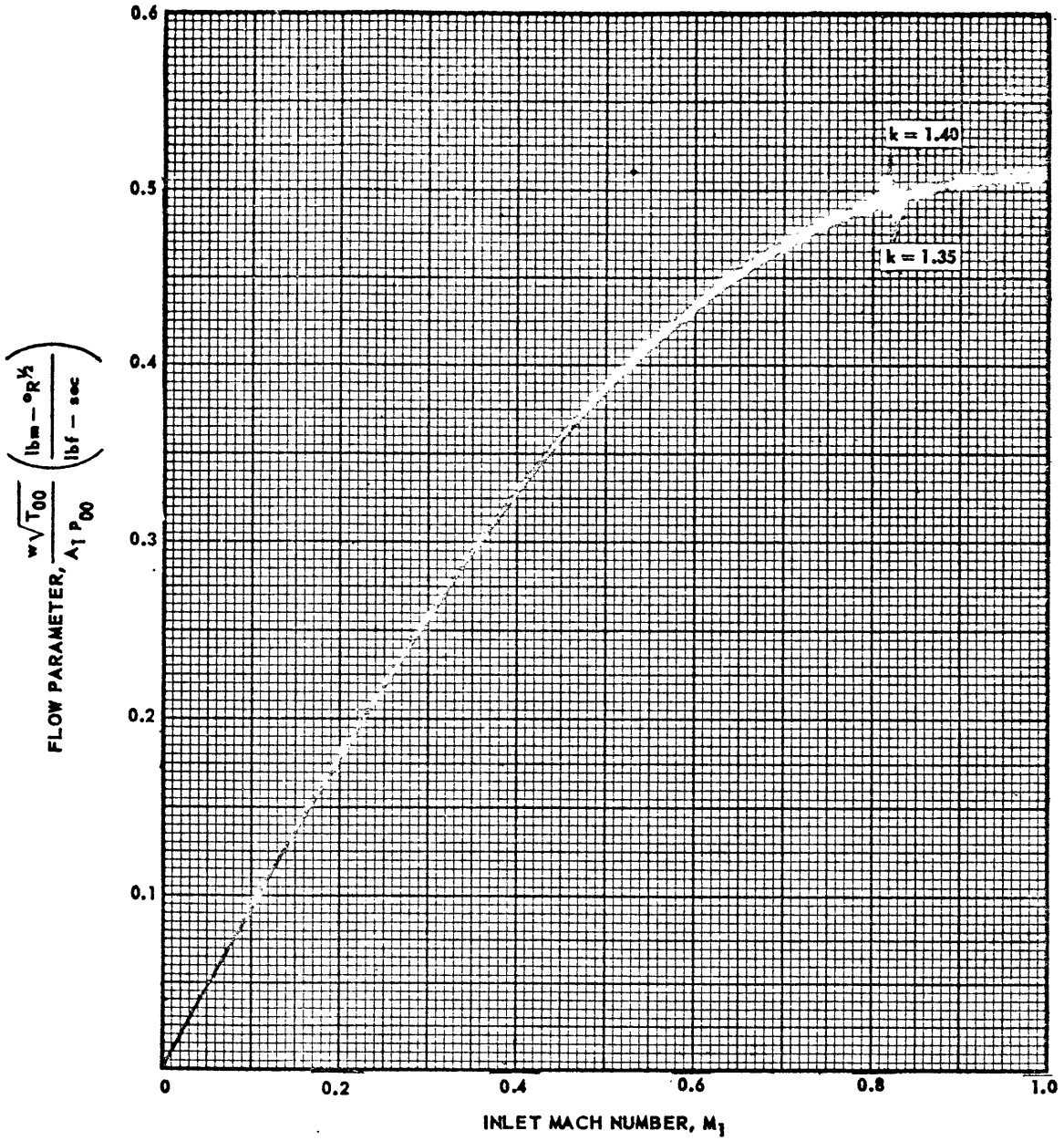

FIG. 30 CALIBRATION CHART NO. 1 FOR INLET MACH NO.

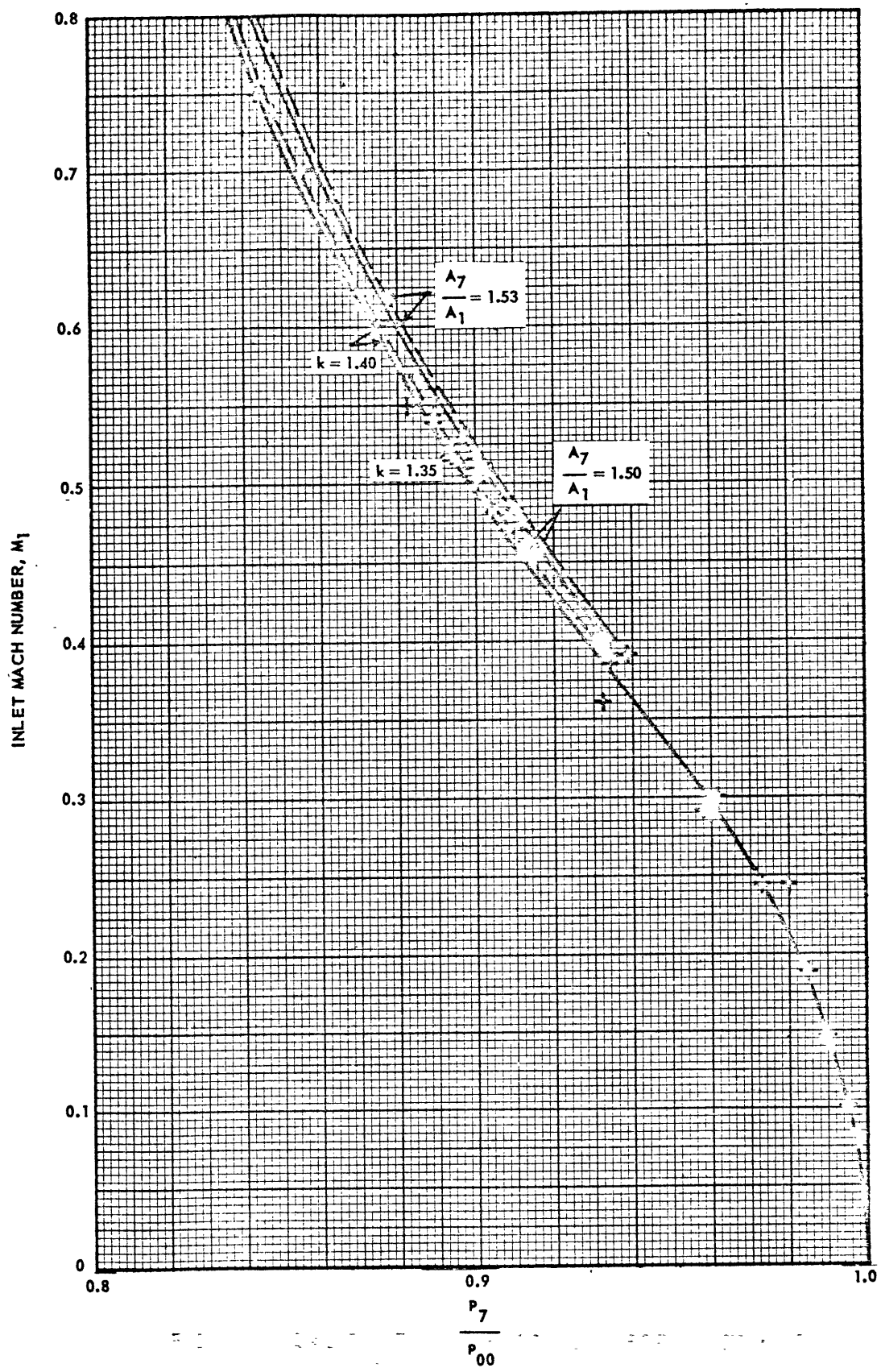

FIG. 31 CALIBRATION CHART NO. 2 FOR INLET MACH NO.

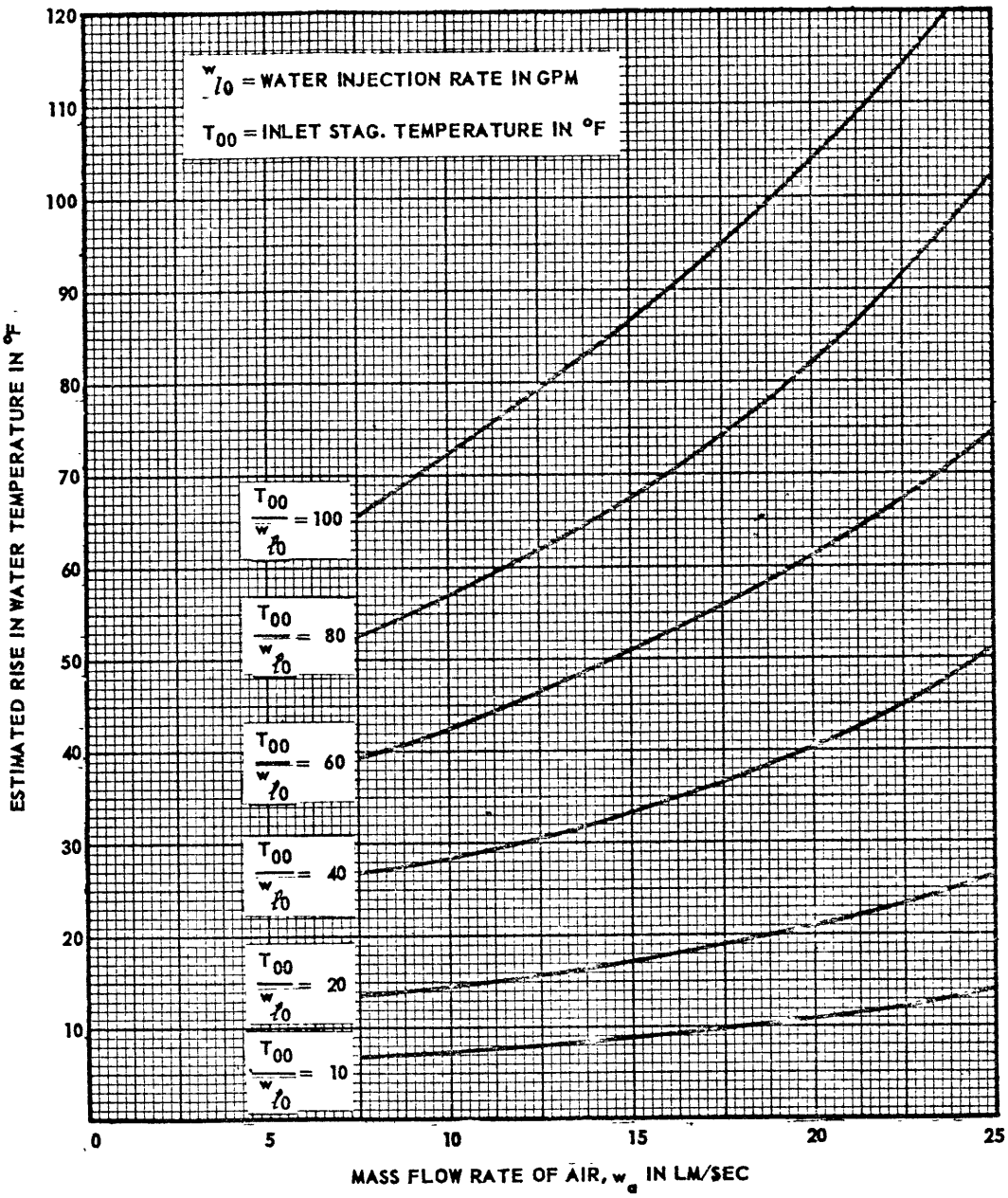

FIG. 32 ESTIMATED RISE IN TEMPERATURE OF WATER FLOWING UP TO INJECTION POINT

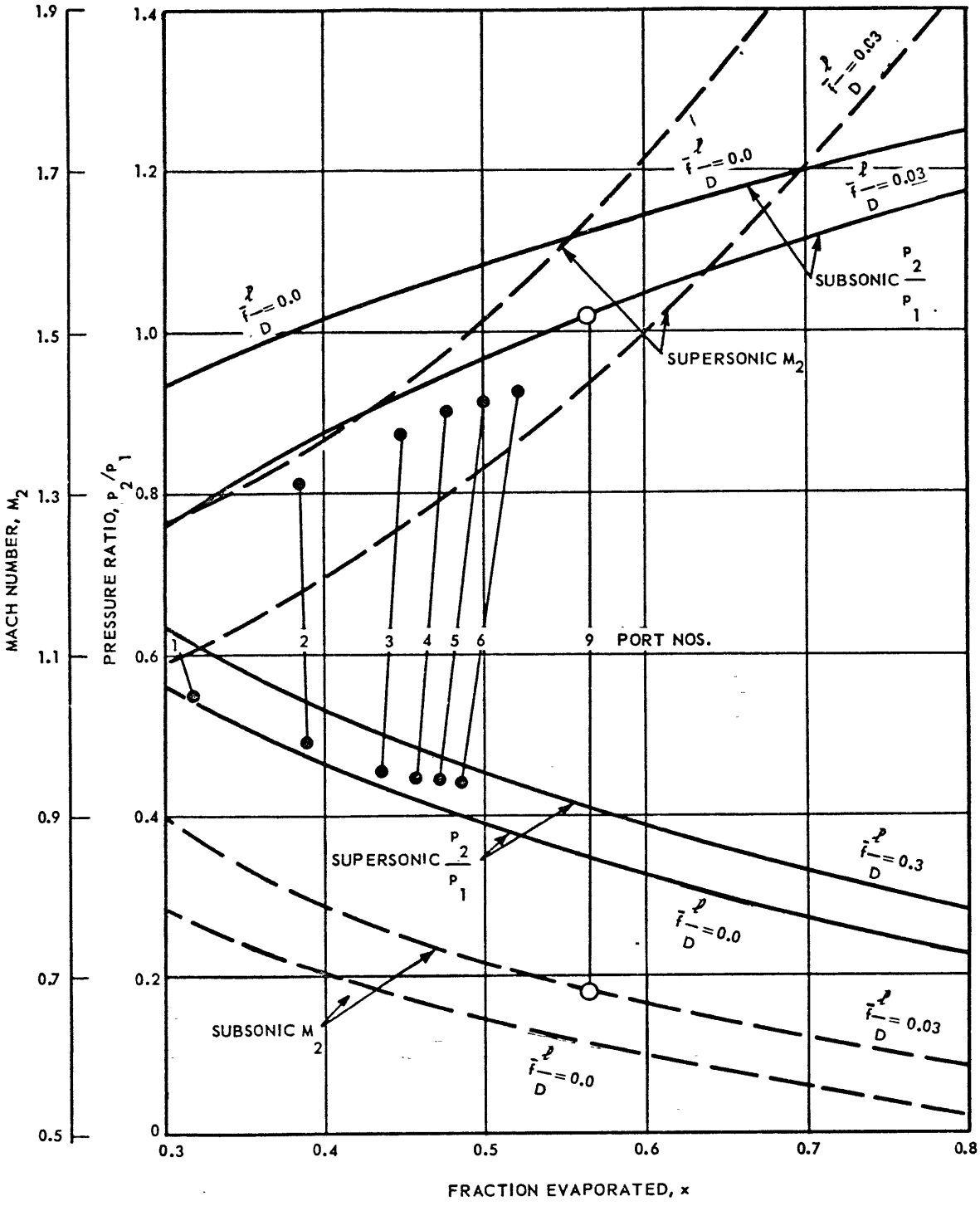

FIG. 33 ILLUSTRATING RESULTS OF DISCONTINUITY ANALYSIS AND METHODS EMPLOYED TO DETERMINE APPARENT FRICTION FACTOR AND HUMIDITY.